Classification of Birimian Gold Occurrences Using their Geological and Geochemical Attributes: Case Study in South Ashanti Belt, Ghana

Seidu Alidu

February 2007

Errata sheet

For the MSc. thesis by Seidu Alidu, (AES)

Classification of Birimian Gold Occurrences Using their Geological and Geochemical attributes: Case Study in South Ashanti Belt, Ghana.

Page	**Location**	**Change**	**Add**
Opening Page	Thesis Assessment Board	-	**Dr. S.P. Vriend-Univ. of Utrecht, Dr. T. Woldai (ITC)**
Opening Page	Observer	**Dr. J.B.de Smeth** (Programme Director)	-
i	Abstract P2L7	"downstream dilution **to** derive"	-
10	Section 2.4.1 P1L3	"oven-dried overnight at **50 ^{0}C**"	-
10	Section 2.4.1 P1L4	"minus **-80 mesh was** then"	-
36	Section 4.3 P1L3	"(i.e. **0-80, and 80-100**)".	-
47	Section 5.2 P1L2	"Ashanti Belt (See Section **2.3**)"	-

Note!

- P means Paragraph
- L means Line

Classification of Birimian Gold Occurrences Using their Geological and Geochemical Attributes: Case Study in South Ashanti Belt, Ghana

by

Seidu Alidu

Thesis submitted to the International Institute for Geo-information Science and Earth Observation in partial fulfillment of the requirements for the degree of Master of Science in Geo-information Science and Earth Observation, Specialisation: **Earth Resources Exploration**.

Supervisors:
Dr. E.J.M. Carranza
Drs. J.B. de Smeth

Thesis Assessment Board
Prof. Dr. F.D. van der Meer (Chairman)
Prof. Dr. S.B. Kroonenberg (External)
Dr. E.J.M. Carranza (1st Supervisor)
Drs. J.B. de Smeth (2nd Supervisor)

Observer:
Dr. P. van Dijk (Programme Director)

INTERNATIONAL INSTITUTE FOR GEO-INFORMATION SCIENCE AND EARTH OBSERVATION
ENSCHEDE, THE NETHERLANDS

Disclaimer

Abstract

This research study has two main objectives. First, to determine mesothermal gold deposits occurrences in the South Ashanti Belt having spatially similar geochemical and geological attributes. Second, to determine whether a training set of spatially similar gold deposit occurrences result in a better predictive model of gold deposit prospectivity than a training set of randomly selected gold deposit occurrences.

The first research objective was achieved in the following way. Multi-element geochemical attributes at locations of the known gold deposit occurrences were determined from stream sediment geochemical data, which was performed in the following way 2-step catchment basin analysis. First, influence of lithology and scavenging by Fe and Mn oxides were removed from the uni-element geochemical data by way of multiple regression analysis in order to derive uni-element geochemical residuals. Second, the uni-element geochemical residuals were corrected for effects of downstream dilution o derive uni-element dilution-corrected geochemical residuals. Two types of geological attributes were considered at locations of the known gold deposits occurrences: (1) proximity to faults/fractures; and (2) proximity to greenstone lithologies. The uni-element dilution-corrected residuals and the geological attributes at locations of the known gold deposit occurrences were then subjected to principal components (PC) analysis to derive principal component scores reflecting anomalous surficial multi-element geochemical and geological associations at those locations. Two PCs (PC1 and PC3) were considered to reflect surficial geochemical-geological associations at the locations of known gold deposit occurrences. A scatter plot of PC1 scores versus PC3 scores reveals that 26 out of the 31 gold deposit occurrences have spatially similar surficial geochemical-attributes.

The second research objective was achieved in the following way. The 26 gold deposit occurrences with spatially similar geochemical-geological attributes were used as a training set in weights-of-evidence modelling to derive a predictive map of gold deposit prospectivity. Predictor maps used include the PC1 scores, proximity to faults/fractures, proximity to greenstone lithologies, and proximity to granitoid intrusives. A set of randomly selected gold deposit occurrences was also used in weights-of-evidence modelling to derive another predictive map of gold deposit prospectivity. The results of predictive mapping by way of weights-of-evidence modelling indicate that the gold deposit prospectivity map derived from the training set of gold deposit occurrences with spatially similar geochemical-geological attributes is better than the prospectivity map derived from the training set of randomly selected gold deposit occurrences.

The overall results of this study show (a) the usefulness of stream sediment geochemical data for re-classification of mineral deposit occurrences to be used as training data in predictive mapping of mineral prospectivity and (b) the usefulness of spatial data integration in mineral prospectivity mapping.

Acknowledgements

I wish to express my profound gratitude to the International Institute for Geo-Information Science and Earth Observation (ITC) for providing me with the fellowship to study in this unique institution. My special thanks also to Ghana Geological Survey for allowing me to study abroad.

I am greatly indebted to Dr. John Carranza my first supervisor for his invaluable suggestions, and critical reviews of the manuscripts without which the quality of this research study would not have reached its present state. However, errors and limitations of this study are due to my stubbornness.

My special thanks go to Drs Boudewijn de Smeth my second supervisor and tutor. I would like to thank you for the critical review of my manuscript and guidance during my stay in the Netherlands. Thanks very much for your support throughout the course. I would also like to thank Dr. Simon Vriend for his help and suggestions in this research work.

I would like to express my deep and sincere gratitude to Mr. Emmanuel Owusu for the data for this research. I also thank you very much for the help, advice, suggestions and words of encouragement you gave me throughout my course at ITC.

My sincere thanks go to Dr. Ernst Schetselaar, Drs. Frank Ruitenbeek, Prof. Dr. Freek Van der Meer, Dr. Tseshai Woldai, and Dr Paul Van Dijk (Programme Director). I am also grateful to all the staff of ESA department.

I thank my fellow course mates Gabriel Data (Uganda), Sisay Ayalew (Ethiopia), Md Shajahan (Bangladesh), Waew, Apuntre, Saownee (The Thai Ladies), Maria (Venezuela), Martin Rojas (Costa Rica), Amare, Ephraim, Sahle (Ethiopian brothers) and Shreekamal (Nepal) for your assistance and company during the period of study.

Thanks to the Ghanaian student community of Enschede, especially to Abdul Hanan Abu Iddrisu, Mathew Boafo, Eric Mensah Ocantey, Leslie Pobee, Michael Aduah, and Regina Brown-Mensah.

To the ITC Muslim community, I say thanks for the spiritual support.

I am greatly indebted to my parents and siblings for their encouragement, prayer and support throughout the course. If this has been an achievement it is for you.

Above all, I thank the Almighty God for granting me the strength and wisdom, without his will all these would not have been possible.

February, 2007
Enschede, The Netherlands

Table of contents

List of figures

List of tables

Chapter 1: Introduction

1.1. Background to research

Classification of mineral deposit occurrences is important, because they are never identical, and sometimes one deposit-type may include a range of variation (Cox, 1983). Each deposit-type can be represented by an idealized mineral deposit model, one that has all the typical characteristics of the group (Bonham-Carter, 1994). Mineral deposit classification involves characterization and grouping of mineral deposits according to the attributes or features they exhibit. The traditional way of mineral deposit classification is based largely on geologic characteristics of mineral deposits such as their gangue and ore mineralogy, host rock lithology, wall rock alteration, timing, and depth of ore formation, as well as geologic settings. The conventional way of mineral deposit classification has evolved into mineral deposit models, which classify mineral deposit not only on the basis of their geologic characteristics but also their geochemical characteristics and the genetic processes by which they form (Cox and Singer, 1992). Boyle (1979) classified gold deposits based on their geologic and geochemical settings and characteristics, and stated that classification of gold deposits based on their geologic and geochemical settings is much more valuable than if based on their origin be it magmatic, hydrothermal, sedimentary, or otherwise.

Classification of mineral deposit occurrences is essential to mineral prospectivity mapping, because only one type of mineral deposit occurrences should be used in the analysis. Knowledge about the spatial distribution and spatial association of mineral deposit occurrences of the type sought with certain geochemical anomalies and certain geological features is essential to mineral prospectivity mapping. A-priori knowledge of the geological-geochemical characteristics of known mineral deposit occurrences of the type sought is therefore essential in predictive modelling of exploration targets.

1.2. Research problem definition

In many areas in developing countries where mineral resource development is a major contributor to national economy, the a-priori knowledge of mineral deposits is mainly about the metal commodity (e.g., gold) but the deposit types are not fairly well known because the main focus is on metal extraction and not on mineral deposit studies. This situation constitutes a problem in predictive modelling of new exploration targets.

In this study, it is hypothesized that analysis of stream sediment multi-element geochemical data could provide an additional value to mineral deposit classification. The justification for this hypothesis is that chemical elements can be leached from rocks and mineral deposits, and then transported into streams by clastic and hydromorphic dispersion processes. Therefore, anomalous geochemical signatures that can be defined from stream sediment multi-element geochemical data should reflect the types of mineral deposits present in a study area. It is hypothesized further that mineral deposits situated in zones with the same or similar anomalous geochemical signature probably belong to the same type of deposits. In addition, a group of mineral deposit occurrences situated in zones with similar geological attributes and stream sediment geochemical signature are more likely to represent the same type of deposits.

1.3. Research questions

The study seeks to answer the following questions:

- Are the different major types of gold deposits in the study area reflected by stream sediment geochemical data?
- Do spatial distributions of stream sediment geochemical data portray spatial distributions of lithologic units depicted in a published geological map?
- How can different types of gold deposits be classified based on their geological attributes and geochemical signature at their locations?

- How does mineral prospectivity map derived from a training set of mineral deposit occurrences with similar geological attributes and geochemical signatures compare with that derived from a training set of randomly selected mineral deposit occurrences?

1.4. Research objectives

The objectives of this research are as follows:

- To derive training set(s) of gold deposit occurrences in the South Ashanti Belt, Ghana, with similar geological attributes and geochemical signature.
- To compare results of mineral prospectivity mapping based on a training set of mineral deposit occurrences with similar geological attributes and geochemical signatures and based on a training set of randomly selected mineral deposit occurrences.

1.5. Research methodology

The South Ashanti Belt in Ghana is selected as the test area for the research hypothesis and related questions, because of controversy about classification of the gold deposits there. The flow chart of the main research methodologies followed in this research is shown in Figure 1.1.

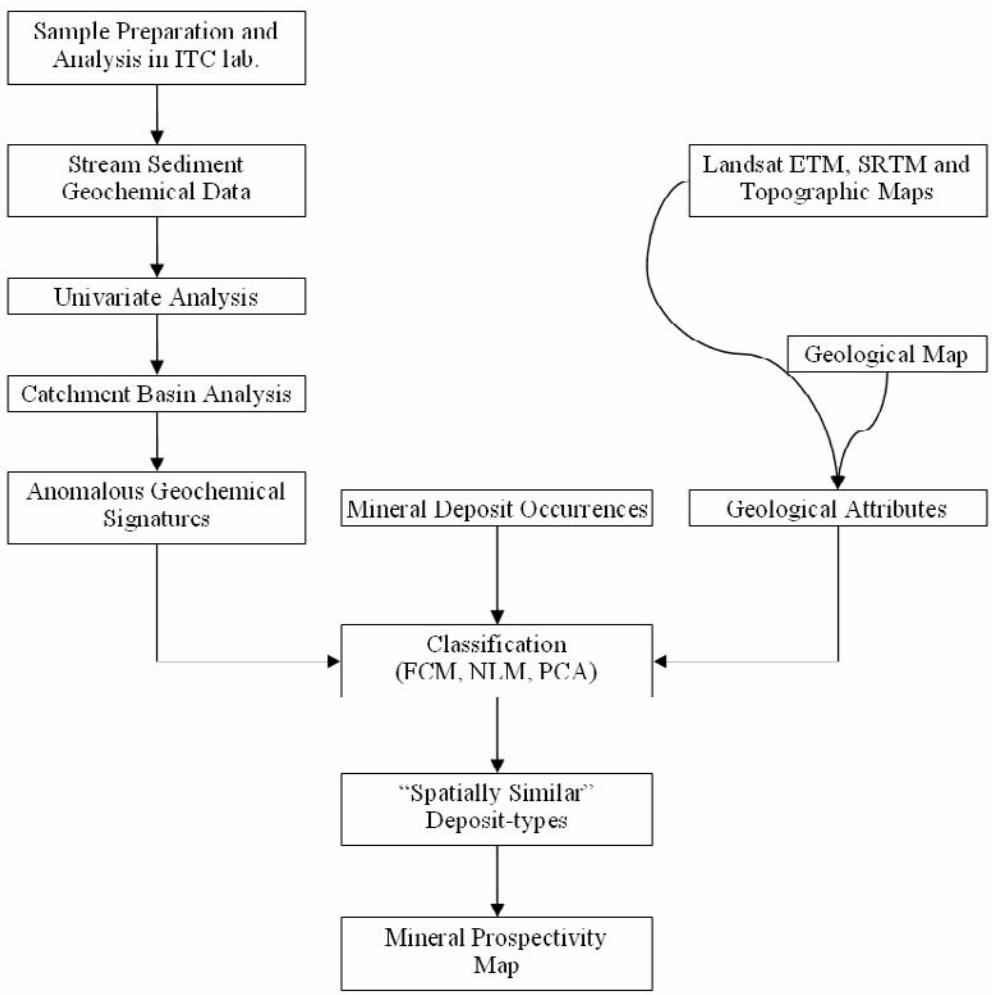

Figure 1.1: Flow chart of methodology for geochemical-geological attribute classification of mineral deposits.

1.5.1. Geochemical data analysis

Geochemical data from 405 stream sediment samples were obtained by ICP-OES determinations for Cu, Pb, Zn, Ag, As, Mn, Fe, Ni, Cr, Co, Li, Ca, V, Mo, Cd, Sb, Sr, and Ba at the ITC laboratory.

The samples had already been analysed for Au in Ghana. Frequency distribution, histograms, and cumulative frequency plots were used to define populations present, after which the catchment basin approach was used in modelling of geochemical anomalies.

1.5.2. Classification of mineral deposits

Derived geochemical residuals and geologic attributes at deposit locations are used as inputs to principal component (PC) analysis for classification of gold occurrences. The analysis aims at determining inherent element associations in the structure of the correlation matrix into a number of de-correlated PCs or groups of elements that together account for the total variability of the original data.

1.5.3. Mineral prospectivity mapping

Deposit recognition criteria (DRC) or indicative geological features of mineral deposits were defined according to established models of the deposit-class under study. Maps representing DRC were used as predictor variables and map of deposit occurrences with similar geological attributes and geochemical anomalies was used as target variable in mineral prospectivity mapping. A map of randomly selected mineral deposit occurrences was also created and used as training data (target variable) to create another mineral prospectivity map.

1.6. Datasets

Available datasets used in this study are:

- Locations of gold deposit occurrences
- Geological map (1:250, 000)
- Geochemical data from 405 stream sediment samples analyzed for 18 elements
- Shuttle Radar Topography Mission (SRTM) imagery
- Topographic map

1.6.1. SRTM data

The SRTM image was used to delineate lineaments and faults. Faults and fractures serve as conduit for mineralized fluids, and are therefore important indicative geological features for mineral prospectivity mapping.

1.6.2. Topographic data

The drainage networks in the topographic map were digitized and subsequently used for the generation of stream sediment sample catchment basins.

1.6.3. Geological map

Data from hardcopy geological map were scanned and the resulting scanned raster formats were digitized to capture lithological contacts, and faults/fractures.

1.6.4. Locations of gold deposit occurrences

At locations of known gold deposit occurrences, geochemical anomalies and geological attributes (e.g., distance to faults, etc.) were extracted and used as input data in the classification analysis.

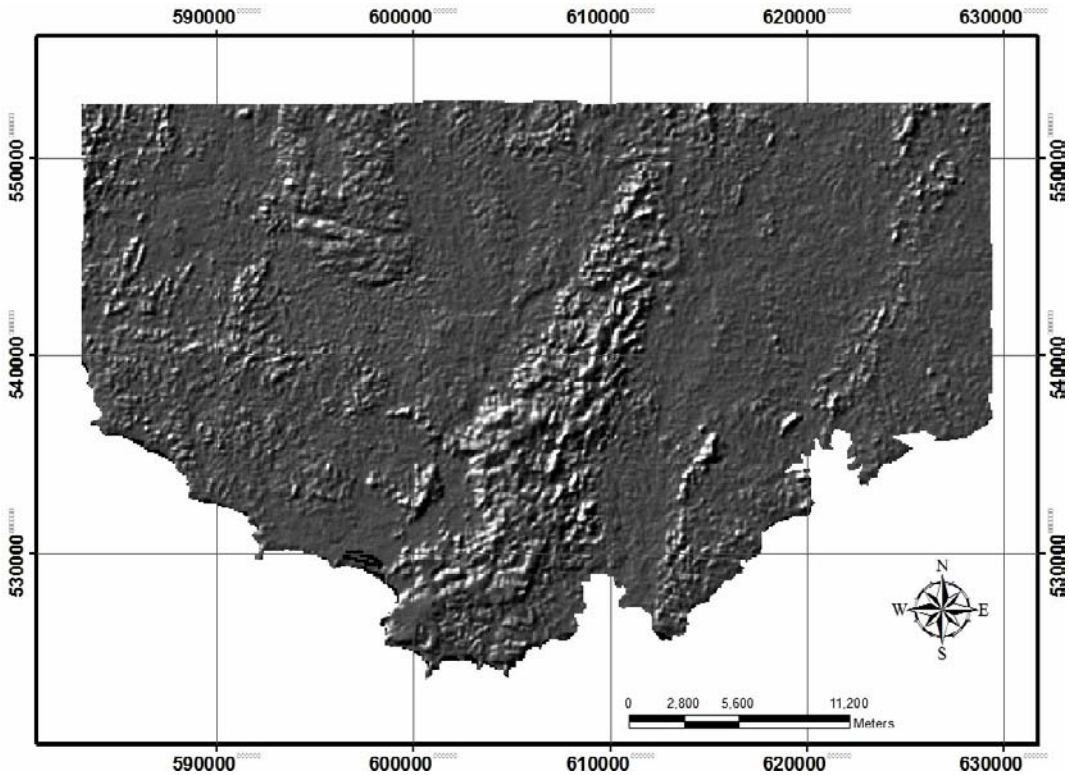

Figure 1.2: SRTM image of the study area.

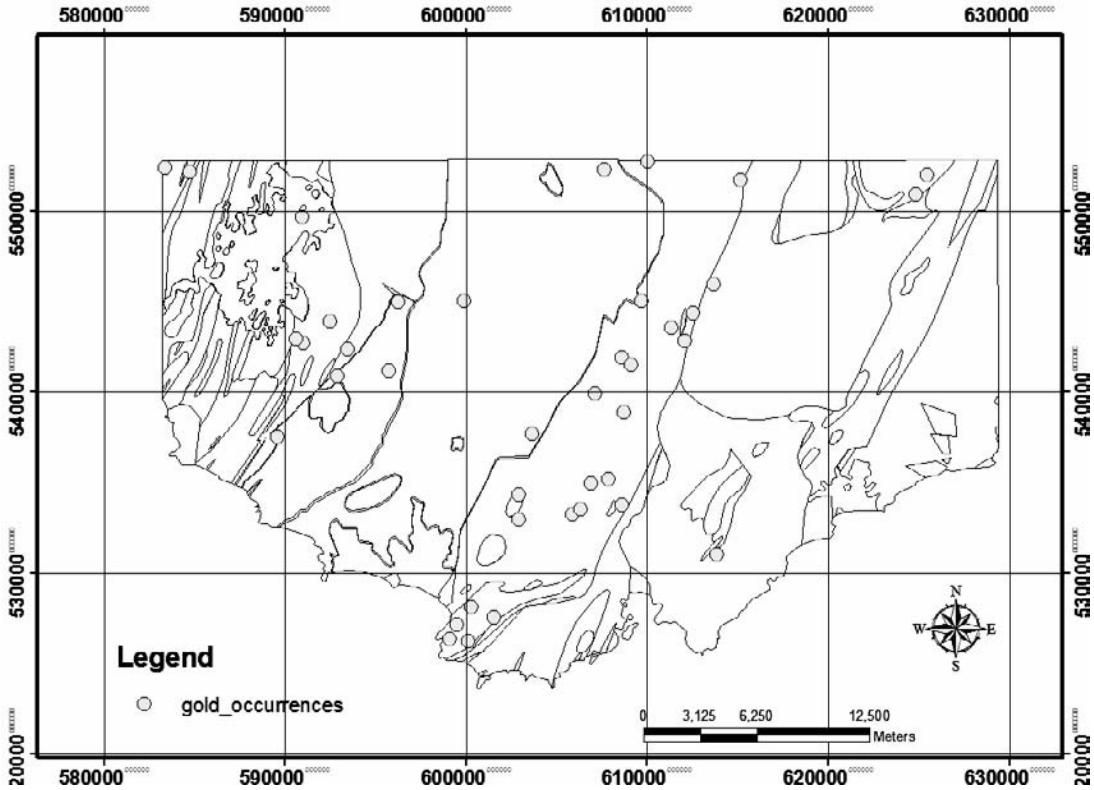

Figure 1.3: Locations of gold deposit occurrences

1.7. Software

The different types of software used in this research were as follows:

- ArcGIS 9.2 - for digitizing and editing of geological map
- ILWIS 3.1 - for generation of catchment basins and for analysis to derive residuals from the geochemical data
- R - for descriptive statistical analysis
- EXCEL - for generating histogram, and cumulative frequency
- ERDAS 8.2

1.8. Thesis outline

The thesis is organised into seven chapters, with a list of references and appendices at the end of the thesis. Chapter 2 describes the regional and local geology of the study area with respect to its mineralisation and geochemical characteristics. Chapter 3 describes univariate analysis of the geochemical data to define populations, as per geological terrains. In Chapter 4, the analysis of geochemical data using catchment basin method to derive residuals is described and discussed. Chapter 5 is concerned with classification of gold deposit occurrences using PCA. Chapter 6 discusses mineral prospectivity mapping. The deposit recognition criteria are defined based on an established model of the deposit class under study. Spatial association analysis is described for derivation of predictor maps, which are integrated to generate prospectivity maps. Chapter 7 presents major conclusions of the study and provides recommendations.

Chapter 2: The Study Area

The study area is located in the southwestern part of Ghana. It is situated within UTM coordinates 525000N to 555000N and 584000E to 620000E, covering an area of 1,080 sq. km (Figure 2.1). The local physiography of the area is controlled by the NE-SW geologic trend and consists of narrow valleys and ridges. Local elevations are generally in the range of 50 to 90 m.

2.1. Regional geology and mineralisation

Five parallel, approximately evenly spaced, volcanic gold belts, consisting of mainly low grade metamorphic, tholeiitic lavas (MORB chemistry), characterize the Birimian Supergroup of Ghana (Leube et al., 1990). Volcanoclastic sediments occur interbedded within the basaltic flows of all volcanic belts. The belts are separated by basins containing isoclinally folded wackes, argillitic sediments, and granitoids (Figure 2.1). A chemical facies (chert, Mn-rich rock, Ca-Fe-Mg carbonates, carbon-rich rock, sulphide-rich rock) predominantly occurs at the transition zone between belt volcanics and basin sediments.

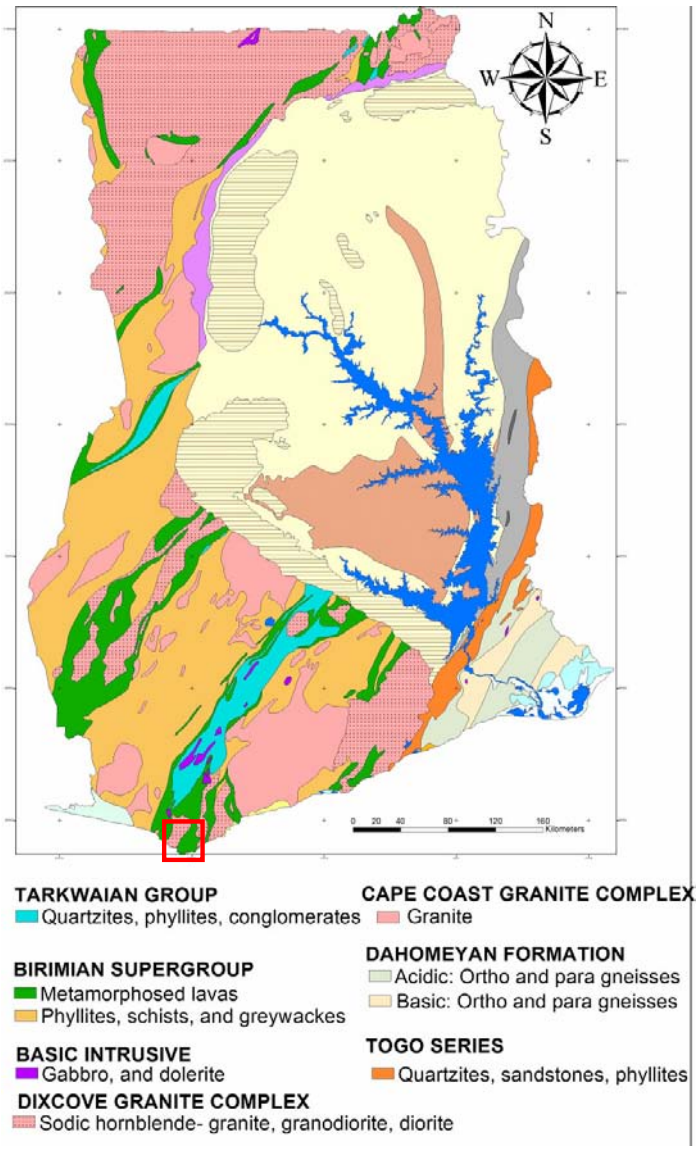

Figure 2.1: Geological map of Ghana (Ghana Geological Survey, 1996). The study area is in red box.

On a regional scale, the vast majority of the Birimian gold deposits occur along the flanks of the volcanics. Mesothermal gold deposits occurrences in the Birimian of Ghana are of two (2) major types, the disseminated–sulphide type (DST), and the quartz vein type (QVT) (Leube et al., 1990). According to Leube et al. (1990), the major differences between DST and QVT with respect to their ore mineralogy are: QVT contain visible 'free gold', whereas DST carries gold largely as submicroscopic inclusions in sulphides. The Ashanti belt is the most outstanding of all the volcanic (greenstone) gold belts in Ghana. This is due largely to the fact that it is host to the major gold mines in the country.

2.2. Geology of the study area

The study area forms part of the South Ashanti Belt, and features wide varieties of lithologies, structures, and types of gold occurrences. It is underlain mainly by Birimian metavolcanics, volcanoclastics, and granitoids (Figure 2.2).

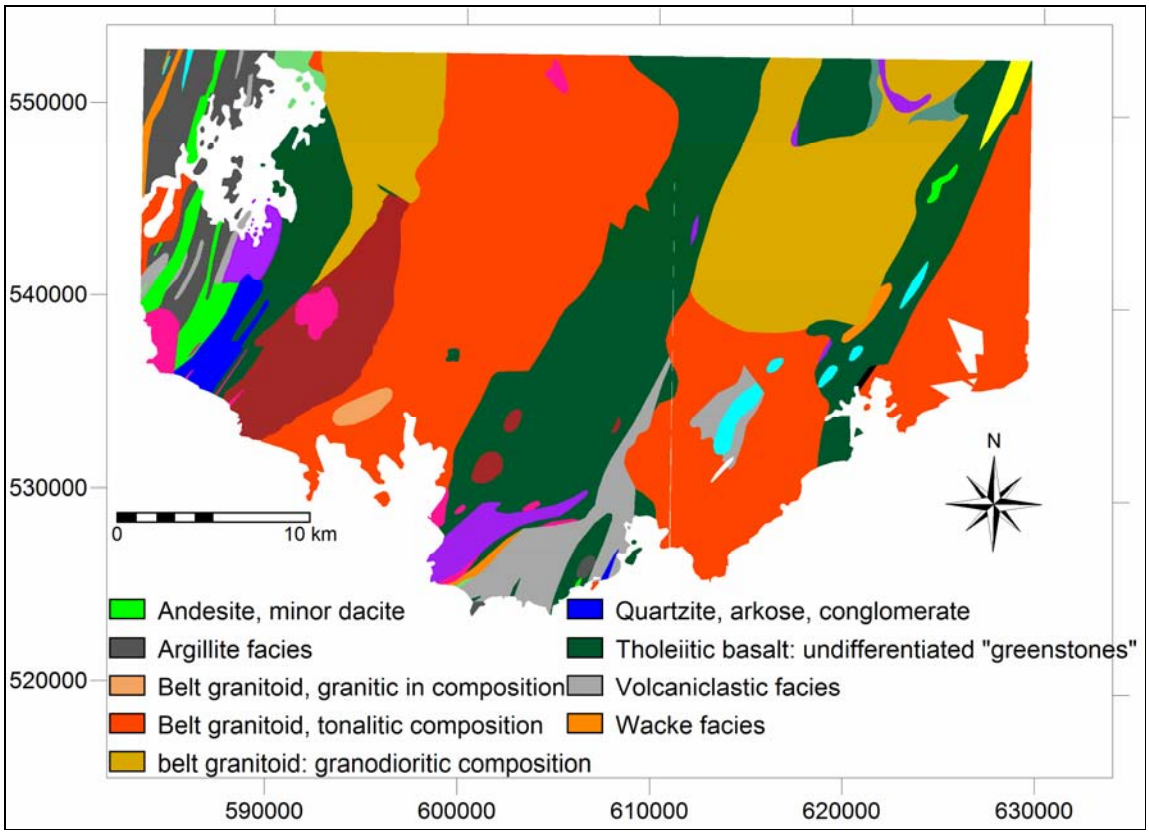

Figure 2.2: Geological map of South Ashanti Belt (after Loh et al., 1996)

2.2.1. Birimian metavolcanics ("greenstones")

The Birimian metavolcanics in the South Ashanti Belt are composed of tholeiitic basalts, which are generally massive but in some places display pillow lava structures. Sylvester et al. (1992) noted that in some areas within the South Ashanti Belt, there are indications of units with calc-alkaline felsic volcanics. Other rock units of Birimian metavolcanics within the study area include andesites, dacites, and few rhyolitic rocks. The rock units show a general NNE-SSW trend. They are composed of fine- to medium-grained pyrite, sericite, and carbonate, chlorite, epidote, and quartz as accessory minerals. As opposed to belt granitoids, chemical sediments and metasedimentary terrains, which tend to produce relatively flat topography, greenstones in the study area form ridges.

2.2.2. Metasediments and chemical sediments

The transition zone between greenstones and basin sediments are characterized by a variety of chemical sedimentary rocks. The chemical sedimentary rocks are cherts, manganiferous, sediments, Fe-Mg-Ca carbonates, and sulphide bearing sediments. "Corridors" characterized by the above chemical sediments frequently follow the margins of the volcanic belts and may attain several hundreds of kilometers wide. The belt-basin transition on the western flank of the study area is marked by lenses of chert NW of Asanta village, manganiferous argillites near Salman village, and the widespread presence of disseminated sulphide. The last is expressed as elevated arsenic content in soils in the area (Bartholomew, 1961).

2.2.3. Volcanoclastics and ultramafic rocks

Volcanoclastics in the study area consist of chloritised glass fragments; sand-to silt-sized, partly reworked pyroclastics (Leube et al., 1990). Further southeast, volcanoclastic and metavolcanic units occur interbedded with marine clastics that include numerous horizons of manganese-rich chemical sediments. Along the coast, metavolcanics have been intruded by ultramafic rocks of varying composition from peridotite to pyroxenite and dunite (Loh et al., 1996). There are abundant sills and feeder dikes with a common affinity to tholeiitic basalts.

2.2.4. Belt-type granitoids

In between the volcanic bands, there are extensive batholiths of belt-type intrusive complexes. The belt-type intrusive complexes are dominantly granodiorite in composition but in some phases are characterized by high radiometric potassium content (Griffis, 1998). Unlike the basin-type granitoids, which are intensely foliated, the belt-type granitoids in this study area rarely show any evidence of foliation, even near the contacts with volcanic rocks.

2.2.5. Gabbro

Gabbro makes up only a minor part of the suite of intrusive rocks in the South Ashanti Belt. Gabbro intrudes metasediments and chemical sedimentary facies located west of the study area. Gabbroic rocks associated with Akitekyi ultramafic complex occur intermittently alongside the outer flanks of the complex.

2.3. Gold mineralisation in the study area

Gold deposit occurrences in the study area are mesothermal auriferous arsenopyrite, and quartz vein mineralization (i.e. both DST and QVT). These gold deposit occurrences feature disseminated sulphides in which pyrite and arsenopyrite host important amounts of gold. They also feature extensive quartz veining and stockwork systems in which visible gold is quite common. Auriferous quartz veins and lenses in sheared fissure zones are filled with black lustrous graphitic material.

The mineral assemblage in either DST or QVT gold deposit occurrences is essentially a gold-sulphide association (Dzigbodi-Adjimah, 1993). The main sulphide minerals include pyrite, arsenopyrite, sphalerite, chalcopyrite, and minor galena. Mineralogical and geochemical studies conducted by Dzigbodi-Adjimah (1991) along a Birimian ore channel at the Prestea goldfields shows that metavolcanic rocks contain higher amounts of Mn, As, Cr, and Sb. Auriferous quartz veins contain high trace element contents of Zn, Pb, Cu, Fe, As, Sb, and Cd, whereas non-gold containing quartz veins have low contents of these elements. Mineralogical and chemical studies in the Ashanti Belt (Amanor et al., 1991) indicate high correlation of Ag, As, Zn, Cu, Pb, Ni, Sb, and Cr, with gold. These elements could be considered as pathfinder elements. They also reported that graphitic zones occur as loci for gold-quartz veins and that methane/propane ratio correlate very well with gold and could be used as pathfinders.

The most favoured host rocks of gold deposits in the study area are metavolcanics and volcanoclastic units. Milesi (1989) recognized that these lithologic units are largely confined to the 'tectonic corridors' that display complex, multi-phase structural features, which control the mineralization. These tectonic corridors are typically concentrated along the margins of various Birimian metavolcanic belts and adjacent metasedimentary basins.

2.4. Stream sediment geochemical data

A total of 405 stream sediment samples at a sampling density of 1 sample per 1.0 km^2 were collected from 1st, 2nd, and 3rd order streams at sites above the confluence as in the areas shown in Figure 2.3. As much as possible, sediments from as near the centre of the streams were collected to avoid sampling bank-slip material. On-the-spot descriptions of the samples including soil type, colour, texture, were recorded. GPS readings were also taken to determine accurate locations of sampling sites. Each stream sediment sample comprises materials taken from a 2-m radius and then made into a composite. The stream sediment samples were wet-sieved over -75 µm mesh in order to standardize the material, before 200-300 g of the samples was filled into pre-labelled plastic bags. At the field camp, the samples were sun-dried.

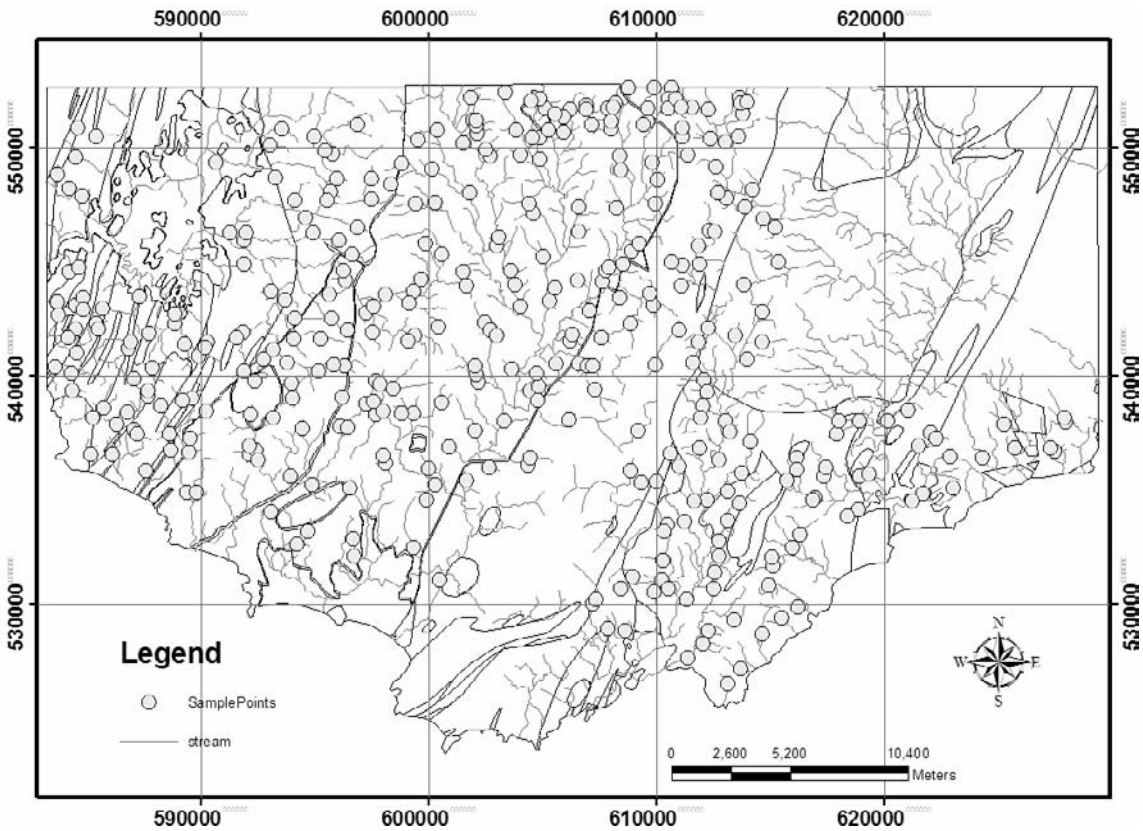

Figure 2.3: Locations of stream sediment sampling sites in the study area.

2.4.1. Chemical analysis

The procedures established by the Forum of European Geological Surveys (FOREGS) were followed during field sampling and chemical analysis of the samples in order to ensure maximum quality geochemical data. The stream sediment samples were oven-dried overnight at 500ºC at the ITC laboratory prior to sample decomposition. Sample fraction of minus -80 mesh (<75 µm) was then collected for subsequent chemical analysis. For each sample, 500 mg of -80 mesh fraction was placed in a test tube, and was decomposed by adding 2 ml acid mixture of HCl, HNO_3 and water. For assessment of precision and accuracy of the laboratory procedures, randomly selected replicate samples some analytical standards were included in a batch of samples and treated exactly the same as original samples. Each sample was then homogenized by shaking on a vortex shaker and then a batch of samples was placed in a shaking hot water bath at 80ºC for 3 hours. After digestion, the samples were diluted to 10 ml using distilled water and then homogenized again. To finally prepare element determination, residues in the sample solution were allowed to settle, after which the liquid portion of the solutions were decanted into new test tubes cocked with a stopper. Multi-element determinations

from the prepared sample solutions were carried out using inductively coupled plasma-optical emission spectrometry (ICP-OES). The sample solutions were aspirated into the ICP-OES instrument where the elemental emission signal is measured for Cu, Pb, Zn, Ni, Cr, Co, V, Mn, Fe, Cd, Ag, As, Sb, Mo, Ba, Li, Ca and Sr. The stream sediment samples had already been analysed for Au in a laboratory in Ghana.

2.4.2. Quality assessment

It is critical to assess the quality of the geochemical data before they are used for analysis and interpretation. Geological-geochemical characteristics of gold deposit occurrences can be masked by substantial errors from the data collection and laboratory procedures. Substantial procedural errors can also cause variations in the geochemical data other than variation due to geology or geochemical processes. The quality of the data will be assessed using scatter plots, 10% precision plots (Thompson et al., 1978) and by performing analysis of variance (ANOVA) on 12 duplicate samples.

2.4.2.1. Scatter plots of duplicate analyses

Scatter plots of the duplicate analyses provide a graphical display of the sample pairs in relation to an ideal 45º line. Deviation of the scatter plots from the 45º line (Figure 2.4) was the criterion used to determine the quality of the geochemical data. The results show that analytical data for all the elements is satisfactory except for Li, Sb, and As.

Figure 2.4: Scatter plots of duplicate chemical analyses.

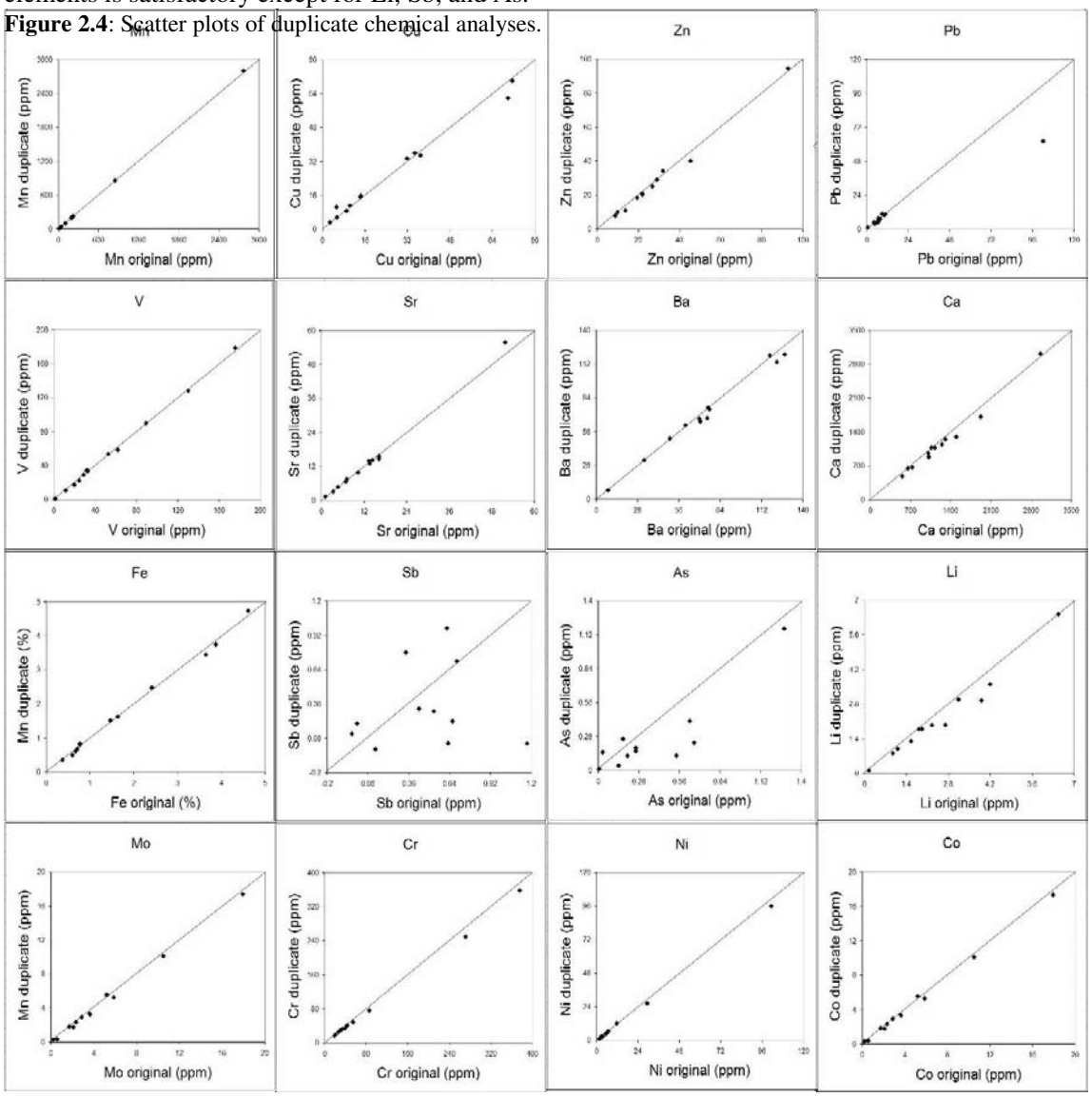

2.4.2.2. Thompson-Howarth precision plots

The precision (P) of an analytical method at a 95% confidence level is defined by (Thompson, 1983) as

$$P=(2S_c/C)*100\%$$

where S_c is the standard deviation of the range of elements concentrations and C is the mean of the range of element concentration of the duplicate samples.

Quantitative information on precision can be obtained from duplicate analyses. In this research, 12 samples have duplicate analyses. The absolute difference $|x_1-x_2|$ between pairs of duplicate element determinations (x_1, x_2) were plotted as a function of mean concentration [i.e., $(x_1+x_2)/2$] on a Thompson-Howarth 10% precision control chart (Thompson and Howarth, 1978). On such a chart (Figure 2.5), the 90th and 99th percentiles of absolute difference between duplicate measurements as a function of mean concentration (assuming a normal distribution of error) have been drawn as the lower and upper diagonal lines, respectively. If 90% or more of the points falls below the 99th percentile, then the duplicate analytical data has 10% precision or better. Thus, the higher the proportion of points that falls below the 90th and 99th percentile lines, the better the precision; the lower the proportion of points that falls below the lines, the worse the precision.

The plots in Figure 2.5 show that precision of analytical data for Fe, Sr, Co, V, and Ba is better than 10%. The precision of analytical data for Cu, Zn, Cr, and Ca is approximately 10%. Results of assessment of analytical data using the 10% precision control chart are summarized in Table 2.1.

Table 2.1: Quality of analytical data based on 10% precision model by Thompson and Howarth (1978).

Element	% of points below the 90th percentile line	% of points below the 99th percentile line	Assessed precision
Fe	91	100	Better than 10%
Mn	73	82	Worse than 10%
Cu	75	92	Approx. 10%
Zn	83	92	Approx. 10%
Pb	38	54	Worse than 10%
As	30	30	Worse than 10%
Sb	27	27	Worse than 10%
Mo	75	83	Worse than 10%
Cr	82	100	Approx. 10%
Ni	55	83	Worse than 10%
Co	91	100	Better than 10%
V	91	100	Better than 10%
Sr	91	100	Better than 10%
Li	42	75	Worse than 10%
Ba	91	100	Better than 10%
Ca	67	100	Approx. 10%

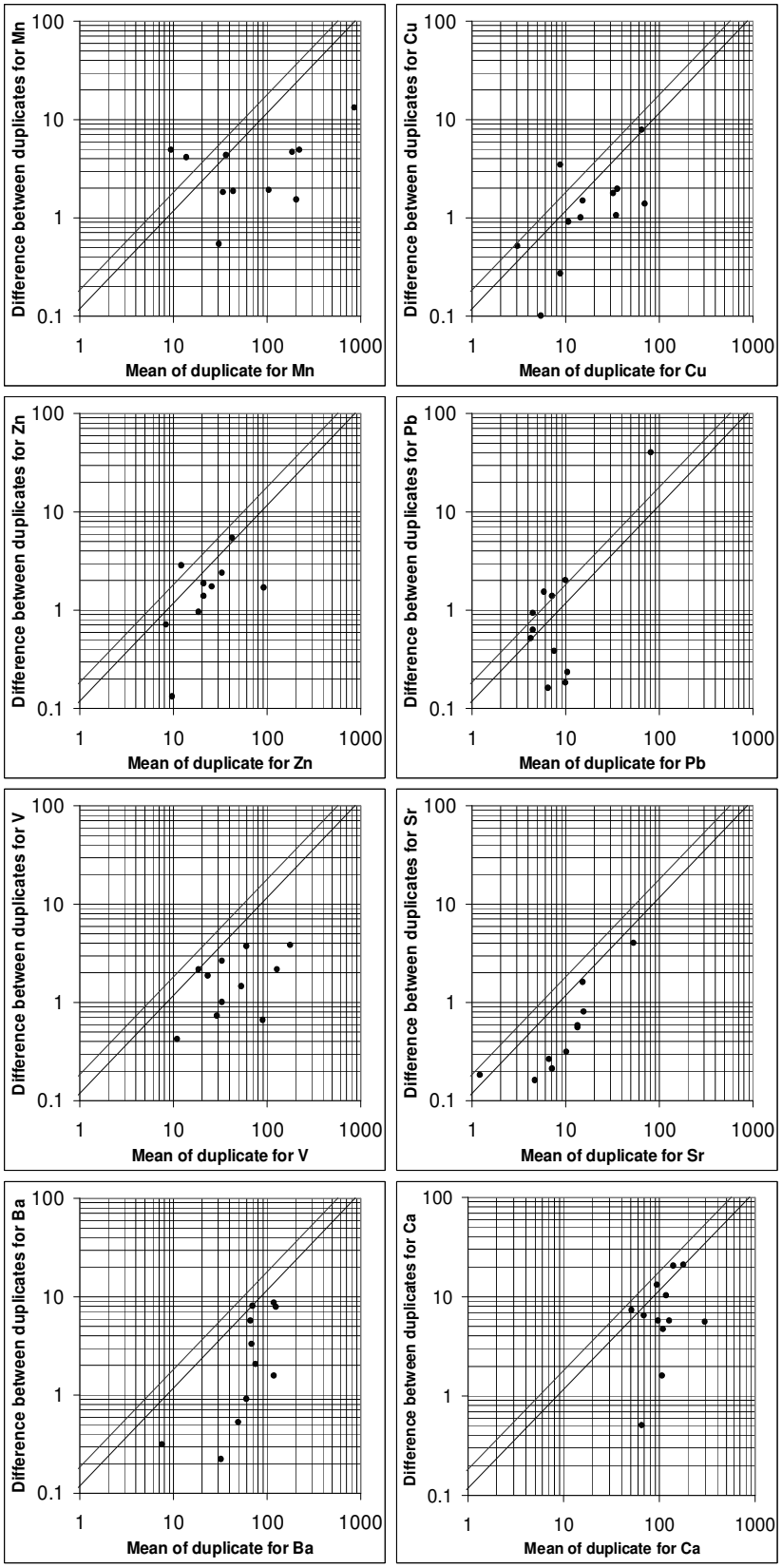

Figure 2.5: Differences and means of duplicate analysis plotted on a 10% precision model control chart by Thompson and Howarth (1978). Upper and lower diagonal lines are 99th and 90th percentiles, respectively.

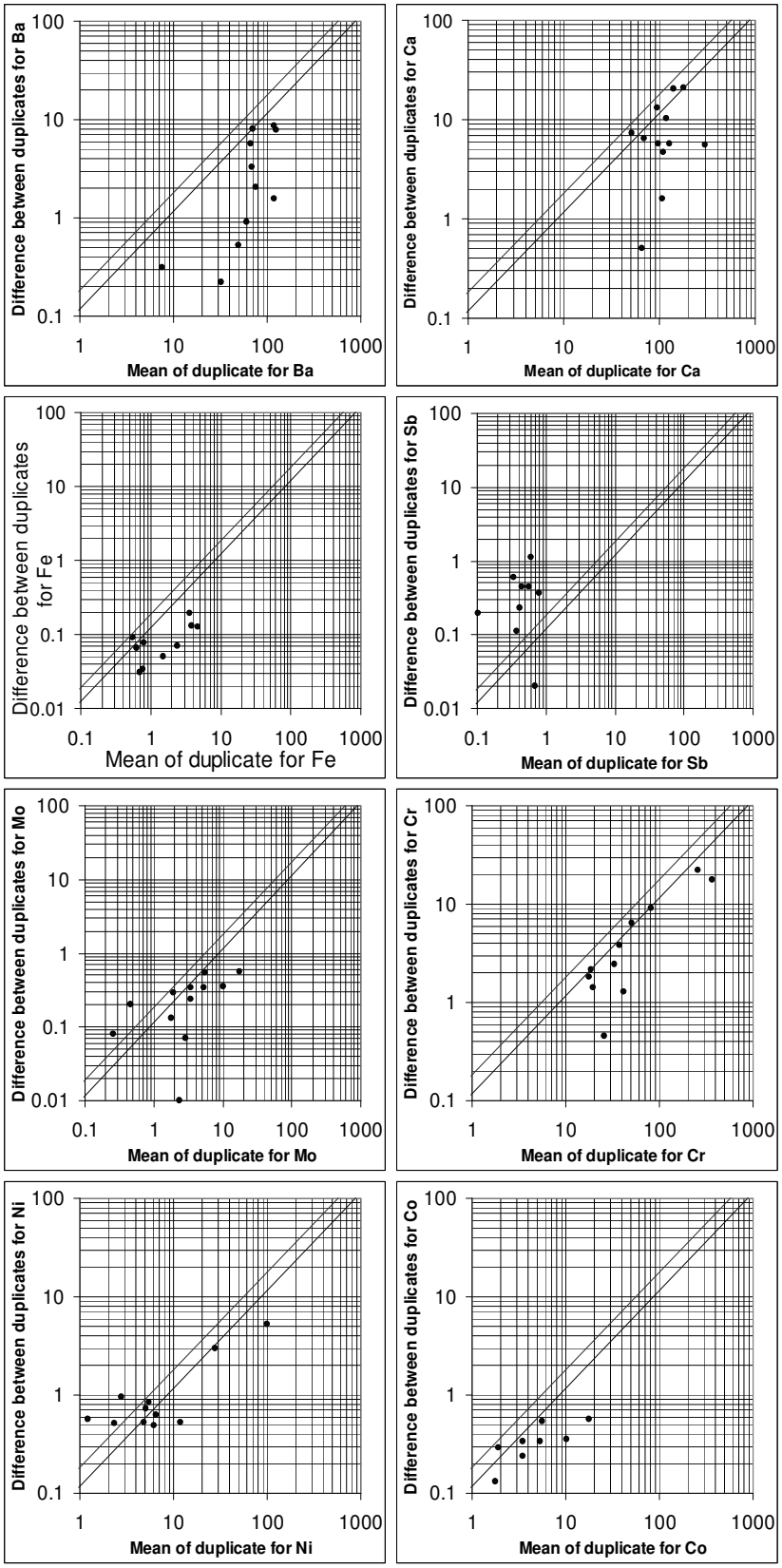

Figure 2.5: Continuation

2.4.2.3. Analysis of variance

It is critical that all variations in a geochemical data resulting from analytical errors (analytical variance, δ_a^2) be quantified and separated from the true geochemical patterns (geochemical variance, δ_g^2). A properly constituted suite of sampling and analytical duplicates can be decomposed into its sampling, analytical, and geochemical components by analysis of variance (ANOVA). The duplicate element determinations were analysed using a simple nested one-way ANOVA method (Ramsey et al., 1992). The analysis allows decomposition of the total variance of duplicate sample measurements into variance due to procedural errors and variance due to geochemical behavior of the population in the study area. This analysis thus aims to obtain confidence that should be placed in the interpretation of the geochemical data.

In the simple nested one-way ANOVA method followed, the total variance (δ_t^2) can be described by the following relationship:

$$(\delta_t^2)=(\delta_g^2)+(\delta_a^2).$$

Because the duplicate samples are a subset of the whole data set, the equation is better written as:

$$MS_t=MS_g+MS_a$$

where *MS* is the mean squares, which are estimated from the corresponding sum of squares (*SS*) and calculated as follows:

$$SS_t=\sum_1^n X^2-\frac{\left(\sum_1^n X\right)^2}{n}$$

$$SS_g=\frac{\sum_1^i\left(\sum_i^j X\right)^2}{j}-\frac{\left(\sum_1^n X\right)^2}{n}$$

$$SS_a=SS_t-SS_g$$

$$MS_g=\frac{SS_g}{(i-1)}$$

$$MS_a=\frac{SS_a}{i(j-1)}$$

where: SS_t = total sum squares;
SS_g = sum of squares due to geochemical variance;
SS_a = sum of squares due to analytical variance;
MS_g = mean of squares of geochemical variance;
MS_a = mean of squares of analytical variance;
X = individual measurements of the elements concerned;
i = number of samples with duplicate measurements;
j = number of measurements for each sample (= 2)
$n = i*j$ = total number of measurements

An F-value, which is the ratio, MS_g/MS_a can be calculated to determine if the geochemical variance is greater than the analytical variance. The calculated F-value is used to determine significance of estimated variances by comparing the F-value at a selected level of significance (95% in this case) for the respective degrees of freedom (11 and 12 in this study). A critical F-value is then obtained from statistical look-up tables (e.g., Snedecor F statistical model). If the calculated F-value is greater than the critical F-value, then the "true" geochemical patterns can be properly reflected by the analytical measurements. However, if the estimated F-value is less than the critical F-value it means

that the procedural errors are significantly high so that the geochemical patterns within the study area are unrecognizable. If the geochemical and analytical variances are expressed as percentages of the total variance, and if the analytical variance does not exceed 4% of the total variance, then the geochemical data can be considered as satisfactory for geochemical mapping (Ramsey et al., 1992).

Results of the simple nested one-way ANOVA of the duplicate element determinations indicate that analytical data for most elements, except for As and Sb, are satisfactory (Table 2.2).

Table 2.2: Summary of geochemical data quality assessment based on simple nested one way ANOVA of duplicate element determinations. All elements are measured in ppm, except Fe (%).

Element	MS_g (%)	MS_a (%)	Estimated F-value	Critical F-value at α=0.05	Quality assessment
Fe	99.91	0.09	1059.9	2.7	satisfactory
Mn	99.99	0.01	19518.3	2.7	satisfactory
Pb	99.92	0.08	1212.5	2.7	satisfactory
Cu	99.66	0.34	290.8	2.7	satisfactory
As	91.66	8.34	11.0	2.7	poor
Ni	99.89	0.11	890.8	2.7	satisfactory
Co	99.90	0.10	991.7	2.7	satisfactory
V	99.96	0.04	2539.0	2.7	satisfactory
Sr	99.77	0.23	437.5	2.7	satisfactory
Li	98.54	1.46	67.6	2.7	satisfactory
Ba	99.57	0.43	231.2	2.7	satisfactory
Ca	99.36	0.64	155.6	2.7	satisfactory
Cr	99.84	0.16	632.2	2.7	satisfactory
Sb	54.34	45.66	1.2	2.7	poor
Cd	99.53	0.47	210.4	2.7	satisfactory
Zn	99.80	0.20	510.9	2.7	satisfactory
Mo	99.90	0.10	991.7	2.7	satisfactory

2.4.2.4. Summary of reliability of geochemical data

From the three methods employed (i.e., scatter plots, 10% precision plots, and ANOVA) to assess the quality of the geochemical data based on the duplicate element determinations, the following conclusions can be made. The analytical data for the following elements, Fe, Sr. Co, V, Ba, Cu, Zn, Cr, and Ca are of satisfactory quality. The quality of data for Ni, Mn, Li, Pb, As and Mo is rated intermediate, because their precision based on the 10% precision plots is not so high, but their ANOVA is satisfactory. This means that these elements can be used to characterize and classify the underlying lithology and mineral deposit occurrences.

Chapter 3: Geochemical Data Analysis

3.1. Univariate Statistical Analysis

Histograms and cumulative frequency graphs were prepared using Microsoft Excel®. The summary statistics of the untransformed analytical data (Table 3.1) indicate that all the uni-element geochemical data are positively skewed while maximum values of some of the individual elements are also very large. Each uni-element data set was therefore logarithmically transformed in order to reduce the inherent asymmetry and to enhance geochemical contrast in order to properly identify geo-information of interest in the data (Stanley, 2006).

Table 3.1: Elementary statistics of original data for 18 elements analyzed by ICP-OES and skewness of $\log_e$-transformed data. All elements measured in ppm except Au (ppb) and Fe (%).

Element	Minimum	Maximum	Mean	Median	Std Dev.	Skewness	Skewness ($\log_e$ transformed data)
Au	1.00	470	62.08	40	68.99	3.70	-0.30
Fe	0.19	17.13	2.63	1.31	3.18	2.28	0.45
Mn	0.50	9085	212.98	82	620.20	9.69	-0.91
Cu	0.27	124.20	19.20	13.90	18.50	2.10	-0.3
Pb	0.03	100.60	5.40	4.40	6.30	9.90	-1.7
As	0.01	62.42	7.20	4.20	9.20	2.90	-1.90
Cd	0.01	15.73	0.30	0.01	1.40	7.20	1.80
Mo	0.02	209.88	10.20	3.18	16.43	7.60	-0.60
Ni	0.04	272.00	18.20	6.90	34.02	3.80	0.21
Cr	3.13	1588.60	146.30	60.80	248.3	3.30	0.60
Co	0.03	169.41	8.04	2.77	17.20	5.30	0.20
V	0.84	473.53	54.41	24.20	79.56	2.70	-0.08
Ca	412	17796	1129	892	1100.50	10.34	1.64
Sr	0.31	1580.76	11.90	4.58	80.95	19.28	0.74
Ba	2.45	342.58	36.64	23.62	40.20	2.60	0.21
Li	0.11	12.03	2.23	1.40	1.77	2.43	-0.09
Zn	0.18	160.21	21.31	12.96	23.10	2.10	-0.7
Sb	0.01	3.21	0.37	0.23	0.46	2.14	-0.33

3.2. Determination and mapping of uni-element populations

Histograms, cumulative frequency graphs, and probability plots were examined to determine population groups in the uni-element data sets. For uni-element data sets that approximate a Gaussian distribution, the mean and standard deviation were used as the basis for classification of populations in the data (Rose et al., 1979). For uni-element data sets that do not approximate a Gaussian distribution, 'natural breaks' in their cumulative frequency curves were used as basis for classification of populations in the data. The populations identified in each uni-element data set are referred to as A, B, C, and so on in the order of increasing element content.

3.2.1. Nickel distribution

The bimodal character of the Ni histogram (Figure 3.1, left panel) suggests presence of at least two populations, which are separable at approximately the 90th percentile (i.e., 60.1 ppm Ni). The Ni data set is therefore divided into four populations. Population A consist of Ni values <26.5 ppm. Population B consists of Ni values ranging from 26.5 to 60.1 ppm. Population C is comprised of Ni values ranging from 60.1 to 136.4 ppm. Population D is comprised of Ni values > 136.4 ppm.

Population A is associated with belt granitoids, argillite facies, and arkose, all of which are located western half of the study area. Zones bordering basaltic rocks and granitoids are characterized by population B, whereas areas underlain mainly by gabbro are characterized by population C. Population D occurs in very few sample catchment basins, which are underlain by basalts (Figure 3.2).

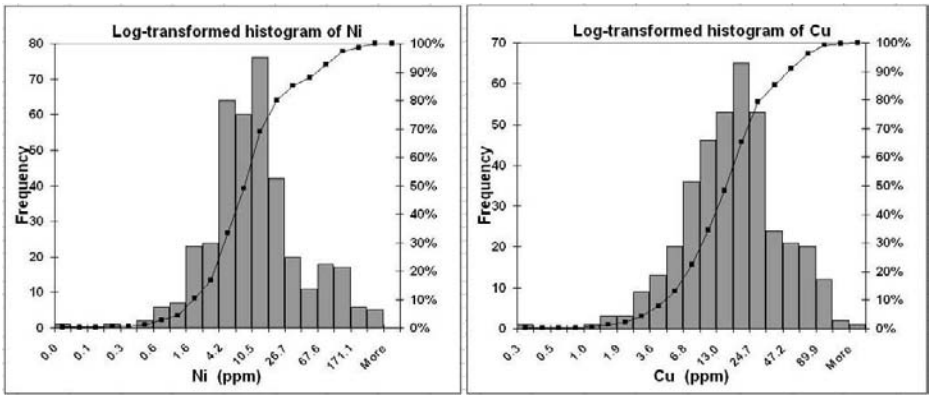

Figure 3.1: Histograms and cumulative frequency curves of $\log_e$-transformed Ni data (left panel) and $\log_e$-transformed Cu data (right panel).

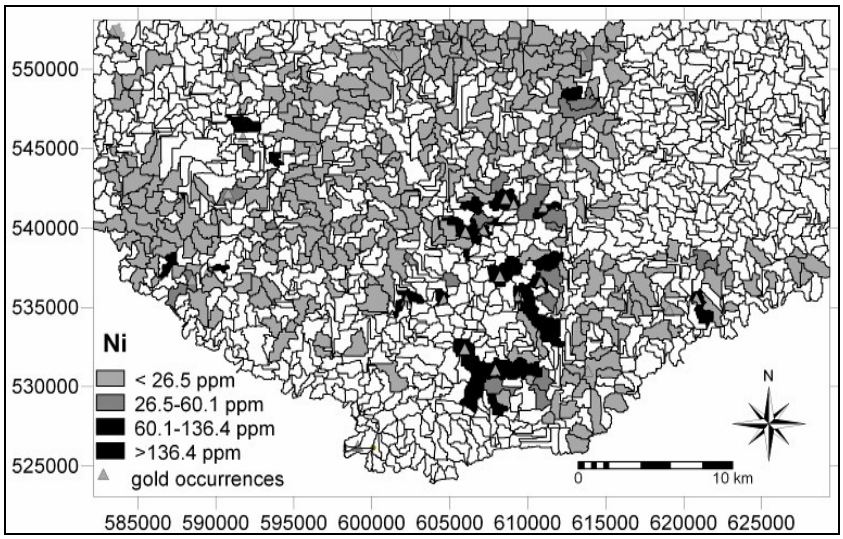

Figure 3.2: Spatial distribution of the Ni stream sediment data in the study area. Grey triangles are locations of known gold deposit occurrences.

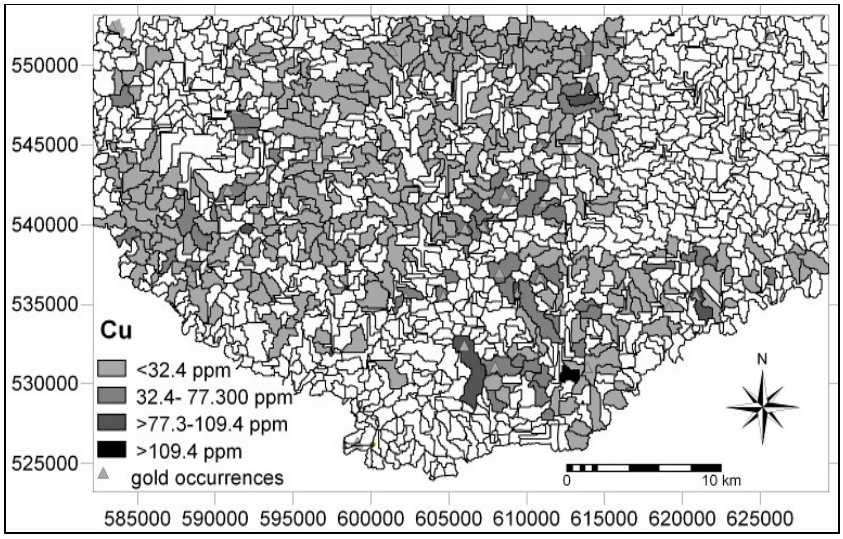

Figure 3.3: Spatial distribution of the Cu stream sediment data in the study area. Grey triangles are locations of known gold deposit occurrences.

3.2.2. Copper distribution

The histogram of $\log_e$-transformed Cu data approximates a unimodal Gaussian distribution (Figure 3.1, right panel). The mean and standard deviation were used to classify the geochemical data. Population A comprises Cu concentrations less than 32.4 ppm, and form the background class. Copper values of 32.4–7 7.3 ppm are considered low anomaly and form population B. Population C consists of Cu concentrations of 77.3–109.4 ppm and is considered as intermediate anomaly. Population D is made up of Cu concentrations of 109.4–124.2 ppm, and is considered to be high anomaly.

Population A of the Cu data characterizes mainly areas underlain by granitoids (Figure 3.3). Population B of the Cu data characterizes mainly areas underlain by greenstones. Sample catchment basins in the western parts of the study area underlain by wacke facies, shale, and quartzite are also characterized by population B of the Cu data. Sample catchment basins with Cu values belonging to either population C or population D are very few but are underlain mainly by greenstones.

3.2.3. Chromium distribution

The histogram for the Cr data indicates presence of at least two populations (Figure 3.4, left panel). Threshold is chosen at the 95th percentile (i.e. 569.9 ppm). The Cr data below 569.9 ppm were classified as populations A (<68.76 ppm), B (68.76-197.9 ppm) and C (197.9-569.9 ppm) or background, low anomaly, intermediate anomaly. Population D consisting of Cr values ranging from 569.9 to 1588.5 ppm and are considered high anomaly.

Background Cr values are spatially associated the granitoids (Figure 3.5). Low Cr anomalies are most situated in samples catchment basins underlain by argillites, volcanoclastics, and quartzites, all of which are located in the southwest portions of the study. Sample catchment basins intermediate to high anomalies of Cr are situated in samples catchment basins underlain by metavolcanic rocks and are spatially associated with known gold deposit occurrences.

3.2.4. Vanadium distribution

The histogram of the vanadium data approximates a normal density distribution (Figure 3.4, right panel). Therefore the V data were classified into four populations based on the mean value plus increments of the estimated standard deviation: population A is <24.1 ppm; population B ranges from 24.1 to 53.5 ppm; population C ranges from 53.5 to 118.5 ppm; population D ranges from 118.5 to 473.5 ppm. Population C of the V data is associated with argillites, and gabbro (Figure 3.6) Sample catchment basins characterized by population D of the V data are situated in areas underlain by volcanoclastics and basalts.

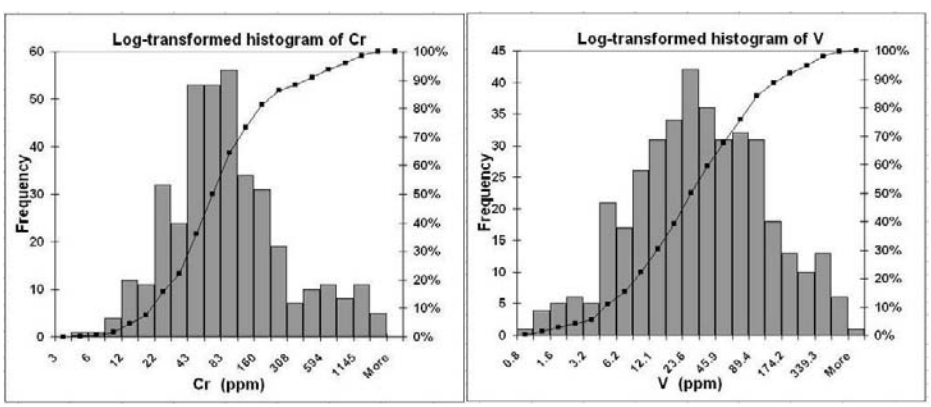

Figure 3.4: Histograms and cumulative frequency curves of $\log_e$-transformed Cr data (left panel) and $\log_e$-transformed V data (right panel).

3.2.5. Iron distribution

The histogram of Fe data shows breaks at the 74th and 94th cumulative percentiles corresponding, respectively, to Fe concentrations of 2.13% and 8.1% (Figure 3.7, left panel). These breaks in the Fe are also noted as inflection points that occur at the 6% and 26% cumulative frequency in the probability graph (Figure 3.7, right panel). The Fe data were thus divided into three populations:

population A consists of Fe values of <2.1%, population B ranges from 8.1 to 17.1%, and population C consists of Fe values >8.1. Population A of the Fe data is predominantly related to the Belt granitoids of tonalitic and granodioritic compositions in the central and southeastern portions of the study area (Figure 3.8). Populations B and C of the Fe data are associated with greenstone rocks.

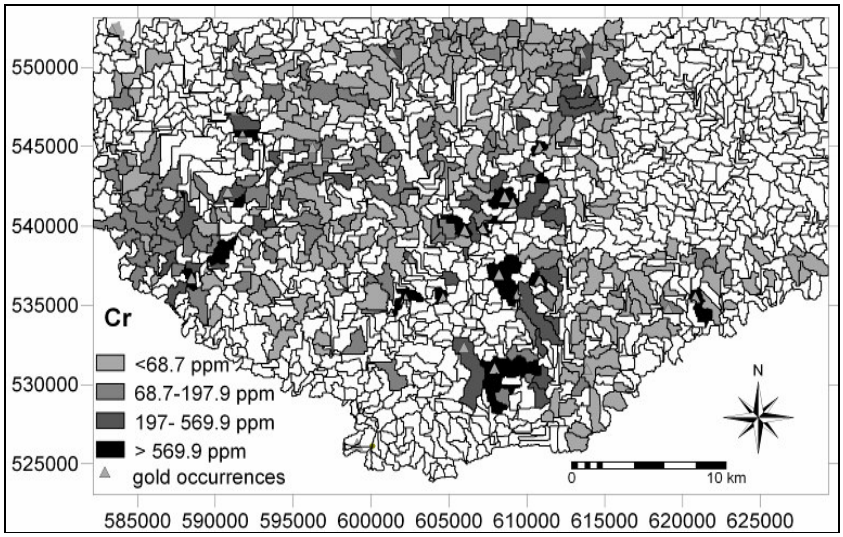

Figure 3.5: Spatial distribution of the Cr stream sediment data in the study area. Grey triangles are locations of known gold deposit occurrences.

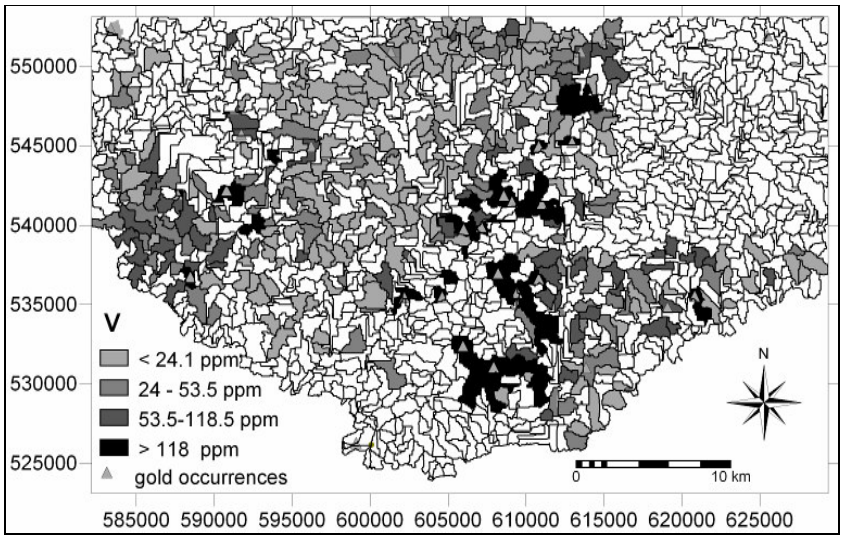

Figure 3.6: Spatial distribution of the V stream sediment data in the study area. Grey triangles are locations of known gold deposit occurrences.

3.2.6. Manganese distribution

The histogram of Mn geochemical data for the entire study area does not show a meaningful distribution in terms of identifying sub-populations. It was therefore decided to subset the geochemical data and to create separate histograms of Mn geochemical data in areas underlain by the two major different lithologies; granitoids and metavolcanics (Figure 3.9).

The histograms of Mn data in granitoid and metavolcanic terrains together show a total of at least three populations. The 97th cumulative percentile (or 734 ppm) in the Mn data in granitic terrains and a break at 481 ppm in the Mn data in metavolcanic terrains are considered to be the break points between at least three populations. Thus, the entire Mn uni-element data is divided into populations A (<481 ppm), B (481-734 ppm) and C (>734 ppm). The spatial distributions of the three populations in the Mn concentrations in the stream sediment catchment basins of the study area (Figure 3.10) are

similar to that of the Fe data (Figure 3.8), suggesting that Mn and Fe concentrations in the stream sediments are likely to be due to the same source or that they might have undergone similar processes in the surficial environment.

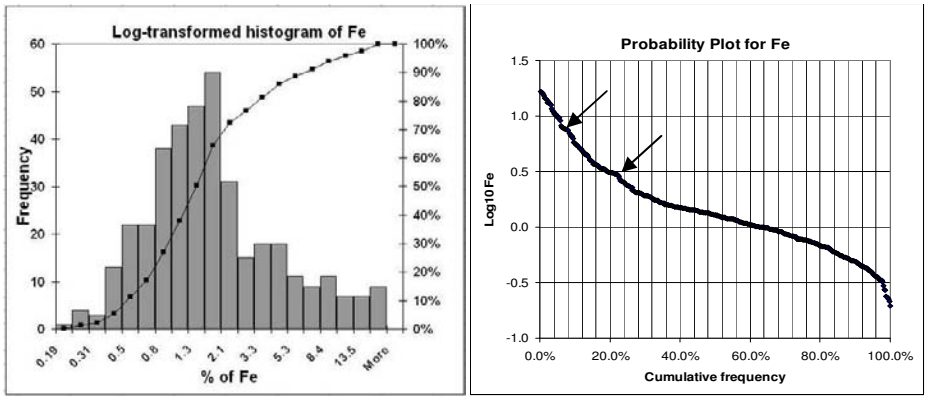

Figure 3.7: Histogram and probability graph of Fe data.

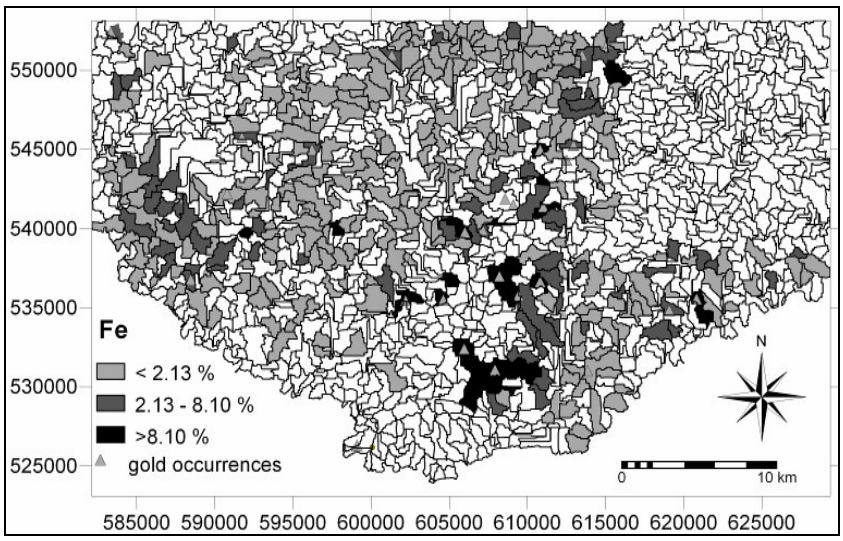

Figure 3.8: Spatial distribution of the Fe stream sediment data in the study area. Black triangles are locations of known gold deposit occurrences.

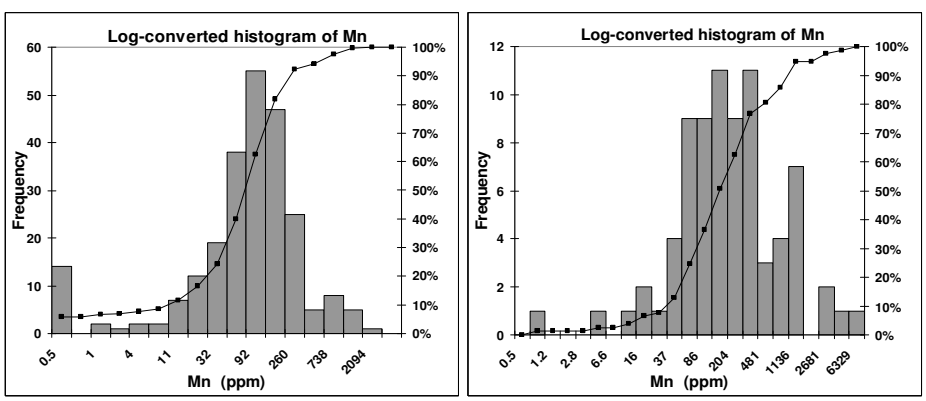

Figure 3.9: Histograms and cumulative frequency curves of $\log_e$-transformed Mn data in granitic terrains (left panel) and in metavolcanic terrains (right panel).

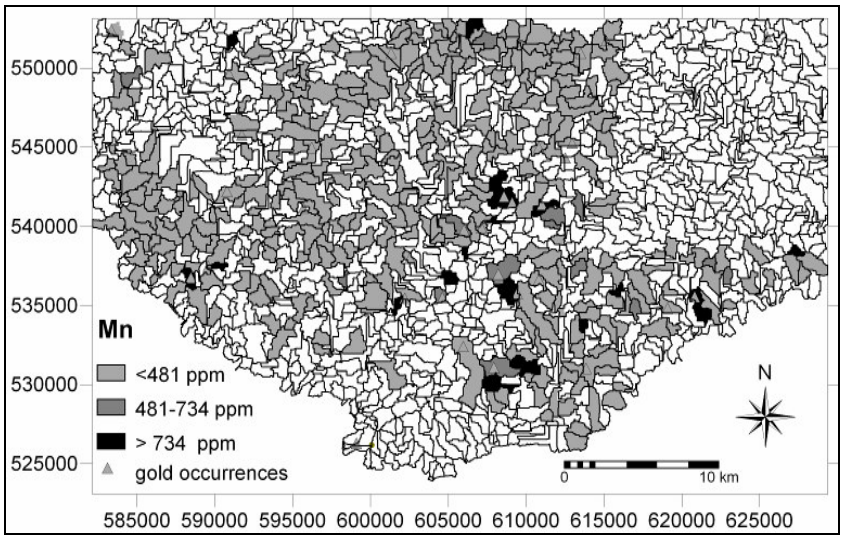

Figure 3.10: Spatial distribution of the Mn stream sediment data in the study area. Grey triangles are locations of known gold deposit occurrences.

3.2.7. Arsenic distribution

The histogram of the $\log_e$-transformed geochemical data for As approximates a Gaussian distribution (Figure 3.11, left panel).The mean and standard deviation $\log_e$-transformed geochemical data for As were therefore used in classification and mapping of populations in the data. Population A consists of As values <8.7 ppm, population B ranges from 8.7 to 15.0 ppm As, population C varies from 15.0-25.8 ppm As, and population D consists of As values >25.8. The spatial distribution of the As geochemical data in the sampled catchment basins is shown in Figure 3.12. Populations C and D show spatial association with greenstone lithologies and with known gold occurrences. Population B is sporadic and does not relate to any specific lithology. Population A is mostly distributed in sample catchment basins underlain by granitoids.

3.2.8. Gold distribution

The histogram of the $\log_e$-transformed Au values is nearly unimodal (Figure 3.11, right panel). The Au data are therefore classified into populations A (<40.2 ppb Au), B (40.2-54.0 ppb Au), C (54.0-97.7 ppb Au) and D (>97.7 ppb Au). Populations A, B and D of the Au data do not relate to specific lithologic units, whereas population C is mostly associated with granitoids (Figure 3.13). Sample catchment basins characterized by population D are sporadic but many of them contain known gold occurrences.

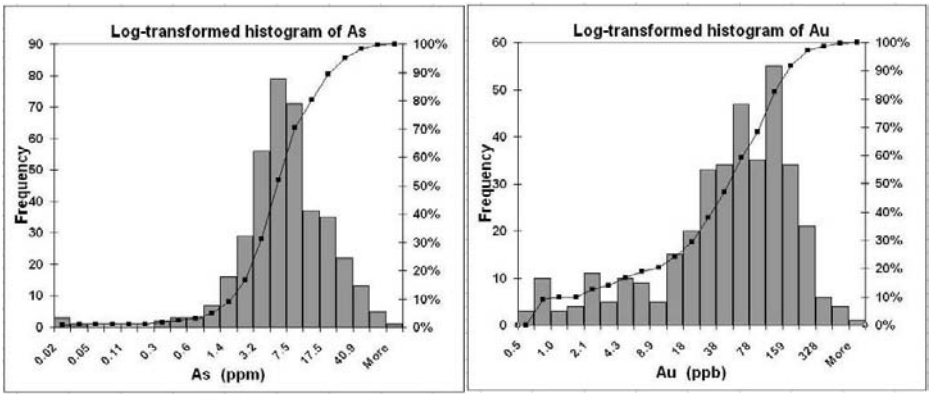

Figure 3.11: Histograms and cumulative frequency curves of $\log_e$-transformed As data (left panel) and $\log_e$-transformed Au data (right panel).

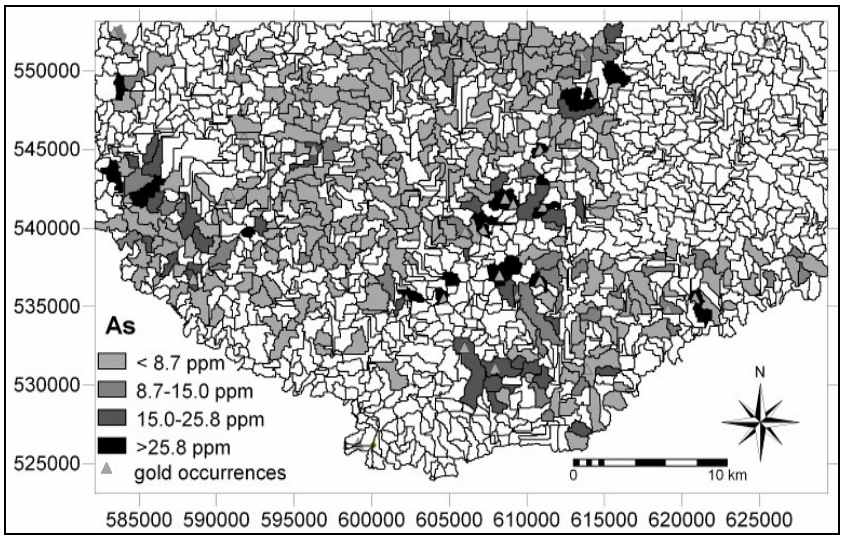

Figure 3.12: Spatial distribution of the As stream sediment data in the study area. Grey triangles are locations of known gold deposit occurrences.

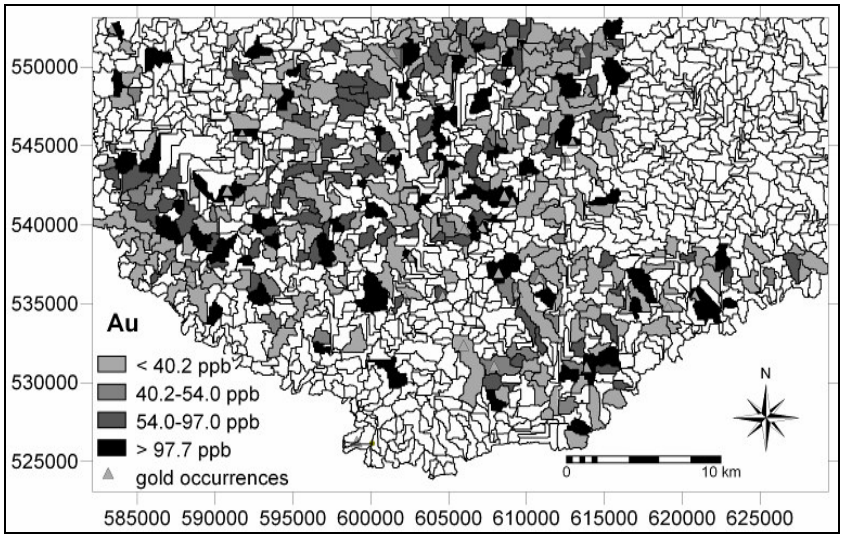

Figure 3.13: Spatial distribution of the Au stream sediment data in the study area. Grey triangles are locations of known gold deposit occurrences.

3.2.9. Zinc distribution

The histogram of Zn data is unimodal and approximates Gaussian distribution (Figure 3.14, left panel). Therefore, the Zn data are divided into four classes to depict its spatial distribution in the stream sediments of the study area (Figure 3.15). Most of Zn concentrations <40.1 ppm is related to granitoids. Zn values of 40.1-73.8 ppm are associated mainly with volcanoclastics in the southwestern portions of the study area. Zn >73.8 ppm are associated mainly with basalts.

3.2.10. Barium distribution

The geochemical data for Ba is unimodal (figure 3.14, right panel) and were divided into four classes (Figure 3.16). Concentrations of Ba <71 ppm mostly relate to granites, while concentrations of Ba >71 ppm mostly related to greenstone lithologies.

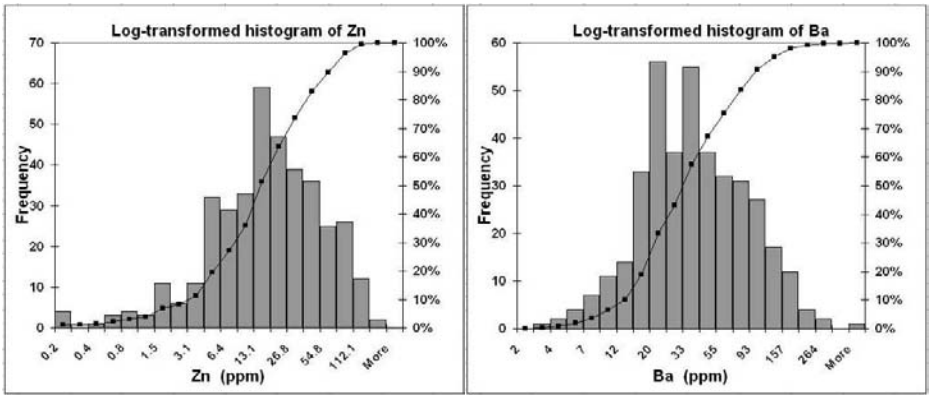

Figure 3.14: Histograms and cumulative frequency curves of $\log_e$-transformed Zn data (left panel) and $\log_e$-transformed Ba data (right panel).

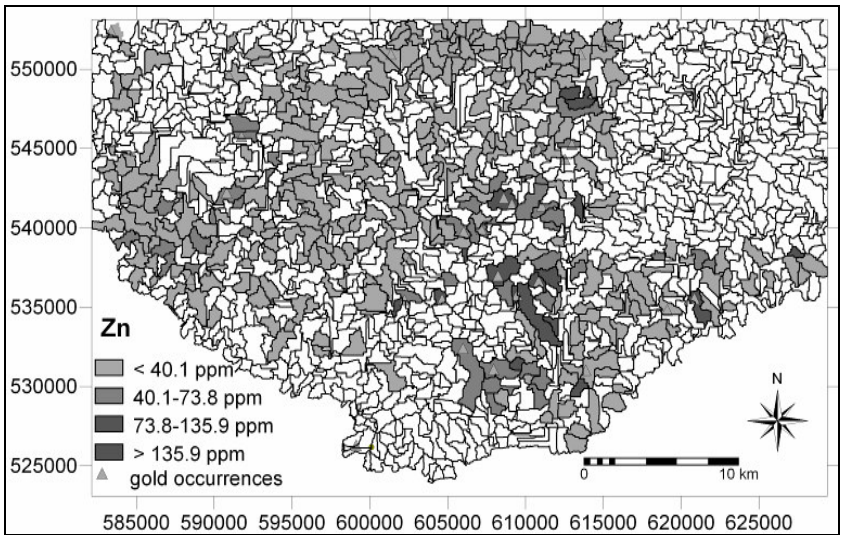

Figure 3.15: Spatial distribution of the Zn stream sediment data in the study area. Grey triangles are locations of known gold deposit occurrences.

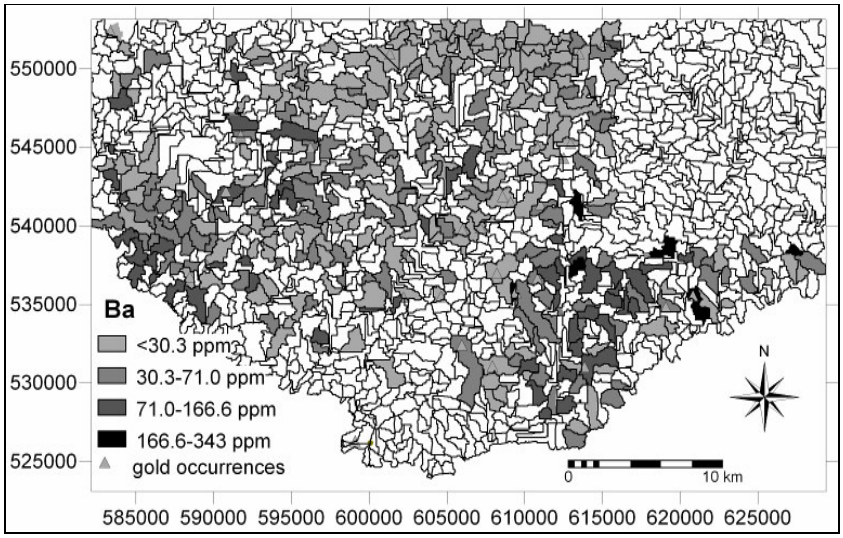

Figure 3.16: Spatial distribution of the Ba stream sediment data in the study area. Grey triangles are locations of known gold deposit occurrences.

3.2.11. Molybdenum distribution

The $\log_e$-transformed Mo geochemical data approximate a Gaussian distribution (Figure 3.17, right panel) and were divided into four classes (Figure 3.18). Mo values <18.6 ppm are predominantly associated with basalts and with some portions of granitoids in the northern sections. Mo values of 18.6-38.7 ppm are mostly associated with granitoids in the western parts. Mo values of 38.7-80.4 ppm are associated with granitoids in the northwestern parts. Only two catchment basins within the study area have Mo content above 80.4 ppm, and these are underlain by metavolcanics.

3.2.12. Strontium distribution

The $\log_e$-transformed Sr geochemical data show a Gaussian distribution (Figure 3.17, right panel), so the mean and standard deviation were used for classification in order to depict its spatial distribution in the study area (Figure 3.19). Most of the study area is characterized by Sr concentrations of <13.5 ppm, whereas the southeastern portions of the study area are characterized by Sr concentrations mostly >13.5 ppm.

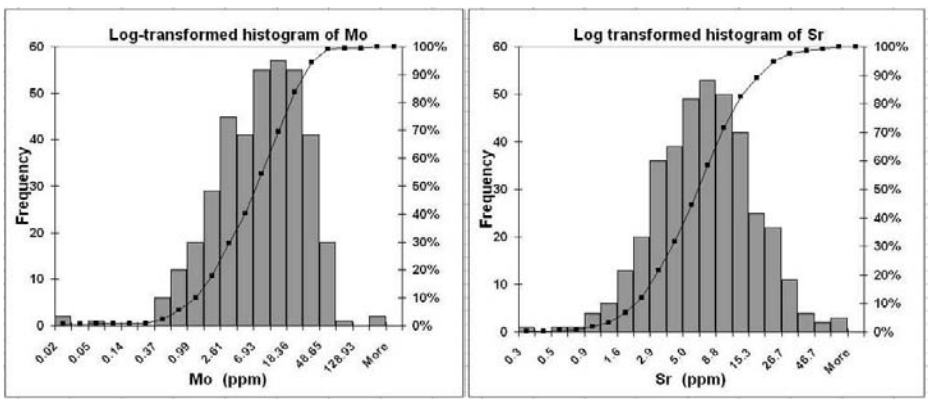

Figure 3.17: Histograms and cumulative frequency curves of $\log_e$-transformed Mo data (left panel) and $\log_e$-transformed Sr data (right panel).

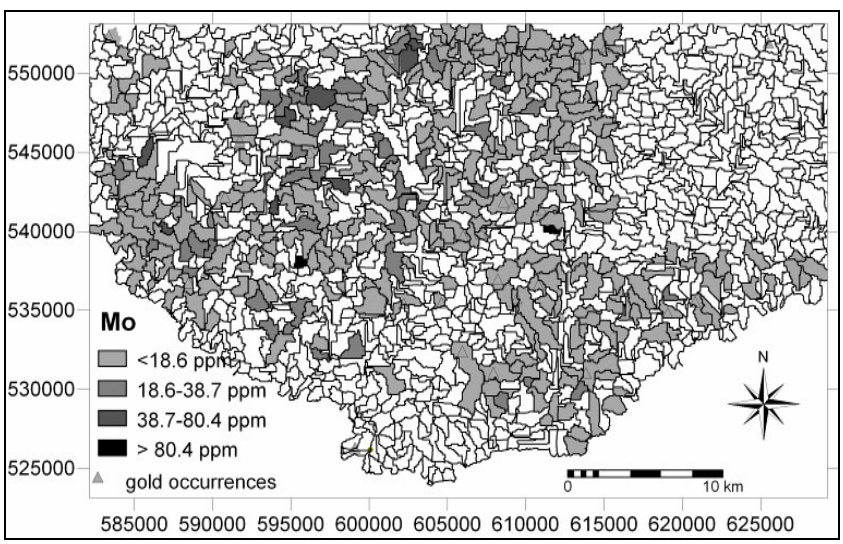

Figure 3.18: Spatial distribution of the Mo stream sediment data in the study area. Grey triangles are locations of known gold deposit occurrences.

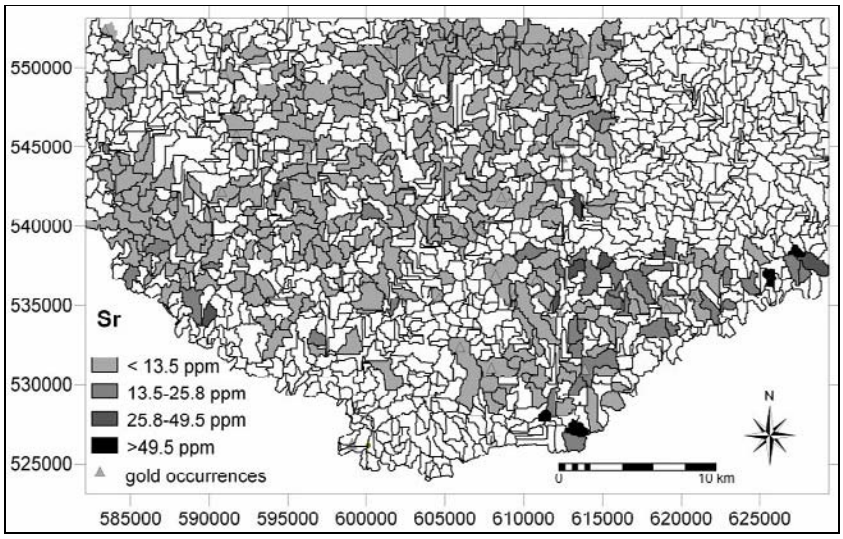

Figure 3.19: Spatial distribution of the Sr stream sediment data in the study area. Grey triangles are locations of known gold deposit occurrences.

3.2.13. Cobalt distribution

The $\log_e$-transformed Co geochemical data are unimodal and approximate a Gaussian distribution (Figure 3.20, left panel) and were divided into four classes (Figure 3.21). Most of the study area is characterized by Co concentrations of <11.4 ppm, whereas the south-central portions of the study area, which are underlain by greenstone lithologies, are characterized by Co concentrations of mostly >11.4 ppm. Co values of >21 show spatial association with known gold occurrences.

3.2.14. Lead distribution

The $\log_e$-transformed Pb geochemical data are unimodal and approximate a Gaussian distribution (Figure 3.20, right panel) and were divided into four classes (Figure 3.22). Most of the study area is characterized by Pb concentrations of <9.8 ppm. Pb values of .9.8 ppm are sporadically distributed in the study area but are mostly in areas underlain by metavolcanics.

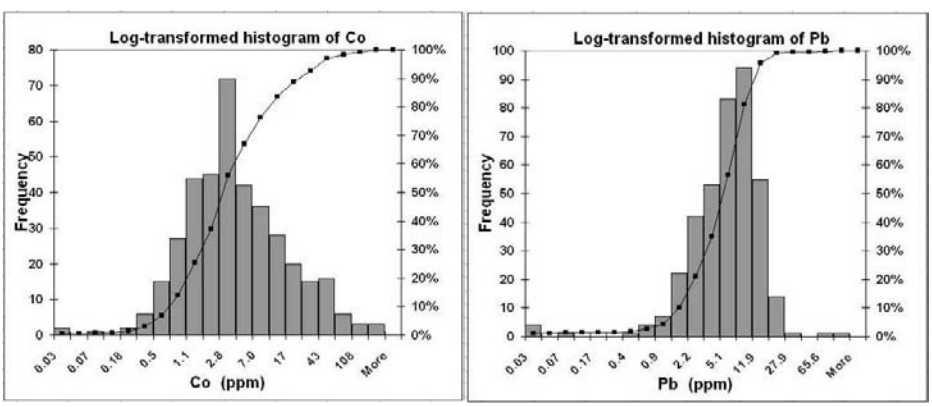

Figure 3.20: Histograms and cumulative frequency curves of $\log_e$-transformed Co data (left panel) and $\log_e$-transformed Pb data (right panel).

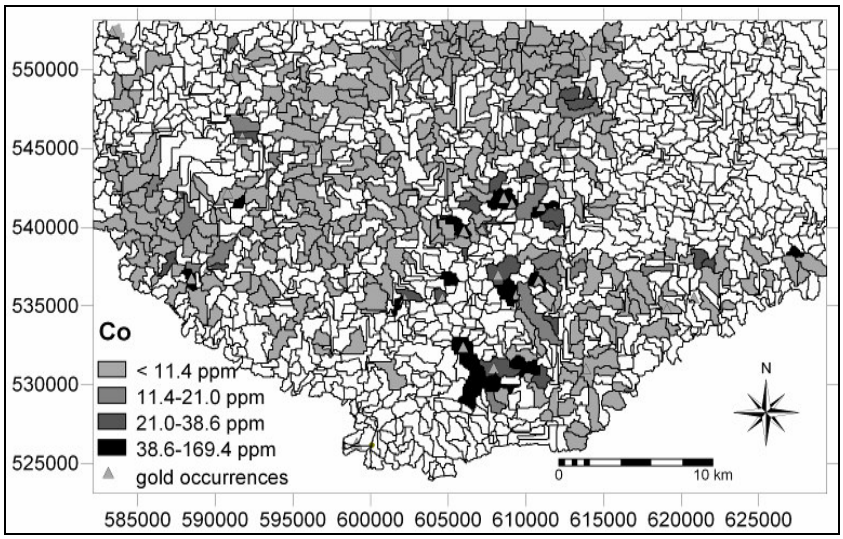

Figure 3.21: Spatial distribution of the Co stream sediment data in the study area. Grey triangles are locations of known gold deposit occurrences.

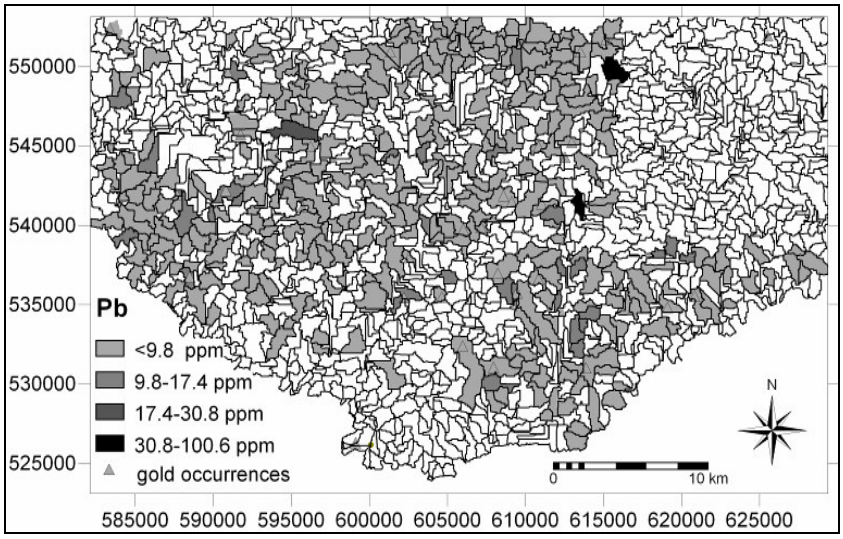

Figure 3.22: Spatial distribution of the Pb stream sediment data in the study area. Grey triangles are locations of known gold deposit occurrences.

3.2.15. Lithium distribution

The histogram of the Li data approximates a Gaussian distribution (Figure 3.23, left panel). The mean and standard deviation estimated of the Li data were thus used for the classification. Concentrations of Li greater than 5.2 ppm pertain mostly to catchments basins underlain by granites and quartzites in the southwestern portion of the study area (Figure 3.24). The central sections of the study area, especially along the belt of greenstone lithologies, are characterized by Li concentrations less than 3.7 ppm.

3.2.16. Antimony distribution

The Sb histogram is almost unimodal (Figure 3.23, right panel). Concentration values of Sb are very low, and so the data were divided into two groups so that the spatial distribution of Sb would be interpretable. Most of the study area is characterized by concentrations of Sb <1.05 (Figure 3.25). Catchment basins with concentrations of Sb >1.05 ppm are sporadic but seem to be distributed mainly where greenstone lithologies exist.

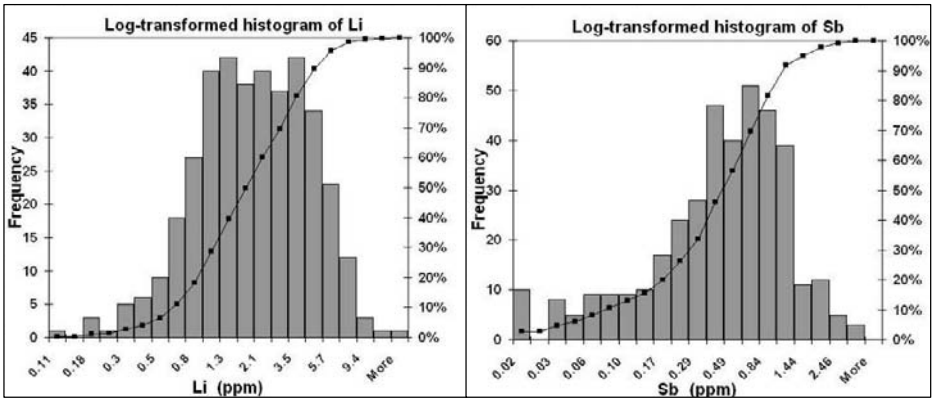

Figure 3.23: Histograms and cumulative frequency curves of $\log_e$-transformed Li data (left panel) and $\log_e$-transformed Sb data (right panel).

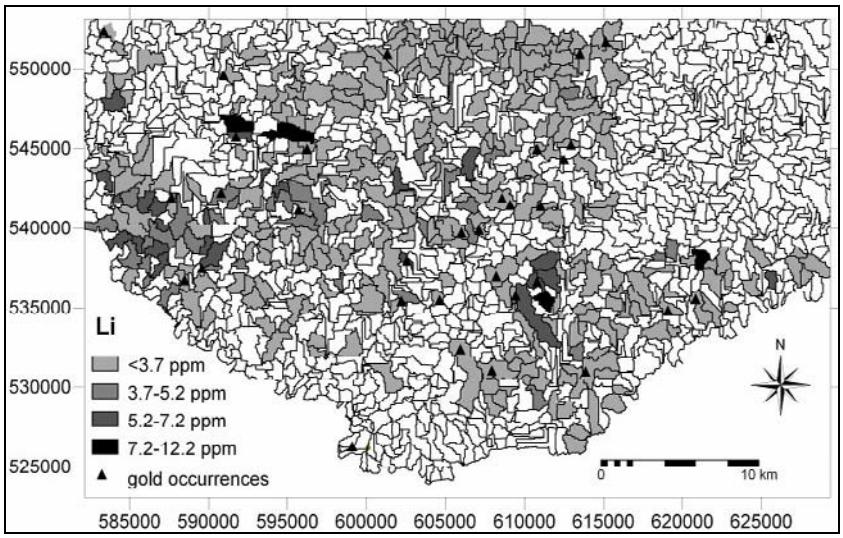

Figure 3.24: Spatial distribution of the Li stream sediment data in the study area. Grey triangles are locations of known gold deposit occurrences.

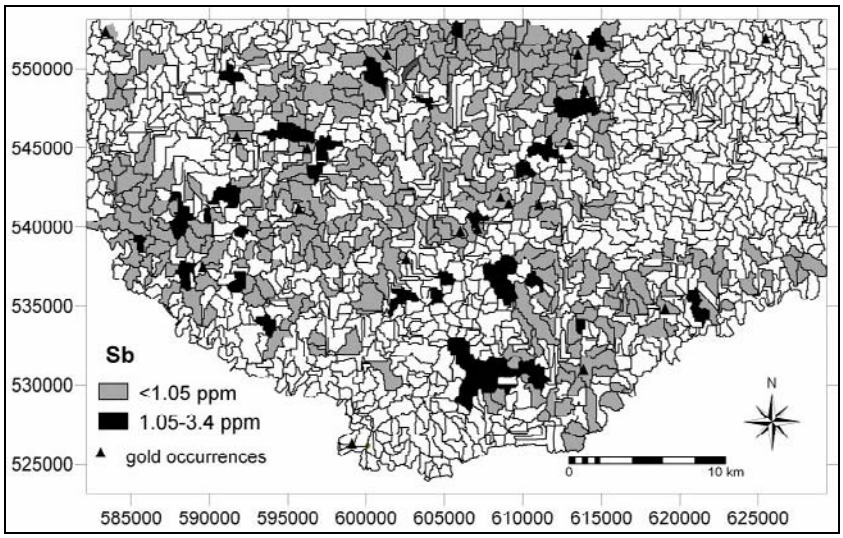

Figure 3.25: Spatial distribution of the Sb stream sediment data in the study area. Grey triangles are locations of known gold deposit occurrences.

3.2.17. Cadmium distribution

The histogram of the Cd data indicates presence of at least two populations (Figure 3.26, left panel). The break point at approximately the 65th cumulative frequency (i.e., 1.1 ppm) was used to divide the Cd data into two groups. Concentrations of Cd <1.1 ppm are distributed mainly in catchment basins located in the northern and central sections of the study area where granitic rocks are dominant (Figure 3.27). Concentrations of Cd >1.1 ppm occur in catchment basins that lie along the belt of greenstone lithologies.

3.2.18. Calcium distribution

The histogram of the Ca data is unimodal but positively skewed (Figure 3.26, right panel). Concentrations of Ca >1536.7 ppm are mainly associated with greenstones (Figure 3.28). Concentrations of Ca between 976.6-1536.7 ppm are associated with volcanoclastics in the southwestern sections of the study area. Areas underlain by granites are characterized by Ca concentrations of <976.6 ppm.

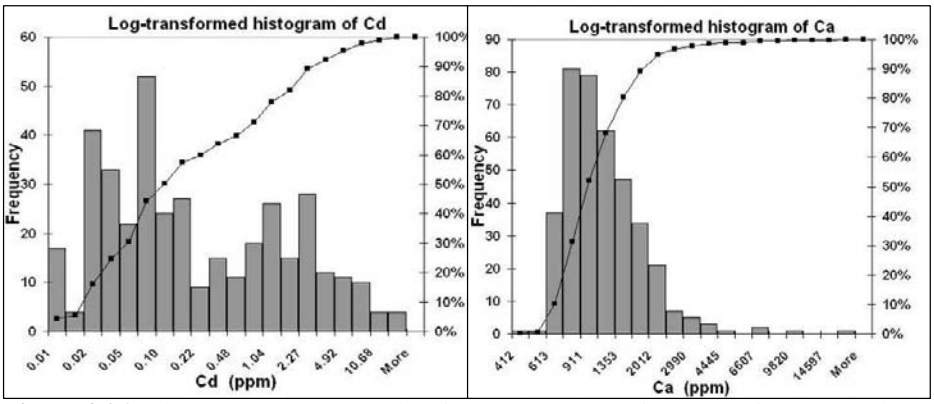

Figure 3.26: Histograms and cumulative frequency curves of $\log_e$-transformed Cd data (left panel) and $\log_e$-transformed Ca data (right panel).

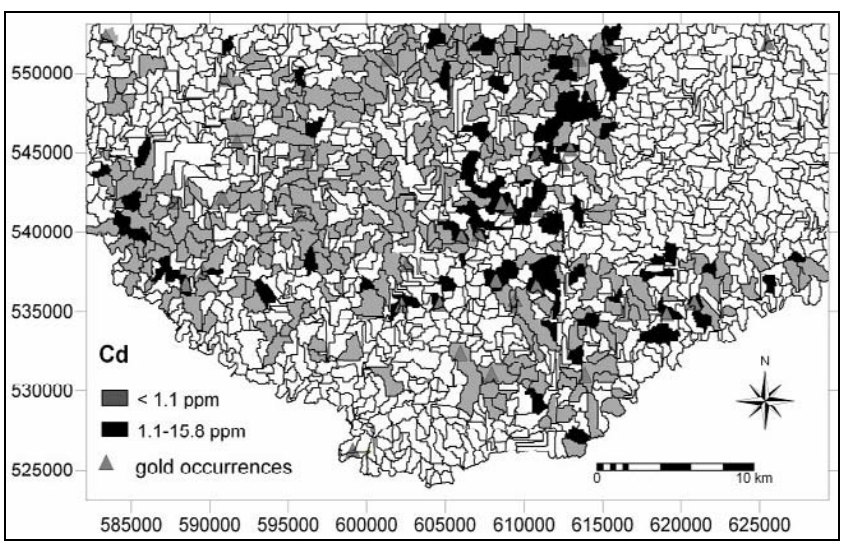

Figure 3.27: Spatial distribution of the Ca stream sediment data in the study area. Grey triangles are locations of known gold deposit occurrences.

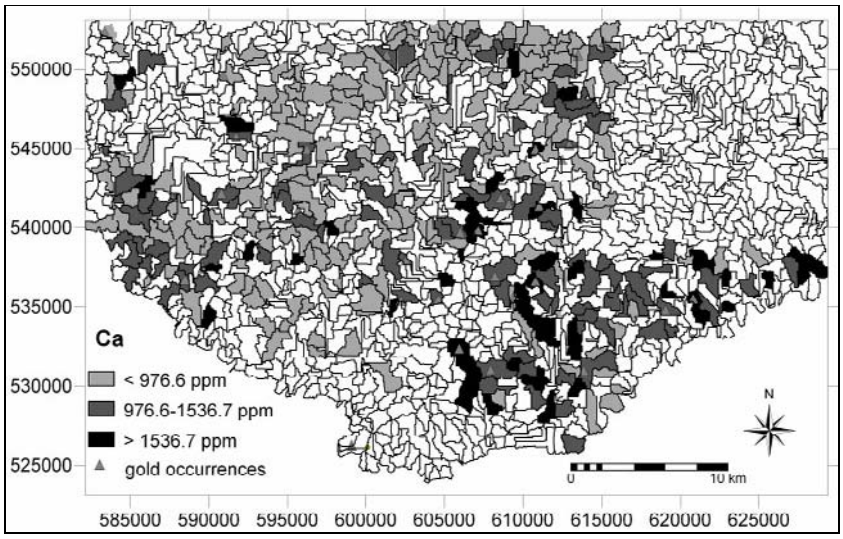

Figure 3.28: Spatial distribution of the Ca stream sediment data in the study area. Grey triangles are locations of known gold deposit occurrences.

3.3. Concluding remarks

The catchment basin geochemical maps show that variations in most of the uni-element datasets are highly influenced by lithology. For instance, higher concentrations of Fe, Mn, Ni, Cu, and V pertain to catchment basins underlain by metavolcanics, while lower concentrations of these elements pertain to areas underlain by granitoids. It can be observed, however, that sample catchment basins that contain a number of known gold occurrences are characterized by intermediate to high concentrations of Ni, Co, Cr, Cu, and Fe. The stream sediment geochemical datasets further analyzed (see next chapter) by quantifying and removing effects of factors unrelated to gold mineralisations in the study area.

Chapter 4: Catchment Basin Analysis

4.1. Introduction

Stream sediments are derived by erosion of materials that eventually find their way into the drainage systems where they are mixed. The geochemical composition of stream sediments is therefore largely influenced by the geochemical composition of lithologic units in the sediment source area. The geochemical composition of stream sediments is also influenced by chemical processes, as many elements could be scavenged by Fe- and Mn-oxides, organic matter, and clays. Factors that influence variations in geochemical composition of stream sediments change from one catchment basin to another. Therefore, stream sediments in every catchment basin have different uni-element background geochemical composition.

The task of estimating local background uni-element composition and subsequently derive geochemical residuals in order to recognized geochemical anomalies, which may be related to mineralization, has been approached in several ways (Rose et al., 1979; Bonham-Carter et al., 1997). In catchment basin analysis, areal proportions of lithologic units in sample catchment basins are used as independent variables and observed uni-element contents as dependent variables in multiple regression analysis to estimate local uni-element contents due to lithology (Bonham-Carter et al., 1987; Carranza et al., 1997; Carranza, 2004).

4.2. Modelling of background uni-element contents

Uni-element content of sediment samples (Y_i) and areal proportions (X_{ij}) of the jth lithologic units in the ith sample catchment basin are used as dependent and independent variables, respectively, in multiple regression in order to estimate local uni-element background content of stream sediments Y_i' in the ith sample catchment basin. The regression model is defined as follows:

$$Y_i' = b_0 + \left(\sum_{j=1}^{m} b_{ij} X_{ij}\right) + e_i \qquad \text{(Equation 4.1)}$$

where e_i represent residual values, which may be positive or negative; $\sum_{j=1}^{m} X_{ij} = 1$; b_0 and b_{ij} are regression coefficients determined by least squares method to minimize the residual errors $\sum_{i=1}^{n} (Y_i - Y_i')^2$. The model implies a simple linear additive mixing relationship between elements contents derived from different lithologic units, with b_0 interpreted as mean uni-element content, and b_{ij} interpreted as mean uni-element composition of the jth lithologic unit in the ith sample catchment basin.

For the independent variables, areal proportions of lithologic units in every stream sediment sample catchment basins were determined using ILWIS, which is a GIS software package developed by ITC. The analysis involved crossing the raster map of lithologic units (Figure 2.2) with a raster map of sample catchment basins. The cross operation results in a table with three columns namely; lithologic units, number of pixels, and area (in m^2). The latter two columns refer to overlap between a lithologic unit and a sample catchment basin. Areal proportion of a lithologic rock unit in a sample catchment basin was then calculated by dividing area of overlap between that lithologic unit and the sample catchment basin by the area of the sample catchment basin.

For the dependent variables, the $\log_e$-transformed uni-element data are used because of their reduced asymmetry. However, by using the $\log_e$-transformed uni-element data, the multiple regression model (Equation 4.1) becomes multiplicative and does not anymore represent the linear additive mixing hypothesis. To alleviate this problem, the multiple regression model is forced through the origin by setting b_0=0 so that the resulting b_{ij}'s are positive and easy to interpret (Bonham-Carter et al., 1987; Carranza et al., 1997).

4.2.1. Effect of lithology on uni-element background

Each of the 18 elements was regressed against areal proportion of lithologic units in sample catchment basins in order to estimate influence of lithology on uni-element background per sample catchment basin. The results of regression analysis are summarized in Table 4.1. The ability of the

independent variables (i.e., areal proportions of lithological unit in sample catchment basins) to account for variation of the dependent variables (i.e., stream sediment uni-element content) is indicated by R^2 expressed as a percentage. It represents the ratio of sum of squares explained by regression to total sum of squares, which indicates goodness-of-fit of regression model between dependent and independent variables. In Table 4.1, the elements are arranged downwards according to decreasing percentage of variation accounted for by the lithological factor. The results show that the lithological factor accounts for >75% of variations in Ca, Cu, Ba, Cr, Mn, V, Zn, Sr and Au; 50-75% of variations in Ni, Pb, Mo, As and Cd; and <50% of variations in Sb, Co, Li and Fe. The results also suggest that other factors account for variations in stream sediment element contents in the study area.

Table 4.1: Results of regression of uni-element contents vs. areal proportion of lithologic units.

Dependent Variables	Regression coefficients (b_j) of independent variables				R^2 (%)
	Granitoids	Basalts	Argillites/Wackes	Volcanoclastics	
Ca	2.999	3.296	3.045	3.073	97.5
Cu	1.005	1.357	1.270	1.634	94.0
Ba	1.786	1.403	1.744	1.492	92.6
Cr	1.741	2.608	1.743	2.128	91.9
Mn	1.740	2.109	1.931	2.595	86.2
V	1.232	1.737	1.473	2.198	85.1
Zn	0.980	1.264	1.210	1.737	80.0
Sr	0.973	0.656	0.763	0.901	78.2
Au	1.406	1.429	1.569	1.334	75.7
Ni	0.724	1.251	0.713	1.558	73.0
Pb	0.540	0.614	0.819	1.043	67.4
Mo	0.838	0.404	0.731	0.593	64.2
As	0.570	0.847	0.693	0.437	51.7
Cd	-0.940	-0.332	-1.071	-1.148	50.7
Sb	-0.515	-0.462	-0.448	-0.266	49.3
Co	0.300	1.218	0.532	0.829	45.4
Li	0.421	0.163	0.408	0.293	29.4
Fe	0.066	0.372	0.180	0.644	22.0

4.2.2. Effect of lithology and metal scavenging on uni-element background

It is important to determine the contribution of other factors to the variations in stream sediment element contents. The effect of co-precipitation with or scavenging by Fe- and/or Mn oxides on variations in the stream sediment uni-element contents in the study area was therefore investigated by using Fe and Mn contents in the stream sediments as independent variables in addition to areal proportions of lithologic units. In Table 4.1 the elements are arranged downwards according to decreasing percentage of variation accounted for by the lithological factor. The results show that the lithological factor accounts for >75% of variations in Ca, Cu, Ba, Cr, Mn, V, Zn, Sr, Au, Ni and Pb; 50-75% of variations in As, Mo, Fe, Cd and Sb; and <50% of variations in Li.

The additional effect of Fe and Mn on the variations in uni-element contents not yet explained by the lithological factor was estimated by subtracting the R^2 values in Table 4.1 from the R^2 values in Table 4.2. The results (Table 4.3) show that the chemical controls (Fe, Mn) account for <5% of variations in Mo, Ca, Au, Sr, Ba, Cu and Cr; 5-10% of variations in Li, Mn, Pb, V and Cd; and >10% of variations in Zn, Fe, As, Ni, Sb and Co. For these latter elements, the chemical factors (Fe, Mn) account for a significant increase in explained variation over that accounted by lithology.

The results of the two regression analyses further show that lithological and chemical factors considered do not account for 100% of variations of each of the elements. This means that other factors, one of which could be mineralization, account for the unexplained variations in element contents. For example, about 20% of variation in Au is not accounted for by the lithological and chemical factors considered.

Table 4.2: Results of regression of uni-element contents vs. areal proportion of lithologic units, Fe and Mn.

Dependent Variables	Regression coefficients (b_j) of independent variables R^2 (%)						R^2 (%)
	Granitoids	Basalts	Argillites/ Wackes	Volcano-clastics	Fe	Mn	
Ca	2.301	2.343	2.363	2.414	-0.177	0.384	98.1
Cu	0.586	0.777	0.725	0.760	0.426	0.224	97.4
Cr	1.094	1.509	1.098	1.322	0.576	0.280	96.3
Ba	0.976	0.838	1.193	1.128	-0.206	0.305	94.0
Mn	1.043	1.650	1.600	1.716	1.365	-	93.4
V	0.97	1.157	1.086	1.316	0.900	0.116	92.7
Zn	0.448	0.450	0.557	0.628	0.577	0.284	91.2
Ni	0.203	0.453	0.070	0.444	0.601	0.277	88.4
Co	-0.200	-0.004	-0.106	0.048	0.775	0.258	82.0
Sr	0.396	0.240	0.576	0.407	-0.098	0.215	80.7
Au	0.857	1.153	1.269	1.069	0.184	0.138	76.7
Pb	0.298	0.370	0.590	0.584	0.378	0.083	74.9
As	0.458	0.467	0.480	-0.186	0.838	0.032	66.6
Mo	0.709	0.318	0.614	0.531	-0.237	0.083	64.7
Fe	-0.595	-0.428	-0.553	-0.341	-	0.380	62.4
Cd	-0.623	-0.255	-0.832	-1.249	1.051	-0.222	59.7
Sb	-0.408	-0.447	-0.372	-0.321	0.393	-0.076	52.3
Li	0.344	0.139	0.298	0.195	0.197	0.038	34.9

Table 4.3: Results of regression of uni-element contents vs. areal proportion of lithologic units, Fe and Mn.

Dependent Variables	% of variation due independent variables		Variability due to Fe and Mn
	Lithology	Lithology + Mn + Fe	
Co	45.4	82.3	36.9
Sb	49.3	62.4	19.0
Ni	73.0	88.4	15.4
As	51.7	66.6	14.9
Fe	22.0	62.4	13.1
Zn	80.0	91.2	11.2
Cd	50.7	59.7	9.0
V	85.1	92.7	7.6
Pb	67.4	74.9	7.5
Mn	86.2	93.4	7.2
Li	29.4	34.9	5.5
Cr	91.9	96.3	4.4
Cu	94.0	97.4	3.4
Ba	92.6	94.0	2.6
Sr	78.2	80.7	2.5
Au	75.7	76.7	1.0
Ca	97.5	98.1	0.6
Mo	64.2	64.7	0.5

4.2.3. Removal of the effects of lithology and Mn-Fe Scavenging

The regression coefficients of independent variables given in Table 4.2 were used to estimate local uni-element background in the ith sample catchment basin due to lithology and to Mn-Fe scavenging effects (Carranza and Hale, 1997) using the following equation:

$$Y_i' = (\sum_{j=1}^{m} b_{ij} X_{ij}) + b_{Mn} Mn_i + b_{Fe} Fe_i \qquad \text{(Equation 4.2)}$$

where b_j, b_{Mn} and b_{Fe} are the regression coefficients of the lithologic and chemical controls, X_{ij} are areal proportions of j=1,2,…,m lithologic units in sample catchment basin i; and Mn_i and Fe_i are $\log_e$ transformed concentrations of these elements for sample i.

Removal of estimated local uni-element background concentrations due to lithology and Mn-Fe scavenging effects from the measured uni-element concentrations results in geochemical residuals ($Y_i - Y_i'$), some positive others negative residuals. Positive geochemical residuals mean enrichment in uni-element concentrations, whereas negative geochemical residuals mean depletion of uni-element concentrations. The former could suggest anomalous geochemical controls (e.g., mineralization), while the latter could suggest other controls in the surficial environment (e.g., adsorption to clays or organic matter, which are not considered in stream sediment sampling). Positive geochemical residuals are therefore of interest in mineral exploration.

4.2.4. Correction for downstream dilution

The magnitude of geochemical residuals (i.e., $Y_i - Y_i'$) are controlled by factors such as downstream dilution due to mixing of stream sediments derived from various and mostly non-anomalous sources in sample catchment basins. Bonham-Carter and Goodfellow (1984, 1986) used the following equation, a formula based on the relation developed by Hawkes (1976), to correct for downstream dilution.

$$Y_a A_a = A_i (Y_i - Y_i') + Y_i' A_a \qquad \text{(Equation 4.3)}$$

where Y_a is element content due to an anomalous source with exposed area A_a, Y_i is element content in the ith sample catchment basin with area A_i, and Y_i' is background element content due to non-anomalous sources with surface area A_i–A_a. By assuming that a unit area of anomalous source contributes to stream sediments (i.e., A_a= 1 km^2), Bonham-Carter and Goodfellow (1984, 1986) further proposed a mineralization rating (R_i) for the ith sample catchment basin by using the following formula:

$$R_i = A_i (Y_i - Y_i') + Y_i'. \qquad \text{(Equation 4.4)}$$

However, Carranza and Hale (1997) argue that by using Equation 4.4 to correct for downstream dilution estimates of local uni-element background content due to controls unrelated mineralization (i.e. Y_i') are added back. Rose et al. (1979) indicated that the term $Y_i' A_a$ in Equation 4.3 can be neglected if A_i is much larger than A_a. By assuming further a much smaller unit area of 1 hectare (i.e., A_a=0.01 km^2) of exposed mineralization contributes to stream sediments in every sample catchment basin, Carranza and Hale (1997) proposed the following formula to correct geochemical residuals for the effects of downstream dilution:

$$Y_a = 100 \cdot A_i (Y_i - Y_i'). \qquad \text{(Equation 4.5)}$$

In this study, Equation 4.5 is adopted to correct geochemical residuals for effects of downstream dilution. In the following section, spatial distributions of dilution-corrected geochemical residuals are mapped to examine visually their spatial association with known gold occurrences in the study area

4.3. Spatial distribution of uni-element dilution corrected residuals

To examine the spatial distributions of the dilution-corrected geochemical residuals they were classified as either negative or positive and then the positive residuals were further classified based on their cumulative frequency percentiles (i.e., 0-80, 80-85, 85-90, 90-95 and 95-100). This classification scheme of the dilution-corrected geochemical residuals is applied in order to enhance high positive dilution-corrected residuals, which would be of mineral exploration interest.

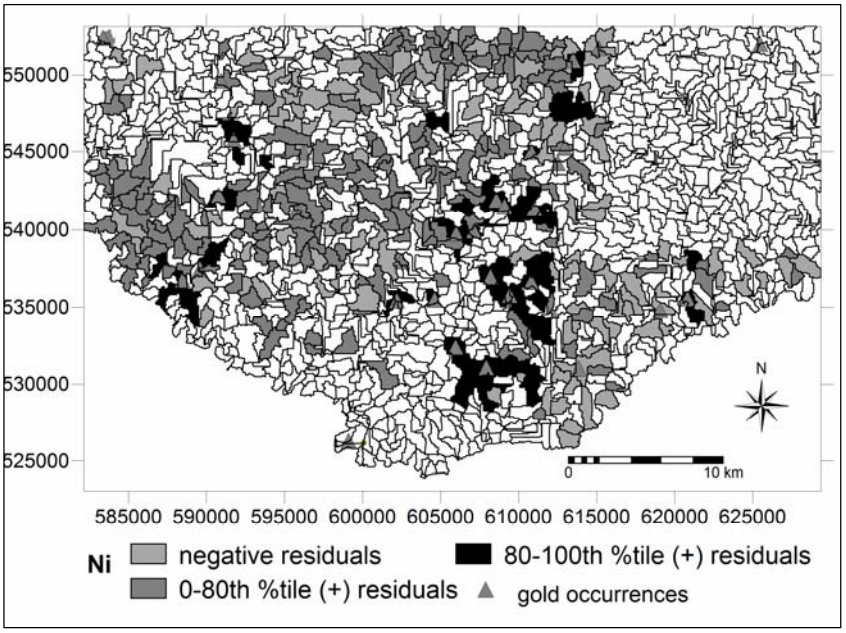

Figure 4.1: Spatial distribution of dilution-corrected Ni residuals.

4.3.1. Nickel residuals

Negative Ni residuals and positive Ni residuals below the 80th percentile are associated with areas underlain by granitoids (Figure 4.1). Sample catchment basins with positive Ni residuals above the 90th percentile are mostly underlain by greenstone lithologies.

4.3.2. Copper residuals

Catchment basins with negative Cu residuals and positive Cu residuals below the 80th percentile are mainly underlain by granitoids (Figure 4.2). Sample catchment basins with positive Cu residuals above the 90th percentile are mostly underlain by greenstone lithologies.

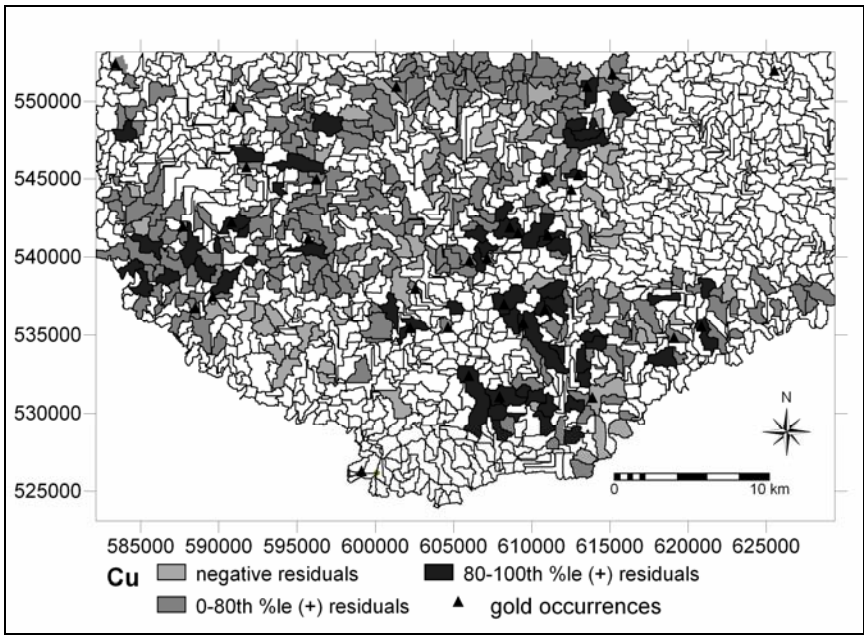

Figure 4.2: Spatial distribution of dilution-corrected Cu residuals.

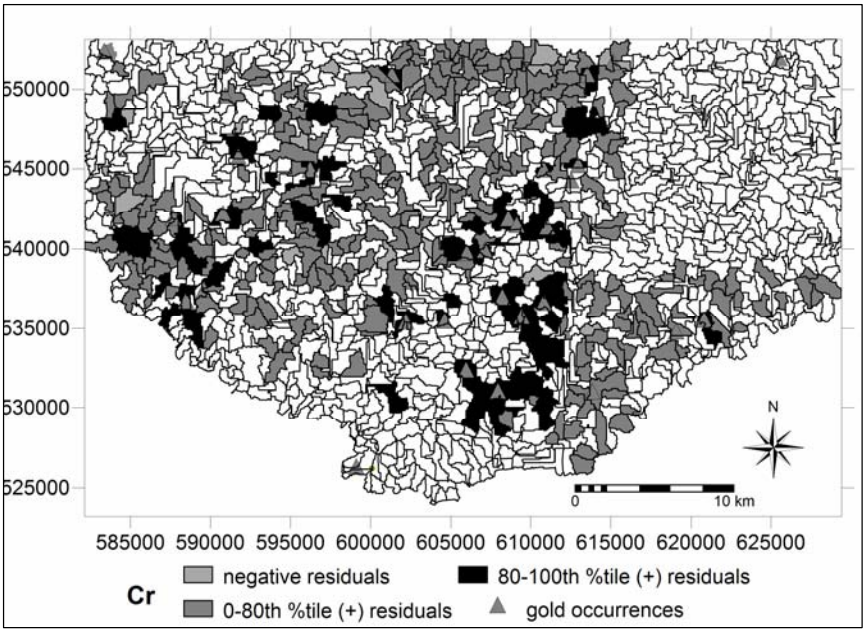

Figure 4.3: Spatial distribution of dilution-corrected Cr residuals.

4.3.3. Chromium residuals

Catchment basins with negative Cr residuals and positive Cr residuals below the 80th percentile are mainly underlain by granitoids (Figure 4.3). Sample catchment basins with positive Cr residuals above the 90th percentile are mostly underlain by greenstone lithologies.

4.3.4. Vanadium residuals

Catchment basins with negative V residuals and positive V residuals below the 80th percentile are mainly underlain by granitoids (Figure 4.4). Sample catchment basins with positive V residuals above the 90th percentile are mostly underlain by greenstone lithologies.

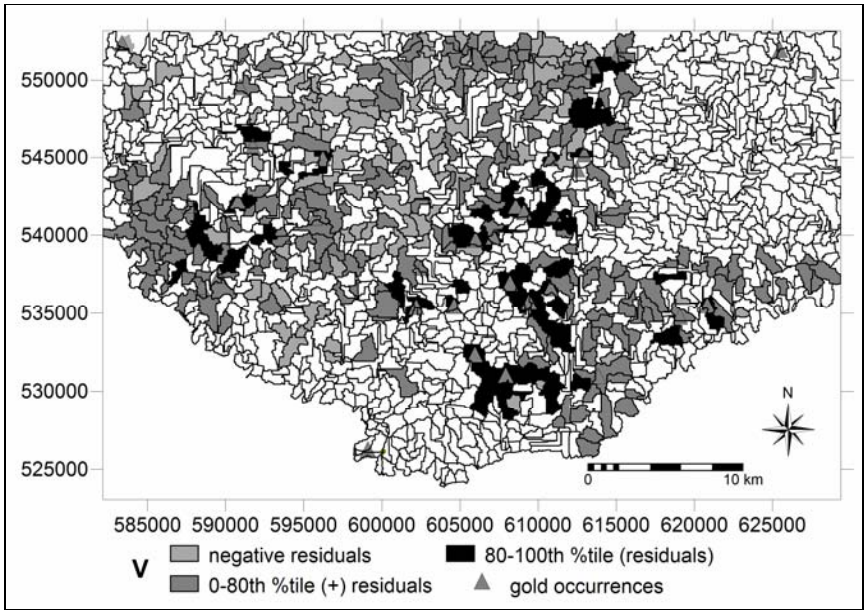

Figure 4.4: Spatial distribution of dilution-corrected V residuals.

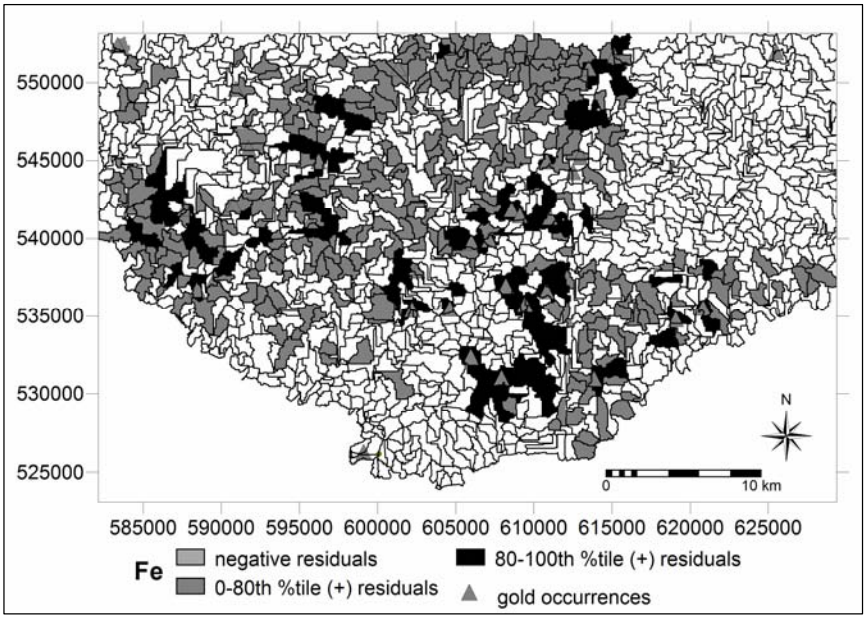

Figure 4.5: Spatial distribution of dilution-corrected Fe residuals.

4.3.5. Iron residuals

Most of the study area is characterized by negative Fe residuals and positive Fe residuals below the 80th percentile (Figure 4.5). Sample catchment basins with positive Fe residuals above the 90th percentile are mostly underlain by greenstone lithologies.

4.3.6. Zinc residuals

Catchment basins with negative Zn residuals and positive Zn residuals below the 80th percentile are mainly underlain by granitoids (Figure 4.6). Sample catchment basins with positive Zn residuals above the 90th percentile are mostly underlain by greenstone lithologies.

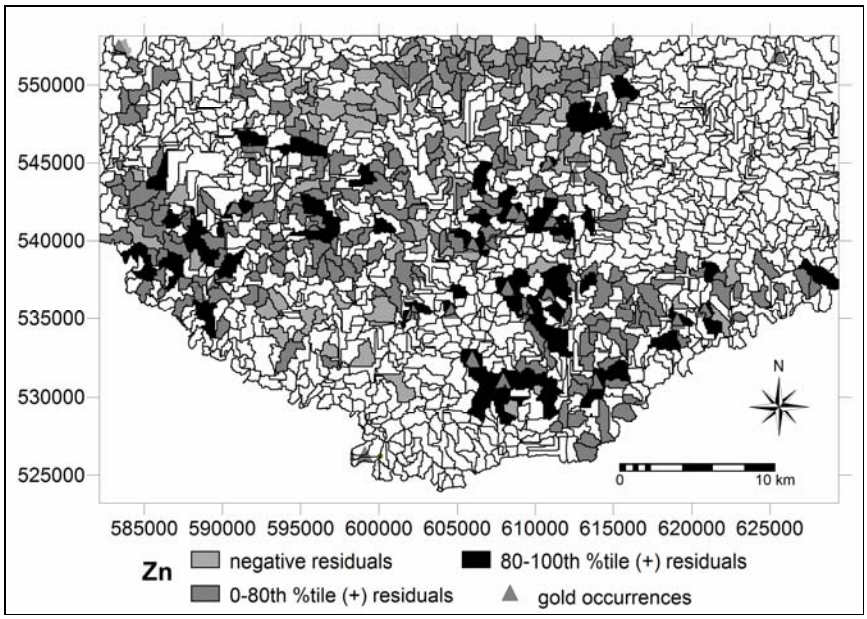

Figure 4.6: Spatial distribution of dilution-corrected Zn residuals.

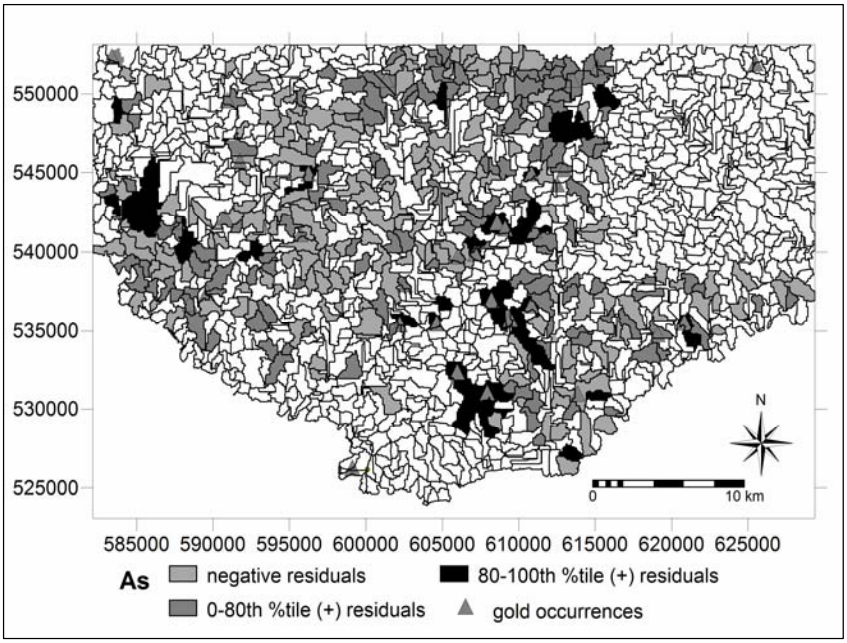

Figure 4.7: Spatial distribution of dilution-corrected As residuals.

4.3.7. Arsenic residuals

Catchment basins with negative As residuals and positive As residuals below the 80th percentile are mainly underlain by granitoids (Figure 4.7). Sample catchment basins with positive Zn residuals above the 85th percentile are mostly underlain by greenstone lithologies.

4.3.8. Molybdenum residuals

Areas underlain by greenstone lithologies are characterized mostly by negative Mo residuals, whereas areas underlain by granitoids are characterized mostly by positive Mo residuals (Figure 4.8). Granitoids in the western half of the study area are characterized by positive Mo residuals above the 90th percentile.

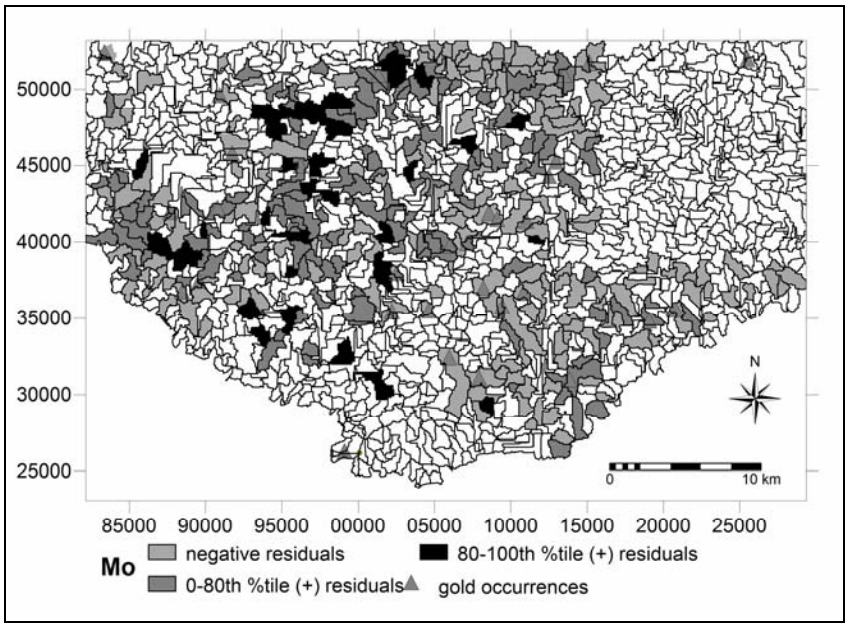

Figure 4.8: Spatial distribution of dilution-corrected Mo residuals.

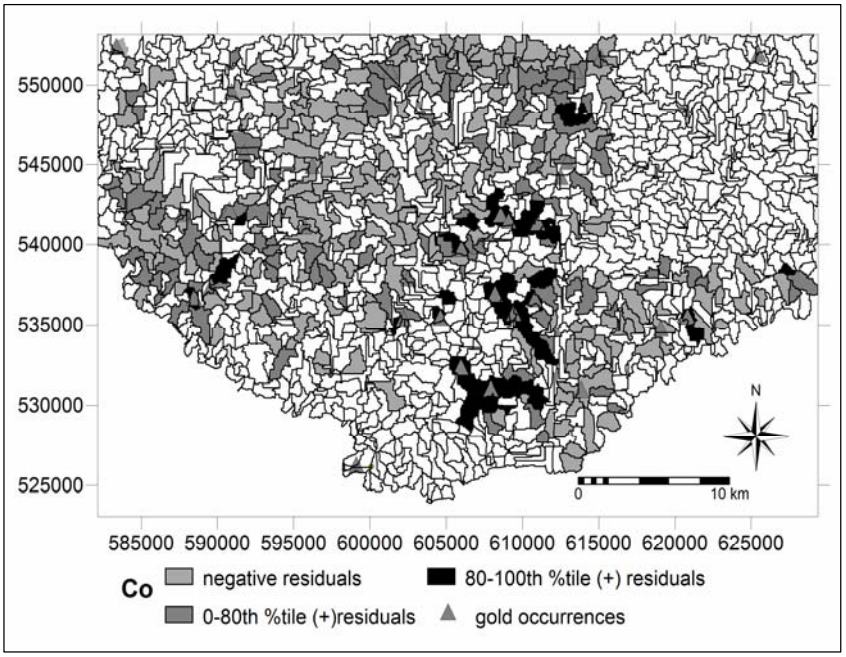

Figure 4.9: Spatial distribution of dilution-corrected Co residuals.

4.3.9. Cobalt residuals

Catchment basins with negative Co residuals and positive Co residuals below the 80th percentile are mainly underlain by granitoids (Figure 4.9). Greenstone lithologies in south-central parts of the study area are characterized by positive co residuals above the 80th percentile.

4.3.10. Strontium residuals

Areas underlain by greenstone lithologies are characterized mostly by negative Sr residuals, whereas areas underlain by granitoids are characterized mostly by positive Sr residuals (Figure 4.10). Granitoids in the southeastern parts of the study area are characterized by positive Sr residuals above the 90th percentile.

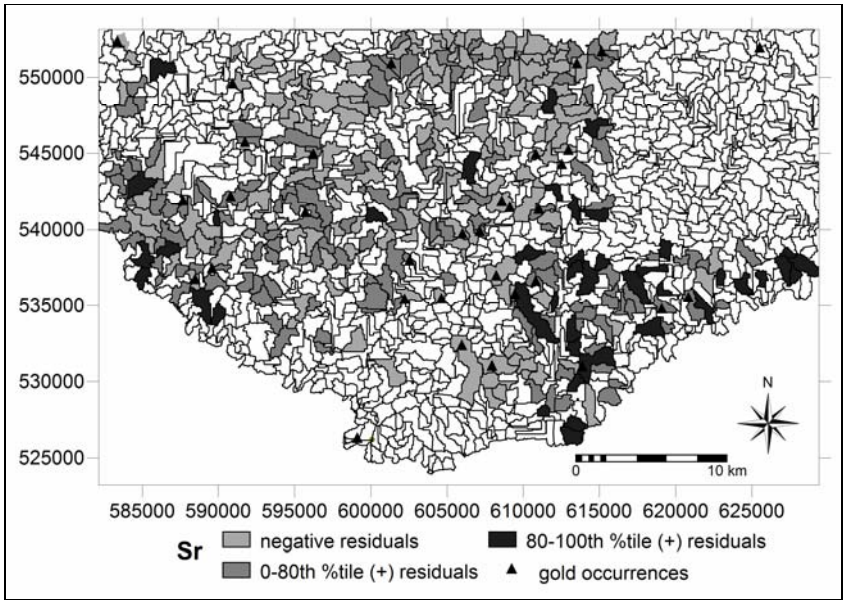

Figure 4.10: Spatial distribution of dilution-corrected Sr residuals.

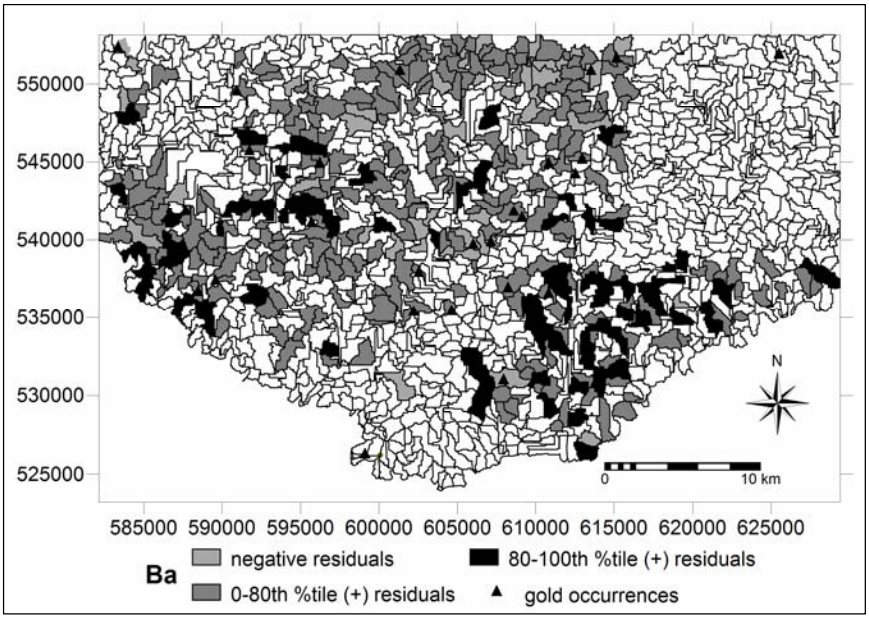

Figure 4.11: Spatial distribution of dilution-corrected Ba residuals.

4.3.11. Barium residuals

Most of the study area is characterized by positive Ba residuals (Figure 4.11). Most negative Ba residuals show spatial association with the granitoid-greenstone contact zones in the north-central parts of the study area. In contrast, most positive Ba residuals above the 90th percentile seem to cluster at or near the granitoid-greenstone contact zones in the south-central parts of the study area.

4.3.12. Gold residuals

Most of the study area is characterized by negative Au residuals and positive Au residuals below the 80th percentile (Figure 4.12). Sample catchment basins with positive Au residuals above the 80th percentile are sporadic.

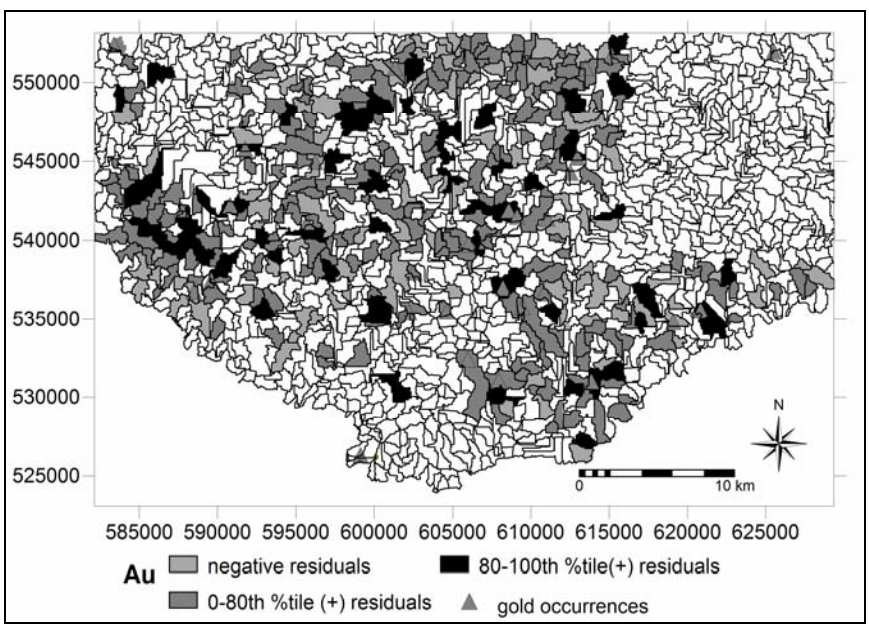

Figure 4.12: Spatial distribution of dilution-corrected Au residuals.

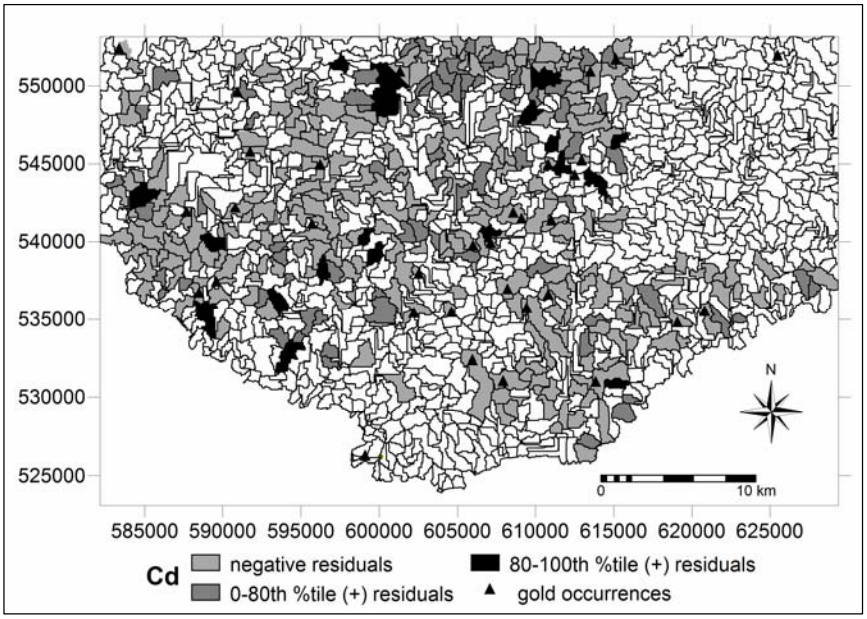

Figure 4.13: Spatial distribution of dilution-corrected Cd residuals.

4.3.13. Cadmium residuals

Most of the study area is characterized by negative Cd residuals (Figure 4.13). Most positive Cd residuals are distributed, however, in areas underlain by granitoids.

4.3.14. Antimony residuals

Most of the study area is characterized by negative Sb residuals (Figure 4.14). Most positive Sb residuals are distributed, however, in areas underlain by granitoids, especially at or near the contact zones with greenstones in the north-central parts of the study area.

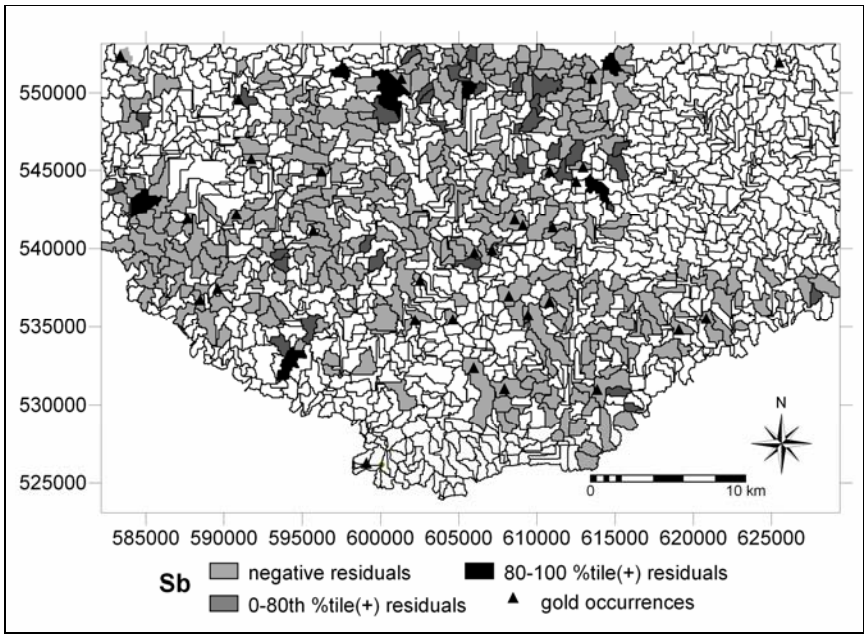

Figure 4.14: Spatial distribution of dilution-corrected Sb residuals.

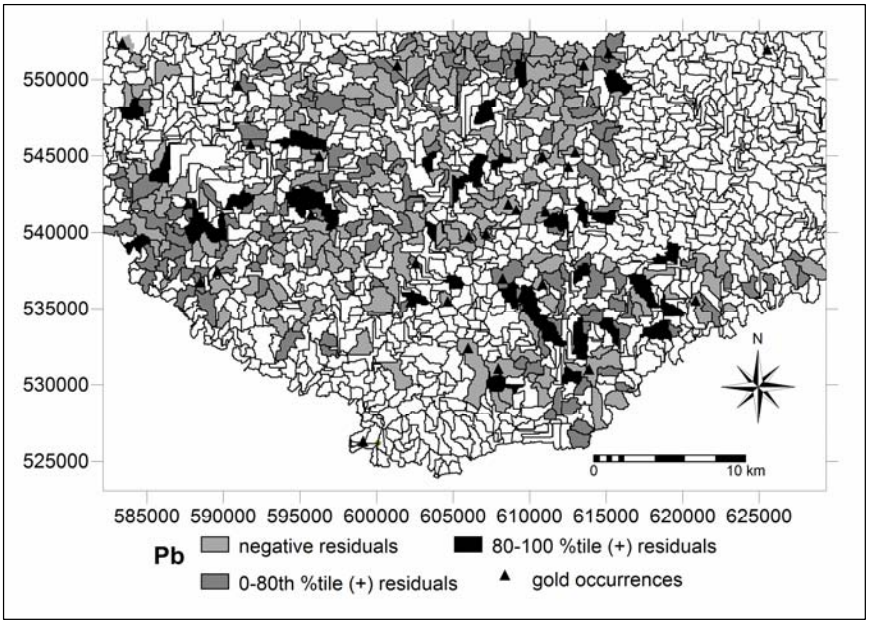

Figure 4.15: Spatial distribution of dilution-corrected Pb residuals.

4.3.15. Lead residuals

Most of the study area is characterized by negative Pb residuals and positive Au residuals below the 80th percentile (Figure 4.15). Sample catchment basins with positive Au residuals above the 80th percentile are sporadic.

4.3.16. Manganese residuals

Negative Mn residuals and positive residuals below the 85th percentile are associated mainly with catchment basins underlain by granitoids (Figure 4.16). Positive residuals of Mn above the 95th percentile are associated with catchment basins underlain by greenstone lithologies and/or containing known gold deposit occurrences.

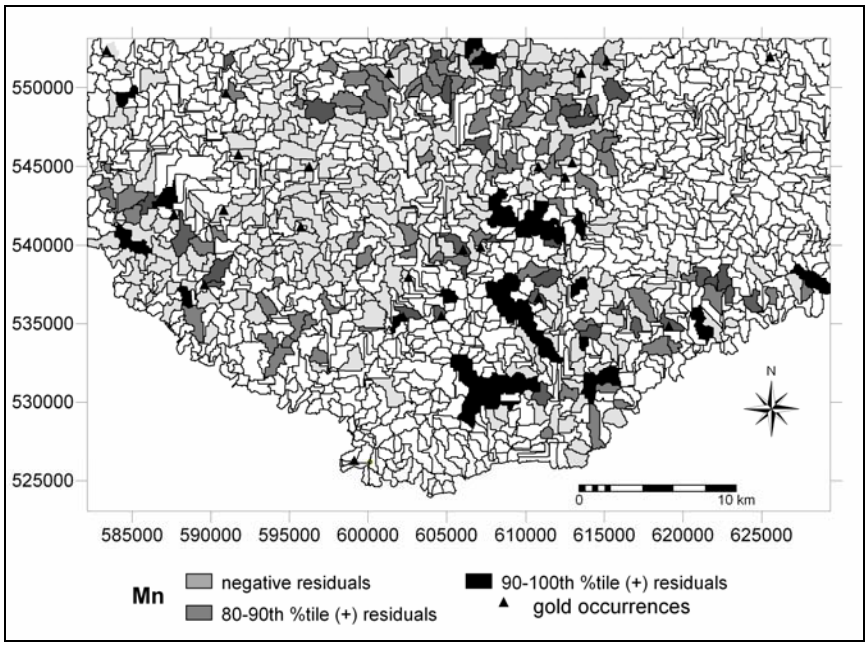

Figure 4.16: Spatial distribution of dilution-corrected Mn residuals.

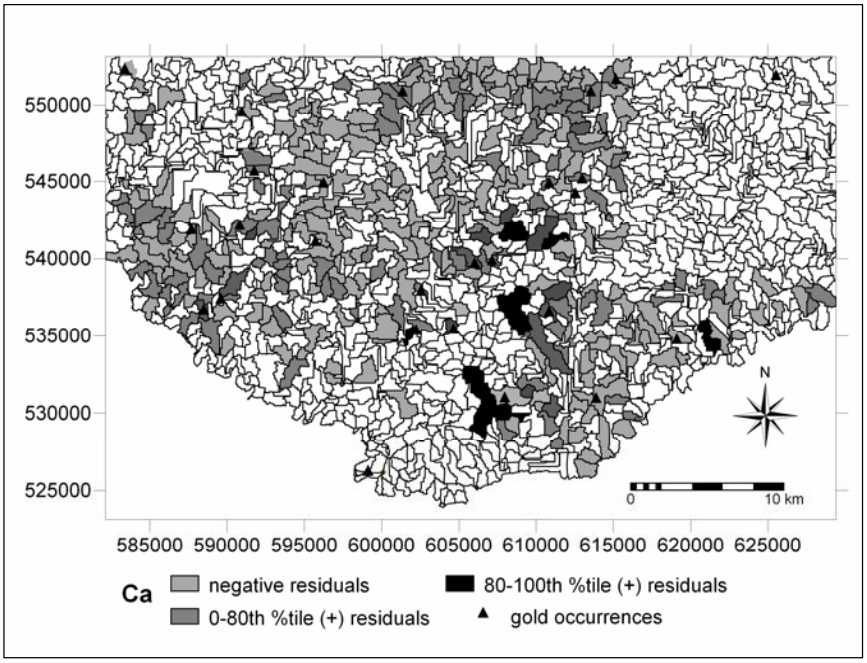

Figure 4.17: Spatial distribution of dilution-corrected Ca residuals.

4.3.17. Calcium residuals

Negative Ca residuals and positive Ca residuals below the 80th percentile are associated mainly with catchment basins underlain by granitoids (Figure 4.17). Catchment basins with Ca residuals above the 80th percentile show spatial association with greenstone lithologies.

4.3.18. Lithium residuals

The study area is characterized mainly by negative Li residuals (Figure 4.18). Catchment basins with positive residuals of Li are very few and scattered, with the range of (0-80) percentile occurring in the southwest of the study area. Most of the gold deposit occurrences are coincidental with negative residuals of Li.

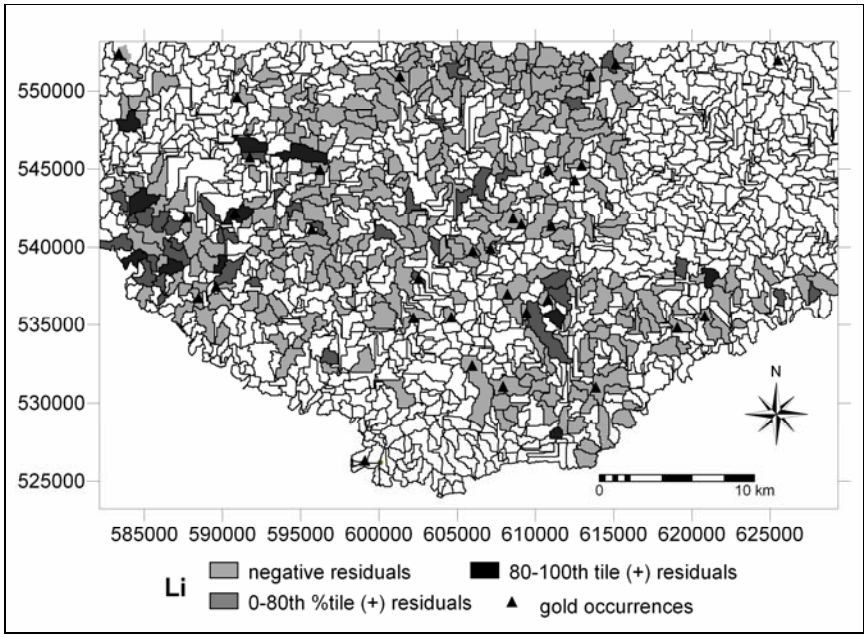

Figure 4.18: Spatial distribution of dilution-corrected Li residuals.

4.4. Concluding remarks

The derivation and dilution-correction of uni-element geochemical residuals resulted in enhancement geochemical contrast mainly between areas underlain by granitoids and areas underlain by greenstone lithologies. There are similarities in spatial distribution of some of the dilution-corrected uni-element geochemical residuals. Dilution-corrected residuals of Ni, Cu, Cr, V and Zn have similar spatial distributions; these elements seem to be enriched in areas underlain by greenstone lithologies, but seem to be depleted or 'normal' in areas underlain by granitoids. Dilution-corrected residuals of Fe, Co, Cd and Sb have similar spatial distributions; these elements do not show enrichment in almost all parts of the study area. Dilution-corrected residuals of Ba and Sr have similar spatial distributions; these elements show enrichment in granitoid terrains, especially in the southeastern part of the study area. Sample catchment basins containing the known gold deposit occurrences have high positive geochemical residuals of Cr, Ni, Co, Au, V and As, but have negative residuals of Ba, Sr, Li, Pb and Cd. In the next chapter, dilution-corrected geochemical residuals at locations of the known gold deposit occurrences will be analyzed for the classification of these mineral deposit occurrences.

Chapter 5: Classification of Gold Deposit Occurrences

5.1. Introduction

In this chapter, data sets comprising derived geochemical residuals at locations of gold deposits, presence and/or proximity to greenstones; and presence and/or proximity to faults/fractures are compiled and subjected to multivariate statistical analysis. This was done so that a spatially similar subset of gold deposit occurrences can be derived from all the known set of gold deposits using their geochemical and geological attributes. The results of the multivariate statistical analysis are interpreted in terms of gold deposit class or metallogeny.

5.2. Geochemical-geological attributes of gold deposits

Based on an earlier discussion of the general characteristics of mesothermal gold deposits in the Ashanti Belt (See Section 2.2), the following geochemical-geological attributes are considered useful for the classification of the gold deposit occurrences in the study area:

a) Geochemical signatures (Dzigbodi-Adjimah, 1992);
b) Presence and/or proximity to greenstones (Leube et al., 1990; (Loh et al., 1995);
c) Presence and/or proximity to faults/shear zones (Loh et al., 1995); (Klemd et al., 2003)

To identify multi-element association reflecting gold deposit occurrences in the South Ashanti Belt, the dilution-corrected residuals at locations of 31 gold deposit occurrences within the sampled stream sediment catchment basins were used in the multivariate statistical analysis. The minimum to maximum range of the dilution-corrected residuals were transformed to the range [0, 1] using the following equation:

$$X_{norm} = (X - X_{\min})/(X_{\max} - X_{\min}) \qquad \text{(Equation 5.1)}$$

where:

X_{norm} = transformed dilution-corrected residuals;
X = value of dilution-corrected residuals;
$X_{\min}$ = minimum value of dilution-corrected residuals;
$X_{\max}$ = maximum value of dilution-corrected residuals.

Faults and fractures play and important role in localising mineralisation. If mineralisation is structurally controlled, then gold deposit occurrences can be expected to occur at shorter distance to the controlling faults/fractures. A map of faults/fractures was compiled by digitization from existing geological maps and also from interpretations of the DEM (Figure 5.1). The map of faults/fractures was rasterized. A map portraying distances away from fault/fractures was then created. This map was used to determine distances of each of the 31 gold deposit occurrences from nearest fault/fracture. The inverse of distance of each gold deposit occurrences to faults/fractures was calculated so that high importance is given to proximity to fault/fractures. The minimum to maximum range of inverse distances of the gold deposit occurrences to faults/fractures were then transformed to the range [0, 1] using equation 5.1.

Greenstone lithologies in the South Ashanti Belt are known to be hosts of gold deposit occurrences (Loh et al. 1995). Therefore, proximity to greenstone lithologies was considered as spatial attribute at locations of gold deposit occurrences. A map of distances greenstones lithologies was thus created. This map was used to determine distances of each of the 31 gold deposit occurrences from greenstone lithologies. The minimum to maximum range of distances of the gold deposit occurrences were then transformed to the range [1,0] so that more gold deposit occurrences located within greenstone lithologies have higher weights than gold deposit occurrences located further away from greenstone lithologies.

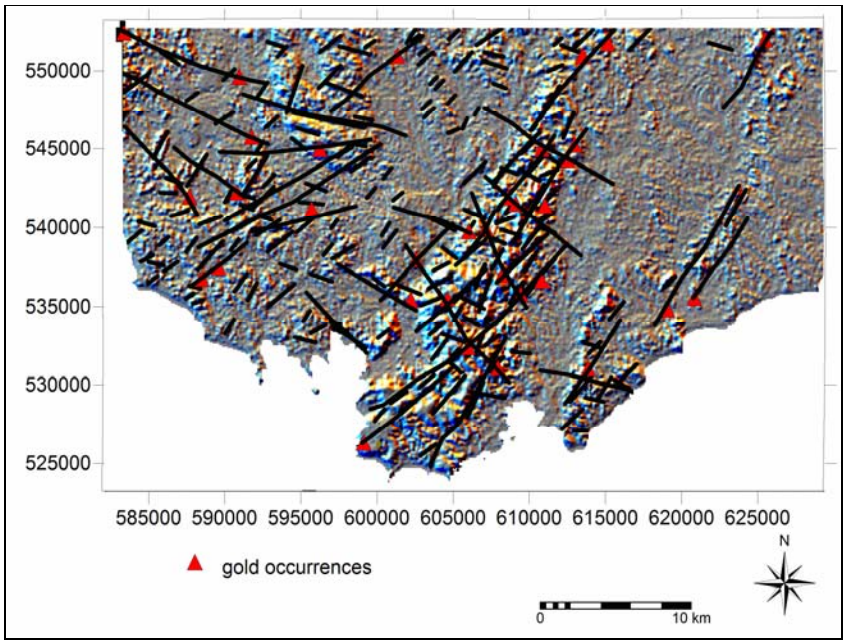

Figure 5.1: Faults and fractures interpreted from shaded-relief image of DEM of the study area.

5.3. Multivariate analysis of geochemical-geological attributes of gold deposit occurrences

The quantified geochemical-geological attributes at location of the 31 gold deposit occurrences in the South Ashanti Belt were subjected to principal component (PC) analysis in order to form uncorrelated linear combinations of the multivariate data. The first PC explains most of the variability in the data. Successive PCs explain progressively smaller portions of the variability in the data. Thus, PC analysis attempts to identify uncorrelated components that may represent different processes. In this study, each PC is interpreted in terms of gold deposit type or metallogenesis.

Table 5.1: PC analysis of geochemical-geological attributes at locations of known gold deposit occurrences.

Elements	Principal Component Loadings				
	PC1	PC2	**PC3**	PC4	PC5
Cu	0.89	0.00	-0.25	-0.06	0.31
Cr	0.87	-0.32	0.17	0.07	-0.13
Ba	0.40	0.88	-0.01	0.11	-0.16
Mn	0.51	0.69	-0.09	0.28	-0.4
V	0.99	-0.05	-0.01	0.03	0.02
Zn	0.96	0.16	0.09	0.09	0.07
Sr	-0.44	0.59	0.47	-0.32	0.17
Ni	0.96	-0.04	-0.11	0.07	0.06
Mo	-0.63	0.05	-0.02	-0.46	0.01
Au	**0.45**	0.13	**0.81**	-0.26	-0.07
Pb	-0.23	0.15	0.32	0.62	0.58
Cd	-0.81	-0.03	0.36	0.27	-0.30
Sb	-0.92	0.00	-0.01	0.35	-0.12
As	**0.80**	-0.20	0.41	0.13	-0.24
Co	0.81	0.42	-0.34	0.13	-0.05
Li	-0.87	0.00	-0.19	0.32	0.15
Ca	0.87	0.15	-0.15	-0.31	0.29
Fe	**0.88**	-0.30	0.01	0.22	-0.19
Proximity to faults/fractures	**0.74**	-0.37	**0.11**	0.06	-0.22
Proximity to greenstone lithologies	**0.57**	-0.05	**0.27**	0.17	0.79
Explained variance (%)	57.9	11.2	8.2	6.9	6.3

Table 5.1 shows the results of un-rotated component matrix of PC analysis. About 77.3% of the variations in gold deposit occurrences in the South Ashanti Belt is explained by the first three PCs. The other PCs are difficult to interpret and are therefore not discussed further.

The PC1 has positive loadings on Cu, Cr, Mn, V, Zn, Ni, Au, As, Co, Ca, Fe, as well as on proximity to faults/fractures and to greenstone lithologies. The association of As, Au and Fe reflects mineral association (gold and arsenopyrite) in the gold deposit occurrences. Its association with proximity to faults/fractures and to greenstones indicates fault/shear-zone-hosted type of gold deposits in the study area.

The PC2 accounts for at least 11% of the total variance. It is characterized by positive loadings on Ba, Mn, Zn, Sr, Mo, Au, and Ca. The PC2 has negative loadings on Cr, V, Ni, Cd, As, Co, and Fe.

The PC3 accounts for at least 8% of the total variance. The high positive loadings on Au and As reflects gold deposits in the study area. The low positive loadings on proximity to faults/fractures and to greenstone lithologies indicate that gold deposit occurrences are located farther from these geological features. Thus, the PC3 probably reflects presence of paleoplacer type of gold deposits in the study area.

Because each PC is a linear combination of multiple variables with the loadings as coefficients of the each variable, the PC(s) representing presence of gold deposit occurrences can be quantified as PC scores. Thus, for each of the 31 gold deposit occurrences, a PC1 score and a PC3 score is calculated. The magnitude of these PC scores can be considered to represent degree of membership in a deposit class. In Figure 5.2, PC1score of 0.0 shows separation between two possible type gold deposit occurrences in the study area.

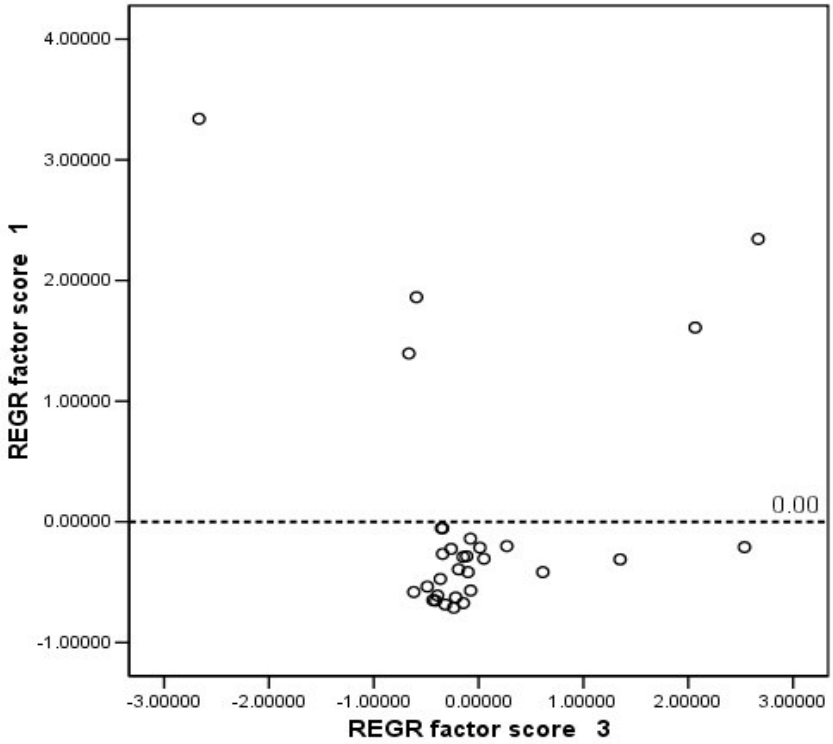

Figure 5.2: Scatter plot of PC1 scores and PC3 scores of gold deposits.

5.4. Concluding remarks

The results of geochemical-geological attribute classification of gold deposits occurrences in the South Ashanti belt show that gold deposits occurrences in the South Ashanti Belt are mainly fault/shear-zone hosted, and paleoplacer types. The results further indicate that both classes of gold deposits (i.e. faults/shear-zone hosted and paleoplacer types) are characterized by As-Fe-Ni-Cr-Cu-Au association. The first principal component (PC1) explained at least 57.9% of the total variance in

gold deposit occurrences in the study area. PC1 relates to gold deposits occurrences that are fault/shear-zone hosted and enriched in As, Fe, Cr, Ni, and Co. It is evident from the results that faults, fractures and shear zones served as channel and subsequent deposition loci of mineralising fluids. Like many fault/shear-zone hosted gold deposits in many places around the world, fracturing and faulting are of primary importance for Au transport, as well as precipitation of native gold, facilitating fluid ascent and probably rapid hydrothermal fluid degassing. The As-Fe-Ni-Cr-Cu-Au association explained by PC1 corroborates reports of spatial association of pyrite/arsenopyrite and chalcopyrite as ore minerals in some parts of the Ashanti Belt especially in the Ashanti gold mine.

The paleoplacer class of gold deposits is explained by the third principal component (PC3), which accounts for at least 8% of the variance in gold deposit occurrences in the study area. It is characterized by high positive loadings on Au and As but low positive loadings on faults and greenstones which suggest that they are at further distance away from faults/fractures systems. The fact that these paleoplacer gold deposits have As-Fe-Au associations, similar to fault/shear-zone hosted class of gold, but are located distances away from faults/fractures suggests that the paleoplacer gold deposits are derived from erosion of mineralised greenstones and fault/fracture zones. In the next chapter, gold deposit occurrences showing spatial similarity (i.e. homogeneous) as shown in Figure 5.2 will be used as training data in mineral prospectivity mapping. The results obtained from the mineral prospectivity mapping using spatially similar training data will be compared with another prospectivity map which will be generated using randomly selected training set of gold deposit occurrences.

Chapter 6: Mineral Prospectivity Mapping

6.1. Introduction

In the previous chapter, gold deposit occurrences showing similar geological attributes and geochemical signatures were derived using principal component analysis. In this chapter the derived spatially similar subset of gold deposits will be used as training data for mineral prospectivity mapping. First, deposit recognition criteria will be defined based on fault/shear-zone hosted gold deposit class. This will be followed by spatial association analysis which will attempt to quantify the association between the indicative geological features and spatially similar gold deposit occurrences using the weight-of-evidence (WofE) method (Bonham Carter, 1994; Carranza and Hale, 1999). Predictor maps are then derived from the spatial analysis and subsequently integrated to generate a prospectivity map. Another prospectivity map will be generated using randomly selected gold deposits occurrences so that the two maps can be compared.

6.2. General characteristics of mesothermal gold deposits

In the 1930's, Lindgren proposed the term 'mesothermal' to refer to epigenetic deposits formed at moderate crustal depths under temperatures in the range of about 200-300°C. Recent works have indicated the range of temperatures and pressures observed in many typical 'mesothermal' deposits goes beyond the general parameters intended by Lindgren. Groves and others (1998) have proposed a revision of terminology and classification of this broad class of lode deposits. The new terminology and classification scheme proposes to adopt the term orogenic gold deposits to refer to this broad type of deposit occurring in a variety of orogenic settings oceanic arc, back arc, accreted terranes, continental arc, back-arc extension (Figure 6.1). Mesothermal gold provinces of Phanerozoic age are characteristically associated with regional structures along which allochthonous terranes have been accreted onto continental margins or arcs. Mesothermal gold deposits, which form at temperatures above 350°C, occur along large breaks or faults in continental crust. They form at depths of 3 to 5 kilometers below the Earth's crust, and appear to be associated with the upward migration of fluids from the Earth's mantle.

6.2.1. Genetic model of gold deposits in the South Ashanti Belt

Gold deposits of Ghana display similarities with mesothermal/orogenic gold deposits (Groves, 1993, Groves et al., 1998). The Ashanti-type of gold occurrences usually features complicated quartz vein systems commonly associated with extensive disseminated sulphides. These early-stage disseminated sulphides host important amounts of gold. Late stage quartz veins and stockwork systems carry visible gold with observed accessory polymetallic sulphides (Figure 6.2). The vein systems almost invariably appear to be related to the NE regional structures (tectonic corridors), which are typically concentrated along the margins of greenstone belts (mainly basalts). The Birimian volcanic belts formed by amalgamation of juvenile island arcs and oceanic plateaus, during which structurally controlled, mesothermal lode-gold deposits were created (Leube et al. 1990; (Milesi et al. 1992). Loh et. al., 1995 have projected fault contacts along the margins of the "Cape Three Points" band of metavolcanics, and airborne digital terrain model have confirmed these NE trending regional fault structures. Satellite images also identify the presence of numerous crosscutting structures, oriented NW, and NNW (Loh et al., 1995). These deposits formed by hot water moving through rocks as the surrounding rocks were uplifted from deep (10 km) in the Earth's crust. The metals in the deposits were extracted from the surrounding rocks by dissolving trace amounts from a large volume of rocks. The metals were then deposited by sudden cooling and/or pressure change as the waters were driven by earthquakes in the Earth's crust.

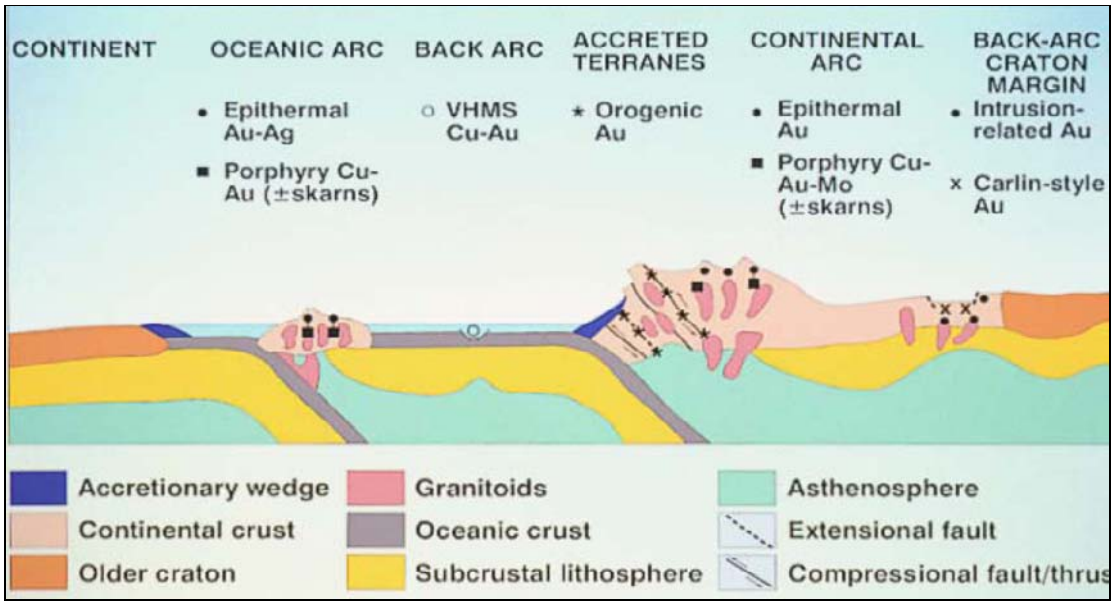

Figure 6.1: Orogenic gold deposits (after Groves et al., 1998).

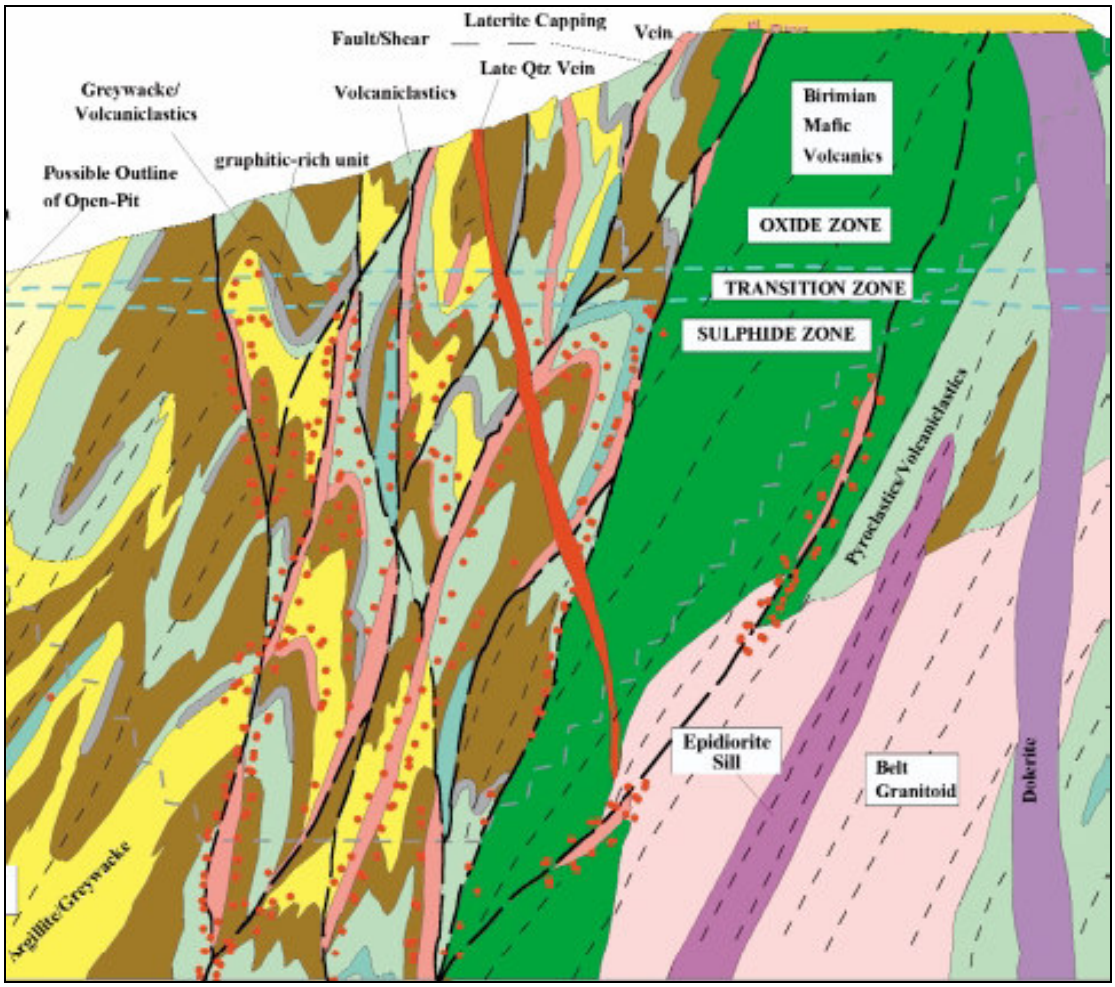

Figure 6.2: Typical Birimian gold vein/disseminated sulphide deposit (adopted from Ghana Minerals Commission, 2002).

6.2.2. Deposit recognition criteria

Based on the general characteristics of mesothermal gold deposits in the Ashanti Belt and elsewhere in the world, the following deposit recognition criteria are considered for the gold deposit in the study area which forms part of the South Ashanti Belt.

a) Host rock lithology (Loh et al., 1995); (Klemd et al., 2003)
b) Presence and proximity to faults/shear zones, (Loh et al., 1995; (Klemd et al., 2003)
c) Geochemical signatures, (Dzigbodi-Adjimah, 1992)
d) Proximity to intrusives.

The most favoured host rocks in the South Ashanti Belt are volcanoclastics units and basalts. The areas along the volcanic belt from the coastline northwards for about 25 km, which are underlain by these lithologic units, have many gold occurrences. There is strong structural control of gold mineralization in the South Ashanti Belt. Gold deposits are sited in second and third order faults and shear zones. Controlling structures range from brittle faults to ductile shear zones with low angle to high angle reverse faults (Klemd et al., 2003). The most important structural features that control gold mineralization are extensive faults and fissure zones (Dzigbodi-Adjimah, 1992). Figure 5.1 shows a shaded relief image of DEM of the study area and interpreted faults/fractures generally NE and NW orientations. Gold is accompanied by the enrichment of the trace elements As, Ag, Au, Cr, and Sb. Auriferous quartz veins are high in trace elements Zn, Cu, Fe, and As (Dzigbodi-Adjimah, 1992).

6.3. Weights-of-evidence modelling of mineral prospectivity

The weights-of-evidence approach to mineral potential mapping uses the theory of conditional probability to quantify spatial association between a set of predictor maps and a set of known mineral deposits (Bonham-Carter and Agterberg, 1990; Carranza and Hale, 1999). The spatial association is expressed in terms of weights-of-evidence for each of the predictor maps. The spatial association of each geologic feature with the mineral occurrences is represented as a binary map, the presence and absence of a predictor pattern. According to Bayes' rule the favourabilty of finding a mineral occurrence given the presence of an indicator pattern is given by:

$$P\{D|B\} = \frac{P\{D \cap B\}}{P\{B\}} = P\{D\}\frac{P\{B|D\}}{P\{B\}} \qquad \text{(Equation 6.1)}$$

where $P\{D/B\}$ is called the posterior probability. It represents the conditional posterior probability of a mineral occurrence given the presence of the indicator pattern; $P\{B\}$ is the prior probability of being in the predictor pattern.

Similarly the conditional probability of finding a mineral occurrence given of an indicator pattern by

$$P\{D|\overline{B}\} = \frac{P\{D \cap \overline{B}\}}{P\{\overline{B}\}} = P\{D\}\frac{P\{\overline{B}|D\}}{P\{\overline{B}\}} \qquad \text{(Equation6.2)}$$

where $P\{D/\overline{B}\}$ is the conditional probability of a mineral occurrence given the absence of a predictor pattern, $P\{\overline{B}\}$ is the prior probability of the area where the indicative feature is absent.

The weight-of-evidence uses odds instead of probabilities [O=P/(1-P)]. It then uses $\log_e$ odds so that evidences can be combined by addition rather than multiplication. Thus, Equation6.2 and Equation6.3 are respectively expressed as

$$O\{D|B\} = O\{D\}\frac{P\{B|D\}}{P\{\overline{B}|D\}} \qquad \text{(Equation 6.3)}$$

$$O\{D|\overline{B}\} = O\{D\}\frac{P\{\overline{B}|D\}}{P\{\overline{B}|\overline{D}\}} \qquad \text{(Equation 6.4)}$$

where $O\{D/B\}$ and $O\{D/\overline{B}\}$ are the respective conditional (posterior) odds of a mineral deposit given the presence and absence of an indicative feature, and $O\{D\}$is prior odds of a mineral deposit. The weights-of-evidence are calculated as:

$$W^{+} = \log_e \frac{P\{B|D\}}{P\{\overline{B}|D\}} \qquad \text{(Equation 6.5)}$$

$$W^{-} = \log_e \frac{P\{\overline{B}|D\}}{P\{\overline{B}|\overline{D}\}} \qquad \text{(Equation6.6)}$$

where W^+ and W^- are the weights-of-evidence when a binary pattern is present and absent, respectively. The W^+ and W^- represent unitless measures of spatial association between mineral deposits and indicator pattern. If $W^+>0$ and $W^-<0$, then it means there is positive spatial association between indicator pattern and the mineral deposits. If $W^+<0$ and $W^->0$, then it implies that there is negative spatial association between mineral deposit and indicator patterns. If $W^+=W^-=0$, then it means there is lack of spatial association between deposits and indicator pattern.

Uncertainty (in terms of variance) of the weights can be calculated by the following expressions,

$$s^2(W^+) = \frac{1}{N\{B \cap D\}} + \frac{1}{N\{B \cap \overline{D}\}} \qquad \text{(Equation 6.7)}$$

$$s^2(W^-) = \frac{1}{N\{\overline{B} \cap D\}} + \frac{1}{N\{\overline{B} \cap \overline{D}\}} \qquad \text{(Equation 6.8)}$$

The spatial contrast, C, is calculated as:

$$C = W^+ - W^- \qquad \text{(Equation 6.9)}$$

The difference of the weights-of-evidence is a measure of overall spatial association, C, between indicator pattern and mineral deposits. If $C>0$, then there is positive spatial association. If $C<0$, then there is negative spatial association between indicator patterns and the mineral deposits. The maximum contrast is useful for determining the cut off distance buffer at which there exist optimal association between linear or polygonal feature mineral deposits.

The standard deviation of C is calculated as

$$s(C) = \sqrt{s^2(W^+) + s^2(W^-)} \qquad \text{(Equation6.10)}$$

Another useful measure is to calculate the studentized value of the contrast, which is a measure of the certainty with which the contrast is known. The studentized C denoted as sigC, is defined as the ratio of C to its standard deviation, $C/s(C)$. This ratio serve to test that spatial association is likely to be real. If sigC>1.96, then it indicates that C is statistically significant (Bonham Carter et al., 1989).

Using the log-odds formulation of Bayes' rule, two or more binary predictor maps can be combined to generate a predictor map using the expression

$$\log_e\{D|B_1^k \cap B_2^k \cap B_3^k ....B_n^k\} = \sum_{j=1}^{n} W_j^k + \log_e O\{D\} \qquad \text{(Equation 6.12)}$$

where the superscript k is positive (+) or negative (-) if the binary predictor pattern is present or absent respectively. A requirement of the Bayes' rule is that all input maps should be conditionally independent of one another with respect to the gold deposit occurrences. If this rule is violated then the resultant map (predictive map) will be biased and over-estimate posterior probability of gold deposit occurrence. The following relation is satisfied if two or more binary predictor maps are conditionally independent.

$$N\{B_1 \cap B_2 \cap D\} = \frac{N\{B_1 \cap D\} \times N\{B_2 \cap D\}}{N\{D\}} \qquad \text{(Equation 6.13)}$$

The left hand side of Equation 13 is the observed number of gold deposit occurrences in the overlap zone of B_1 and B_2. The right hand side is the predicted number of gold deposit occurrences in this overlap zone. A contingency table calculation is used to test the conditional independence of the two binary maps. The chi-square value is then calculated to test the null hypothesis of conditional independence.

$$\chi^2 = \sum_{i=1}^{4} \frac{(observed_i - predicted_i)^2}{predicted_i} \qquad \text{(Equation 6.14)}$$

In prospectivity mapping, where the prior probability is assumed to be the average known deposit point density, an overall test of conditional independence can be applied to determine the total number of predicted deposit points after combining the binary predictor map patterns. The predicted number of occurrences $N\{D\}_{pred}$ can be calculated as the sum of the products of the number of pixels, $N\{A\}$ and their posterior probabilities, P, for all pixels on the map, thus

$$N\{D\}_{pred} = \sum_{k=1}^{m} P_k \times N\{A\}_k \qquad \text{(Equation 6.15)}$$

where there are k=1,2,…m pixels in the posterior probability map. If $N\{D\}_{pred}$ is 10-15% larger than the observed number (i.e., 26 in this case), then the assumption of conditional independence is violated (Bonham-Carter, 1994).

6.4. Gold prospectivity mapping using training set of spatially similar gold deposit occurrences

Spatial data analysis is the process of seeking out patterns and association on maps that help to characterize, understand and predict spatial phenomena (Bonham-Carter, 1994). The occurrence of mineral deposit is not random, their occurrence are linked to favourable geological features. The spatial associations of geologic features and mineral occurrence have to be quantified before data integration. The quantified spatial association illustrates the behavior of each geologic feature with the mineral occurrences. The spatial association between mineral deposit occurrences and geological features such as faults may serve as important geological indicators of mineralization. In this study, 26 gold deposit occurrences found to have similar geochemical-geological attributes were used as training data in the spatial association analysis and in the subsequent mineral prospectivity mapping. The other five gold deposit occurrences were used for predictive model validation.

6.4.1. Spatial association between training set of spatially similar gold deposit occurrences and northeast-trending faults/fractures.

The spatial associations of northeast trending faults are quantified by the weights-of-evidence method. The results of cumulative buffer distances of 255, 428, 625, 842, 1111, 1453, 1916, 2617, 4253, 11310 m, which were crossed with spatially similar gold deposit occurrences is shown in Table 6.1. The contrast, C, in Table 6.1 shows that there is positive spatial association between northeast trending faults/fractures and the spatially similar gold deposit occurrences. The cumulative distance within which there is optimal spatial association between the spatially similar gold deposit occurrences and the northeast-trending faults/fractures is 1453 m. A binary map (Figure 6.3, left panel) depicting zones within 1453 m of northeast trending fault is considered an optimal predictor map for gold mineralization in the study area.

6.4.2. Spatial association between training set of spatially similar gold deposit occurrences and northwest-trending faults/fractures.

Cumulative buffer distances of 353, 787, 1235, 1690, 2180, 2726, 3391, 4360, 6629, and 14159 m were used to create binary patterns of northwest trending faults/fractures. The results of the analysis are shown in Table 6.2. The results show that there is positive spatial association between northwest-trending faults/fractures and the spatially similar gold deposit occurrences. The contrast, C, indicates that the cumulative distance at which there is optimal spatial association between northwest-trending faults/fractures and the spatially similar gold deposit occurrences is 2062 m. The values of W^+ and W within 2062 m are statistically different from zero. Thus, the northwest-trending faults/fractures were buffered at 2062 m and considered optimal predictor map based on C. The binary predictor patterns of NW trending faults is shown in (Figure 6.3, right panel).

Table 6.1: Variation of weights and contrasts for cumulative distances from northeast-trending faults/fractures with respect to training set of spatially similar gold deposit occurrences.

Dist (m)	npixb	npixpd	W^+	$s(W^+)$	W^-	$s(W^-)$	C	$s(C)$	sigC
235	163113	4	0.454	0.50	-0.064	0.213	0.518	0.518	1.0
428	163414	6	0.165	0.408	-0.045	0.224	0.210	0.419	0.5
625	173407	10	0.250	0.316	-0.130	0.250	0.379	0.422	0.9
842	167641	16	0.431	0.250	-0.445	0.316	0.876	0.398	2.2
1111	165626	20	0.432	0.224	-0.775	0.408	1.207	0.464	2.6
1453	166426	24	0.433	0.204	-1.651	0.707	2.084	0.744	2.8
1916	168621	25	0.317	0.200	-2.051	1.000	2.372	1.031	2.3
2617	171585	25	0.180	0.200	-1.634	1.000	1.815	1.008	1.8
4253	162472	26	0.105	0.196	?	?	?	?	?
11310	166579	26	0.000	0.1961	?	?	?	?	?

npixb = number of pixels in every cumulative proximity class.
npixpd = number of pixels in a cumulative class with gold deposit occurrences

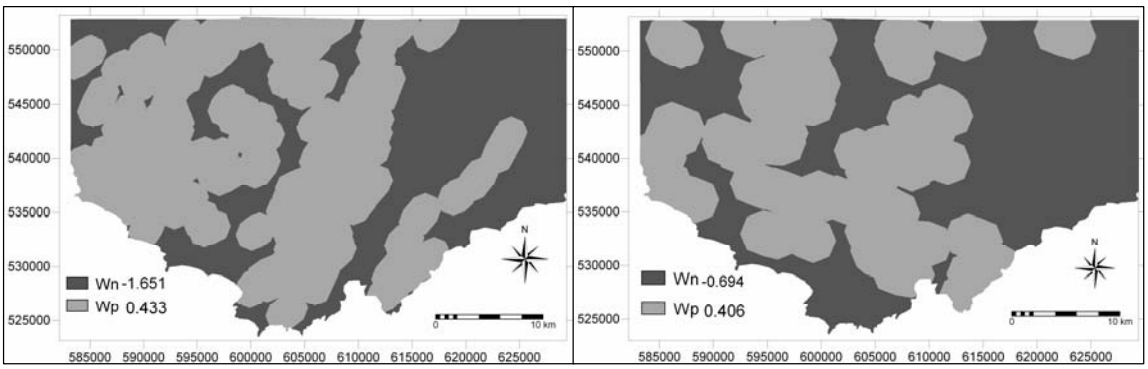

Figure 6.3: Binary predictor pattern of NE-trending faults/fractures (left panel) and NW-trending faults/fractures (right panel).

Table 6.2: Variation of weights and contrasts for cumulative distances from northwest-trending faults/fractures with respect to training set of spatially similar gold deposit occurrences.

Dist (m)	npixb	npixpd	W^+	$s(W^+)$	W^-	$s(W^-)$	C	$s(C)$	sigC
504	165203	4	0.521	0.500	-0.078	0.224	0.599	0.728	1.1
890	168607	9	0.629	0.333	-0.247	0.258	0.875	0.725	2.1
1249	166702	13	0.424	0.302	-0.257	0.277	0.681	0.733	1.7
1625	167060	16	0.377	0.267	-0.365	0.316	0.742	0.732	1.8
2062	166308	20	0.406	0.236	-0.694	0.408	1.100	0.722	2.3
2601	166541	21	0.278	0.229	-0.654	0.447	0.931	0.730	1.9
3291	167743	26	0.357	0.204	?	?	?	0.729	?
4423	166736	26	0.223	0.204	?	?	?	0.713	?
7060	167076	26	0.105	0.204	?	?	?	0.977	?
15500	166908	26	0.000	0.204	?	?	?	?	?

npixb = number of pixels in every cumulative proximity class.
npixpd = number of pixels in a cumulative class with gold deposit occurrences

6.4.3. Spatial association between training set of spatially similar gold deposit occurrences and greenstone lithologies

The variations in contrast *C* for cumulative distances of 284, 769, 1340, 1988, 2705, 3479, 4544, and 8240 m from greenstone lithologies (as host rocks) with respect to spatially similar gold deposit occurrences are shown in Table 6.3. The contrast *C* shows that the cumulative distance at which there is optimal spatial association between the greenstone lithologies and the spatially similar gold deposit occurrences is 284 m. Thus, a binary map of zero to 284 m from greenstone lithologies is an optimum predictor map. Figure 6.4 (left panel) shows areas within and 284 m away from greenstone lithologies

are assigned a weight of 0.862 and areas 284 m beyond the greenstone lithologies are assigned a weight of -0.877.

Table 6.3: Variation of weights and contrasts for cumulative distances from greenstone lithologies with respect to training set of spatially similar gold deposit occurrences.

Dist (m)	npixb	npixpd	W^+	$s(W^+)$	W^-	$s(W^-)$	C	$s(C)$	sigC
284	499356	19	0.862	0.243	-0.877	0.378	1.738	0.4	3.9
769	165833	0	?	?	?	?	?	?	?
1340	168684	20	-0.886	1.000	0.064	0.209	-0.950	1.1	-0.9
1988	166254	21	-0.872	1.000	0.062	0.209	-0.934	1.0	-0.9
2705	168590	22	-0.886	1.000	0.064	0.209	-0.950	1.1	-0.9
3479	166540	23	-0.873	1.000	0.063	0.209	-0.936	1.0	-0.9
4544	166754	24	-0.875	1.000	0.063	0.209	-0.937	1.0	-0.9
8240	166873	26	-0.182	0.707	0.018	0.213	-0.201	0.7	-0.3

npixb = number of pixels in every cumulative proximity class.
npixpd = number of pixels in a cumulative class with gold deposit occurrences

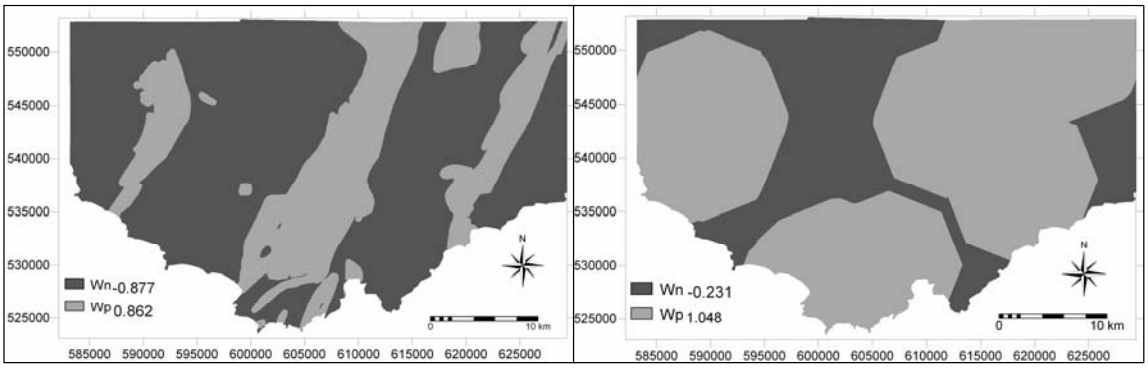

Figure 6.4: Binary predictor patterns of greenstone lithologies as host rocks (left panel) and heat source rocks

6.4.4. Spatial association between training set of spatially similar gold deposit occurrences and granitoids

Cumulative buffer distances of 1219, 2255, 3121, 3938, 4737, 5579, 6498, 7495, 8866, and 13740 m were used to create binary patterns of presence of proximity to granitoid intrusives as heat source rocks. The results of spatial association analysis between spatially similar training set of gold occurrences and heat source rocks are shown in Table 6.4. The results indicate that the cumulative distance at which there is optimal spatial association between the training set of spatially similar gold deposit occurrences and heat source rocks is 6498 m. A binary predictor pattern based on the heat source rocks was created using the weights 1.048 for distances within 6498 m and -0.231 for distances beyond 6498 m. Figure 6.5 (right panel) shows the resulting binary predictor pattern.

6.4.5. Spatial association between training set of spatially similar gold deposit occurrences and favourable geochemical signature

Table 6.5 shows that there is optimum positive spatial association between the training set of spatially similar gold deposit occurrences and the $\geq 90^{th}$ percentile PC1 scores representing favourable geochemical signature. This means that stream sediment sample catchment basins with $\geq 90^{th}$ percentile PC1 scores are anomalous for fault/shear-zone hosted gold deposits. Figure 6.6 shows the resulting binary predictor pattern.

Table 6.4: Variation of weights and contrasts for cumulative distances from granitoid intrusives with respect to training set of spatially similar gold deposit occurrences.

Dist (m)	npixb	npixpd	W^+	$s(W^+)$	W^-	$s(W^-)$	C	$s(C)$	sigC
1219	166336	0	?	?	0.105	0.218	?	?	?
2255	167502	4	0.353	0.577	-0.048	0.236	0.401	0.7	0.6
3121	165869	6	-0.043	0.707	0.005	0.229	-0.047	0.5	-0.1
3938	167626	10	0.352	0.577	-0.048	0.236	0.401	0.7	0.6
4737	166569	11	-0.740	1.000	0.056	0.224	-0.796	1.0	-0.8
5579	166424	12	-0.739	1.000	0.056	0.224	-0.796	1.0	-0.8
6498	167204	19	1.048	0.408	-0.231	0.258	1.279	0.5	2.6
7495	167369	21	-0.052	0.707	0.006	0.229	-0.057	0.6	-0.1
8866	166946	22	-0.742	1.000	0.057	0.224	-0.799	1.0	-0.8
13740	167039	26	-0.050	0.707	0.005	0.229	-0.055	0.6	-0.1

npixb = number of pixels in every cumulative proximity class.
npixpd = number of pixels in a cumulative class with gold deposit occurrences

Table 6.5: Variation of weights and contrasts for percentile classified geochemical signature with respect to spatially similar sets of gold deposits.

Percentile of PC1 scores	npixb	npixpd	W^+	$s(W^+)$	W^-	$s(W^-)$	C	$s(C)$	sigC
<50	1267825	0	?	?	1.505	0.229	?	?	?
50-60	35592	2	0.880	1.000	-0.032	0.236	0.912	1.01289	0.9
60-70	81156	5	0.055	1.000	-0.003	0.236	0.058	0.58300	0.1
70-80	81428	9	0.745	0.707	-0.060	0.243	0.805	0.73191	1.1
80-90	81174	13	0.748	0.707	-0.060	0.243	0.808	0.73482	1.1
90-100	82443	26	2.605	0.277	-1.101	0.408	3.706	0.49407	7.5

npixb = number of pixels in every cumulative proximity class.
npixpd = cumulative number of pixels in a cumulative class with gold deposit occurrences

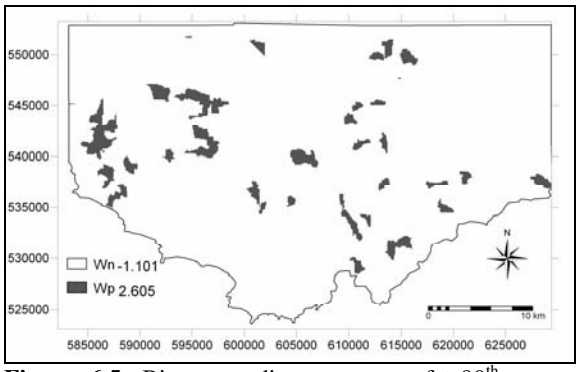

Figure 6.5: Binary predictor pattern of ≥90th percentile PC1 scores representing anomalous geochemical signatures.

6.4.6. Summary of weight-of-evidence results

Table 6.6 shows that among the binary evidence maps the binary map of ≥90th percentile PC1 scores is most statistically significant spatial evidence of gold deposit occurrence in the study area. The presence and proximity to greenstone lithologies is the second most statistically significant spatial evidence of gold deposit occurrence. The presence and proximity to NE-trending faults/fractures is a more statistically significant spatial evidence of gold deposit occurrence than the presence and proximity to NW-trending faults/fractures. The results also show that proximity to granitoid intrusives is a statistically significant spatial evidence of gold deposit occurrence.

Table 6.6: Summary of analysis of spatial associations between geologic features and spatially similar gold deposit occurrences.

Evidence maps	W^+	W^-	**sigC**
Geochemical signature	2.605	-1.101	7.5
Host rocks	0.862	-0.877	3.9
NE-trending faults	0.433	-1.651	2.8
Heat source rocks	1.048	-0.231	2.6
NW-trending faults	0.406	-0.694	2.3

6.4.7. Gold prospectivity map based on training set of spatially similar gold deposit occurrences

The binary predictor maps are integrated to generate a posterior probability map of gold deposit occurrence using equation 6.12, which can also be written as

$$\text{Predmap} = \exp\frac{(-10.639 + wthstrx + wtgeoch + wtheat + wtne + wtnw}{(1 + \exp(-10.639 + wthsrx + wtgeoch + wtheat + wtne + wtnw)} \qquad \text{(Equation 6.16)}$$

where the value -10.639 is the $\log_e O\{D\}$ and $O\{D\}$is the prior odds of gold deposit occurrences of 0.000024. The *wthstrx*, *wtgeoch*, *wtheat*, *wtne*, and *wtnw* are the binary predictor patterns for host rocks, geochemical signatures, heat source rocks, NE-trending and NW-trending fault/fractures respectively.

To validate usefulness of a posterior probability map of gold deposit occurrence prospectivity map in terms of guiding future exploration activities towards other potentially mineralized zones, overall test of conditional independence was performed and three other parameters were determined. Overall test of conditional independence using equation 6.15 determines whether or not resulting posterior map violates the assumption of conditional independence among the input predictors by comparing the number of predicted gold deposits with the number of gold deposit occurrences in the training set. Binary predictor maps which produce bias and over-estimate the observed number of gold deposit occurrences are then rejected. Success rate was calculated as the percentage of spatially similar gold deposit occurrences delineated correctly within mapped potential zones. If the training set is considered as "discovered" deposits, then the prospectivity map should accurately delineate a large proportion of all these deposits. Prediction rate was calculated as the percentage of "undiscovered" gold deposit occurrences (i.e., those not used in weight-of-evidence calculation) delineated correctly within delineated prospective zones. Proportion of mapped potential zones was also determined to show if the predictive model effectively reduces size of target exploration zones where further search for undiscovered gold deposits can be undertaken.

6.4.7.1. Overall test of conditional independence

The gold posterior probability map based on the combination of *wthsrx+wtgeoch+wtheat+wtne+wtnw* satisfied the conditional rule. This is, because, the number of predicted gold deposits which is 626.5, is not more than 15% greater than the number of gold deposits used in the weight-of-evidence calculation which is 624.7. The posterior probability map based on the combination of *wthsrx+wtgeoch+wtheat+wtne+wtnw* is considered statistically valid and will be used to create and validate the mineral potential map. The posterior probability map was then converted into a binary gold prospectivity map (Figure 6.6) using estimate of prior probability of gold deposit occurrence as threshold.

6.4.7.2. Success rate, prediction rate, proportion of potential zones

The posterior probability map was classified into binary map showing favourable zones reflecting mineral potential. Posterior probability values less than 0.00002 (the prior probability of finding a gold deposit) were classified as non-potential zones and values greater than 0.00002 classified as potential zones. The prospectivity map (Figure 6.6) has a success rate of 96% for predicting 25 out 26 of the spatially similar training set gold deposits. The predictive rate of the map is 80% as it is able to predict all the validation gold deposits. The search area delineated by the prospectivity map as potential zones is 30%.

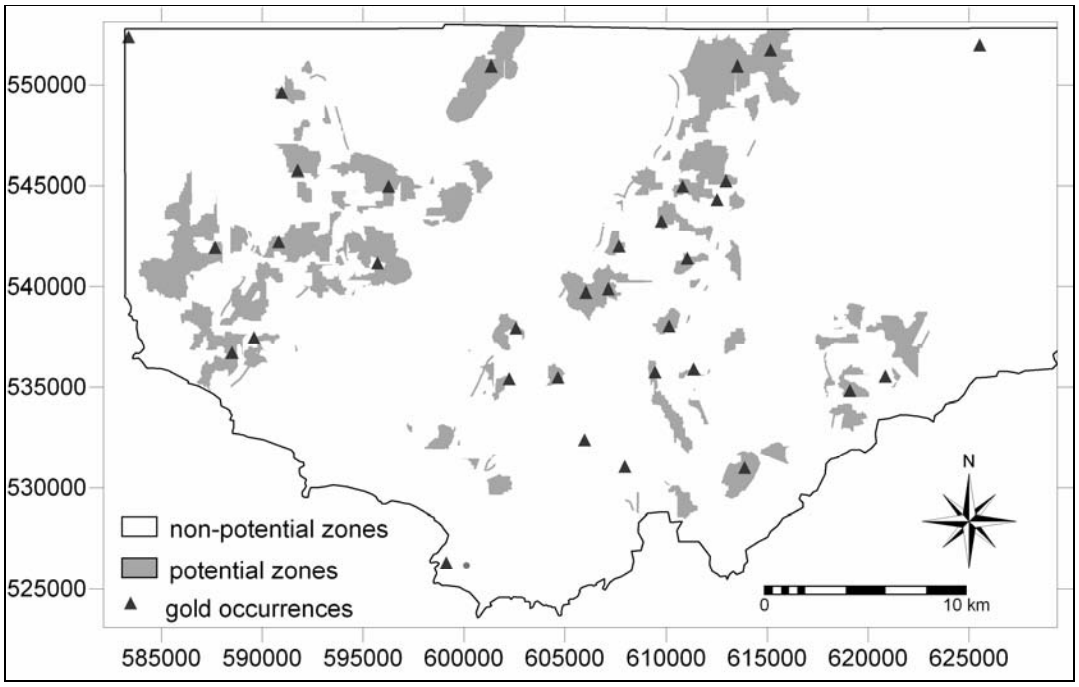

Figure 6.6: Gold prospectivity map of South Ashanti belt based on spatially similar gold deposit occurrences.

6.5. Gold prospectivity mapping using randomly selected gold deposit occurrences

There are 31 gold deposit occurrences in the study area out of which 21 were randomly selected and used as training data for the mineral prospectivity mapping, and the remainder was used for validation. The same indicative geological features used with the spatially similar gold deposit occurrences are used with the randomly selected gold deposits. The indicative features are northeast-trending faults, northwest-trending faults, host rocks, geochemical signatures and heat source rocks.

6.5.1. Spatial association between training set of randomly selected gold deposit occurrences and northeast-trending faults/fractures

The spatial associations of northeast trending faults are quantified by the weights-of-evidence method. The results of cumulative buffer distances of 235, 428, 625, 842, 1111, 1453, 1916, 2617, 4253, and 11310 m which were crossed with randomly selected gold deposit occurrences is shown in Table 6.7. The contrast, C, in Table 6.7 shows that there is a positive spatial association between northeast trending faults/fractures with randomly selected gold deposits at a distance of 842m and beyond. The studentized C, *s(C)*, however, shows that this positive spatial association between the randomly selected gold deposits and the northeast trending faults is not statistically significant. A binary map (Figure 6.7, left panel) depicting zones within 1916 m of northeast trending fault is considered optimal predictor map for gold mineralization in the study area.

6.5.2. Spatial association between training set of randomly selected gold deposit occurrences and northwest-trending faults/fractures

Cumulative buffer distances of 504, 890, 1249, 1625, 2062, 2601, 3291, 4423, 7060, and 15500 m were used to create binary patterns of northwest trending faults/fractures. The results of the analysis are shown in Table 6.8. There is negative spatial association between northwest-trending faults/fractures with randomly selected gold deposit occurrences within cumulative distances of 890 and 1249 m interval. The contrast *C* indicates that the cumulative distance at which there is optimal spatial association between northwest trending faults and gold deposits is 3291 m although the contrast, *C,* is not statistically significant. The values of W^+ and W^- within 3291 m are not statistically

different from zero. The binary predictor patterns of NW trending faults buffered at cumulative distance of 3291m is shown in (Figure 6.7, right panel).

Table 6.7: Variation of weights and contrasts for cumulative distances from northeast trending faults/fractures with respect to randomly selected training sets of gold deposits.

Dist (m)	npixb	npixpd	W^+	$s(W^+)$	W^-	$s(W^-)$	C	$s(C)$	sigC
235	163113	2	0.185	0.707	-0.022	0.258	0.208	0.3	0.7
428	163414	2	-0.509	0.707	0.093	0.2582	-0.601	-0.8	0.8
625	173407	3	-0.018	0.447	0.008	0.289	-0.026	0.0	?
842	167641	7	0.163	0.354	-0.125	0.333	0.288	0.6	0.5
1111	165626	10	0.164	0.316	-0.196	0.378	0.360	0.7	0.5
1453	166426	12	0.164	0.289	-0.310	0.447	0.474	0.9	0.5
1916	168621	17	0.232	0.258	-0.936	0.707	1.168	1.6	0.7
2617	171585	19	0.094	0.258	-0.516	0.707	0.611	0.8	0.8
4253	162472	20	0.045	0.250	-0.529	1.000	0.573	0.6	1.0
11310	166579	21	0.000	0.243	?	?	?	?	?

npixb = number of pixels in every cumulative proximity class.
npixpd = number of pixels in a cumulative class with gold deposit occurrences

Table 6.8: Variation of weights and contrasts for cumulative distances from northwest trending faults/fractures with respect to randomly selected gold deposits.

Dist (m)	npixb	npixpd	W^+	$s(W^+)$	W^-	$s(W^-)$	C	$s(C)$	sigC
504	165203	2	0.173	0.707	-0.021	0.258	0.194	0.647	0.3
890	168607	5	-0.125	0.577	0.029	0.267	-0.154	0.770	-0.2
1249	166702	6	-0.243	0.500	0.088	0.277	-0.331	0.552	-0.6
1625	167060	8	0.029	0.378	-0.020	0.316	0.049	0.490	0.1
2062	166308	14	0.259	0.301	-0.349	0.408	0.608	0.507	1.2
2601	166541	15	0.163	0.289	-0.309	0.447	0.472	0.524	0.9
3291	167743	15	0.163	0.267	-0.531	0.577	0.693	0.630	1.1
4423	166736	17	0.029	0.267	-0.126	0.577	0.155	0.775	0.2
7060	167076	19	0.045	0.250	-0.531	1.000	0.575	0.958	0.6
15500	166908	21	0.000	0.243	?	?	?	?	?

npixb = number of pixels in every cumulative proximity class.
npixpd = number of pixels in a cumulative class with gold deposit occurrences

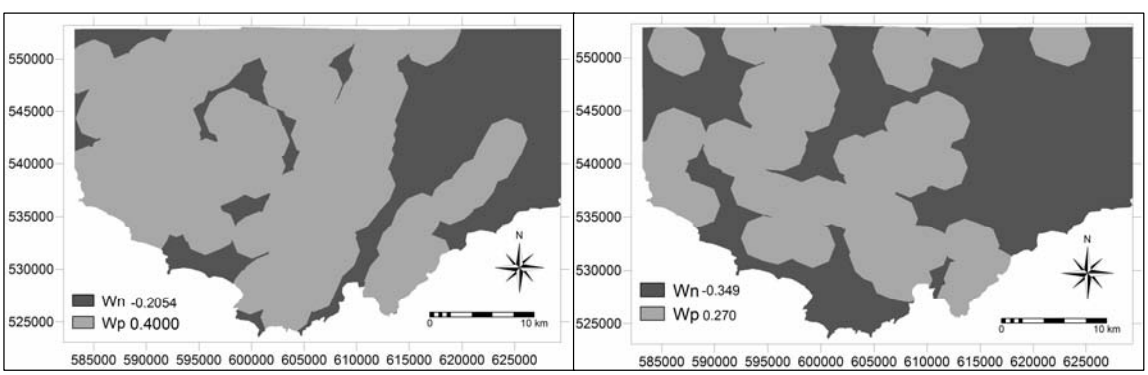

Figure 6.7: Binary predictor pattern of NE-trending faults (left panel) and NW trending faults (right panel).

6.5.3. Spatial association between training set of randomly selected gold deposit occurrences and host rocks

The variations in contrast, *C,* for cumulative distances of 284, 769, 1340, 1988, 2705, 3479, 4544, and 8240 m from host rocks with respect to randomly selected gold deposit occurrences are shown in Table 6.9. The contrast C indicates that there is a negative spatial association between host rocks and

the randomly selected gold deposit occurrences within cumulative distances of 1340 m and beyond. At cumulative distance of 769 m there is a positive spatial association between the host rocks and the gold deposit. A binary map with zones less than 769 m from host rocks is considered an optimum predictor map. Figure 6.8, left panel, shows the binary predictor patterns of host rocks where zones within 769 m are assign a weight of 1.760 and those beyond -0.296.

Table 6.9: Variation of weights and contrasts for cumulative distances from host rocks with respect to randomly selected gold deposits.

Dist (m)	npixb	npixpd	W^+	$s(W^+)$	W^-	$s(W^-)$	C	$s(C)$	sigC
284	499356	4	-0.115	0.500	0.045	0.302	-0.160	0.533	-0.3
769	165833	8	0.700	0.577	-0.118	0.289	0.818	0.629	1.3
1340	168684	10	-0.416	1.000	0.038	0.267	-0.454	1.135	-0.4
1988	166254	14	0.291	0.707	-0.038	0.277	0.329	0.823	0.4
2705	168590	16	-0.416	1.000	0.038	0.267	-0.454	1.135	-0.4
3479	166540	18	-0.403	1.000	0.036	0.267	-0.439	1.098	-0.4
4544	166754	20	-0.405	1.000	0.036	0.267	-0.441	1.103	-0.4
8240	166873	25	0.288	0.707	-0.038	0.277	0.326	0.815	0.4

npixb = number of pixels in every cumulative proximity class.
npixpd = cumulative number of pixels in cumulative proximity classes with gold deposit occurrences

6.5.4. Spatial association between training set of randomly selected gold deposit occurrences and heat source rocks.

Cumulative buffer distances of 1219, 2255, 3121, 3938, 4737, 5579, 6498, and 7495 m, were used for the analysis of spatial association between heat source rocks and randomly selected gold deposit occurrences. The results which are shown in Table 6.10 indicate that there is a negative spatial association between the randomly selected gold deposit occurrences and heat source rocks at cumulative distance of 3121 m and beyond. Even though there is a positive spatial association between heat source rocks and the randomly selected gold deposit occurrences within a cumulative distance of 2255 m, the values of W^+ and *sigC* within this cumulative distance are not statistically significant. A binary predictor pattern based on the heat source rocks was created using the weights 1.109 for distances within 2255m and -0.252 for distances beyond 2255m. Figure 6.8, right panel shows the resulting binary predictor pattern.

Table 6.10: Variation of weights and contrasts for cumulative distances from heat source rock with respect to randomly selected gold deposits.

Dist (m)	npixb	npixpd	W^+	$s(W^+)$	W^-	$s(W^-)$	C	$s(C)$	sigC
1219	166336	3	0.632	0.577	0.105	0.277	?	?	?
2255	167502	7	0.219	0.707	-0.048	0.267	0.247	0.823	0.3
3121	165869	8	-0.464	1.000	0.005	0.258	-0.504	1.008	-0.5
3938	167626	9	-0.474	1.000	-0.048	0.258	-0.515	1.030	-0.5
4737	166569	11	-0.468	1.000	0.056	0.258	-0.509	1.018	-0.5
5579	166424	12	-0.467	1.000	0.056	0.258	-0.508	1.016	-0.5
6498	167204	15	0.221	0.707	-0.231	0.267	0.249	0.830	0.3
7495	167369	19	0.220	0.707	0.006	0.267	0.248	0.827	0.3
8866	166946	21	-0.470	1.000	0.057	0.258	-0.511	1.022	-0.5

npixb = number of pixels in every cumulative proximity class.
npixpd = cumulative number of pixels in cumulative proximity classes with gold deposit occurrences

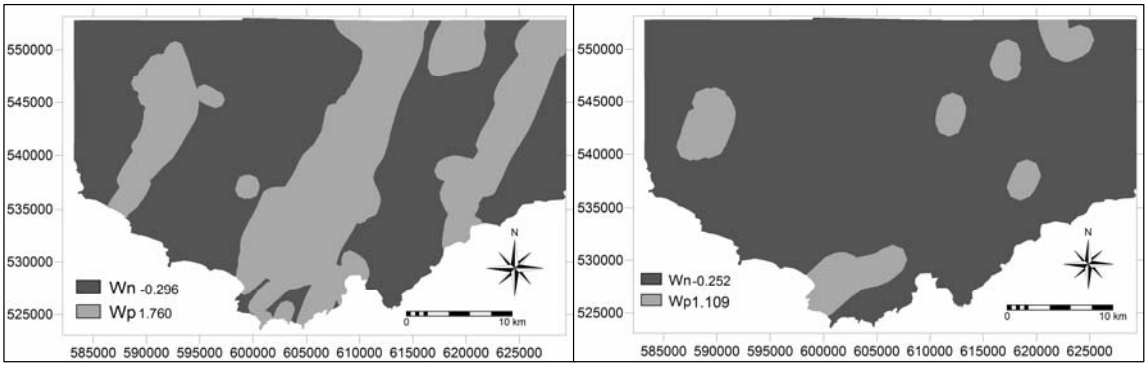

Figure 6.8: Binary predictor patterns of host rocks and heat source rocks

6.5.5. Spatial association between training set of randomly selected gold deposit occurrences and geochemical signatures

Table 6.11 shows that there is a positive spatial association between the randomly selected gold deposit occurrences and the geochemical signatures at 60th percentile and above. There is a strong and statistically significant positive spatial contrast (i.e., sigC>2) at 90th percentile and above. Thus, the percentile class above which there is optimal positive spatial association between the randomly selected gold deposits and favourable geochemical signatures (see section 5.3) is 90. This means that catchment basins with ≥90th percentile PC1 score are the zones with favourable geochemical signatures for gold mineralisation. Figure 6.9 shows the resulting binary predictor pattern where the weight of 1.760 is assigned to catchment basins with ≥90th and -0.296 assigned to catchment basins with less than 90th percentile score of PC1.

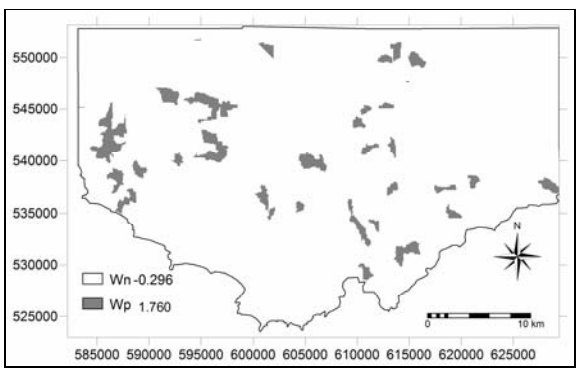

Figure 6.9: Binary predictor patterns of geochemical signatures.

Table 6.11: Variation of weights and contrasts for percentile classified geochemical signature with respect to randomly selected gold deposits.

Percentile of PC1 scores	npixb	npixpd	W^+	$s(W^+)$	W^-	$s(W^-)$	C	$s(C)$	sigC
<50	1267825	4	-0.928	0.500	1.137	0.333	-2.065	0.607	-3.4
50-60	35592	4	?	?	0.022	0.277	?	?	?
60-70	81156	6	0.435	1.000	-0.029	0.289	0.464	1.160	0.4
70-80	81428	10	1.125	0.707	-0.116	0.302	1.241	0.776	1.6
80-90	81174	13	0.435	1.000	-0.029	0.289	0.464	1.160	0.4
90-100	**82443**	21	2.029	0.447	-0.434	0.354	2.463	0.573	4.3

npixb = number of pixels in every cumulative proximity class.
npixpd = cumulative number of pixels in a cumulative class with gold deposit occurrences

6.5.6. Gold prospectivity map based on randomly selected gold deposits

The posterior probability map was classified into binary map showing favourable zones reflecting mineral potential. Posterior probability values less than 0.00002 (the prior probability of finding a gold deposit) were classified as unfavourable zones, and values greater than 0.00002 classified as favourable zones. The gold prospectivity map (Figure 6.10) has a success rate of 90.5% for predicting 19 out of 21 of the randomly selected gold deposit occurrences and 75% as prediction rate.

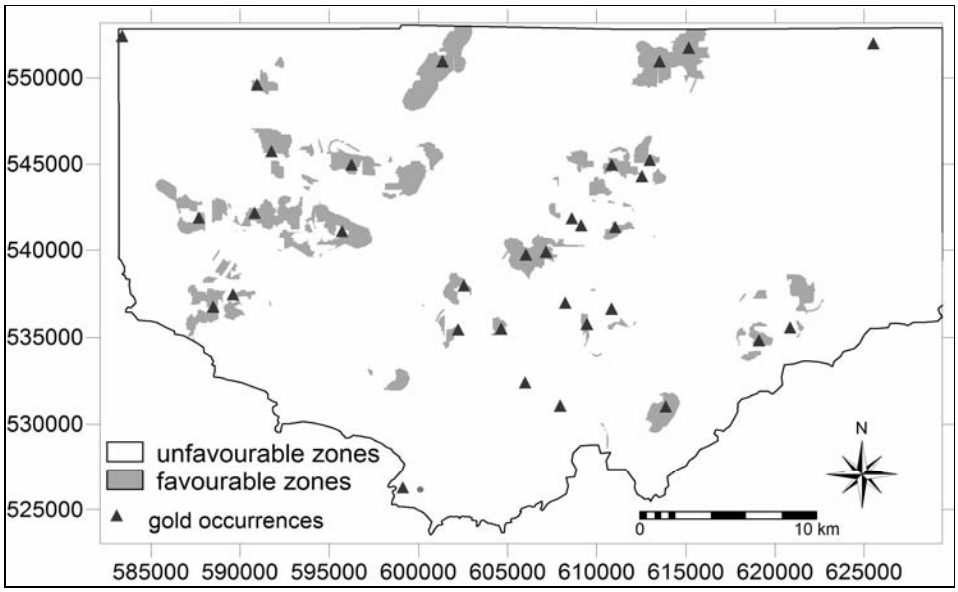

Figure 6.10: Gold prospectivity map for South Ashanti Belt based on randomly selected gold deposits

6.6. Discussion and concluding remarks

A strong and statistically positive spatial association exists between spatially similar gold deposits and fault systems. It is an indication that fault systems serve as favourable structural controls for gold mineralization, and proximity to faults is a good indicator of gold potential. Greenstones are potential host rocks for gold mineralisation in the study area. This is evident from the results of weight-of-evidence calculation involving spatially similar gold deposits and host rocks.

Presence and/or proximity to greenstones are good indicators for gold potential. The strong positive association shown by geochemical signatures in PC1 score and spatially similar gold deposit occurrences suggest that As-Fe-Au-Cr-Ni-V multi-element association could serve as pathfinder elements for gold in the study area. With the exception of favourable geochemical signatures, all the other indicative geological features including northeast trending faults, northwest trending faults, host rocks, and heat source rocks show weak and statistically insignificant positive spatial association with 21 gold deposit occurrences which were randomly selected. This is may be due to the fact that some of the randomly selected gold deposits are not related to faults/fractures or greenstones, because, they may be located at a distance from these geological features.

The prospectivity map generated from gold deposit occurrences with similar geological attributes and geochemical signatures show similarity with prospectivity map created from randomly selected gold deposit occurrences. The similarity in pattern of areas with favourable zones is mainly due to geochemical signatures. Success rate and prediction rates for prospectivity map generated from spatially similar gold occurrences are 96% and 80% respectively, which are higher than that of the prospectivity map generated from randomly selected gold deposits, which has a success rate of 90.5% and 75% of prediction rate.

Chapter 7: Conclusions and Recommendations

7.1. Conclusions

1. A systematic technique for classifying gold deposit occurrences from drainage sediments has been shown using PCA. The technique involves deriving dilution- corrected geochemical residuals, and using those derived geochemical residuals that are coincidental with the gold deposits in a multivariate statistical analysis. Graphical plot of principal component scores would show clustering of spatially similar (homogeneous) gold deposits from the rest.
2. The methodology outlined above confirms the hypothesis and/or research question of this research work that stream sediment geochemical data can portray the presence or absence of different classes of mineral deposits in a study area.
3. The derived geochemical landscape concurred well with the geological terrains delineated in the published geological map used in this research. Catchments basins with high elevations of Fe, Mg and As are associated with basalts, while ultramafic rocks in the southern portions of the study area registered high concentrations of Ni, Cr and V. Concentrations of Ni, Cr, V, Fe, Mg, and As are very low in catchment basins underlain by granitoids where Ba, Sr and Li concentrations are very high.
4. PC analysis showed that gold deposits in the South Ashanti Belt are mainly fault/fracture-hosted gold deposits and paleoplacer gold deposit types. The fault/fracture-hosted gold deposit was shown in PC1 and accounted for at least 57% of the variations in the gold deposits. The paleoplacer type of gold deposits account for 8.2% of the total variance in gold deposits.
5. Spatially similar training set of gold occurrences can be obtained by applying principal component analysis on the geological attributes and geochemical signatures at locations of gold occurrences.
6. Gold deposits in the South Ashanti Belt are characterized by As-Fe-Ni-Cr-Cu-Co-V association as shown by their high positive loadings on PC1.
7. The weights-of-evidence modelling indicate that NE and NW trending faults/fractures, host rocks, mesothermal geochemical signatures, and heat source rocks have strong and statistically positive spatial association with spatially similar gold deposit occurrences in the South Ashanti Belt.
8. Prospectivity map derived from a training set of gold deposit occurrences with spatially similar geological attributes and geochemical signatures have better prediction and success rate than a prospectivity map based on randomly selected mineral deposit occurrences.
9. The results of the prospectivity mapping show that gold mineralisation in the South Ashanti belt is structurally controlled and confined mainly to the tholeiitic basalt and ultramafic rocks of the Birimian metavolcanic belt.

7.2. Recommendations

1. The use of multi-element geochemistry for mineral deposit classification is recommended, because, it provides additional value to mineral deposit classification. Mineral deposit occurrences are associated with suites of elements which are transported and subsequently deposited in catchment basins through mechanical or hydromorphic processes.
2. The results of this study show that there is the need to analyse for Cr, Ni, Cu, Co, V, and Zn which can act as pathfinders for gold. Samples should also be analysed for Fe and Mn in order to check for scavenging effect.
3. In this study the Ag results were all discarded because of high Fe background and Cr peak interference. Ag would have provided an additional insight into the geochemical characteristics of the gold deposit occurrences in the South Ashanti Belt. A more sensitive method should be used to obtain reliable concentrations of Ag.
4. Quality of analytical data should be assessed before any further treatment of the geochemical data. To obtain a reliable interpretation of geochemical data, there is the need to ensure that the measurements are of sufficiently high quality, and that procedural error are not so high that geochemical pattern are indistinguishable from the procedural errors.

5. Further prospective work should be undertaken in the defined target areas to test the predictive capabilities of the prospectivity map. It is recommended further that exploration into Platinum Group of Elements (PGEs) be carried out in the defined target areas especially in areas underlain by ultramafic rocks.

References

Amanor, J.A., and Gyapong, W. A. (1991). "The Geology of Ashanti Goldfields)": In G.O. Kesse (ed), Proceedings of the International Conference on the Geology of Ghana (1988), Geological Society of Ghana, Accra, pp C1-C18.

Bartholomew, R. W., (1961). The Geology of Field Sheets 3 and 5 – Axim NE. Ghana Geological Survey, Archive Report 18 (2 volumes).

Bezdek, J.C., Ehrlich, R. and Full, W. (1984). FCM: the fuzzy c-means clustering algorithm. Computers & Geosciences 10: 191-203.

Bonham-Carter, G. F. (1994). Geographic information systems for geoscientists: modeling with GIS. Kidlington etc., Pergamon.

Bonham-Carter, G.F., Rogers, P.J., and Ellwood, D.J. (1987). "Catchment basin analysis applied to surficial geochemical data, Cobequid Highlands, Nova Scotia." Journal of Geochemical Exploration 29(1-3): 259-278.

Boyle, R.W. (1979). Geochemistry of gold and its deposits: together with a chapter on geochemical prospecting for the element. Ottawa, Geological Survey of Canada.

Carranza, E.J.M. (2004). "Usefulness of stream order to detect stream sediment geochemical anomalies." In: Geochemistry: Exploration, Environment, Analysis, 4(2004)4, pp. 341-352.

Carranza, E.J.M. and Hale, M., (1997). "A catchment basin approach to the analysis of reconnaissance geochemical-geological data from Albay Province, Philippines." Journal of Geochemical Exploration 60(2): 157-171.

Cox, D.P. (1983). U.S. geological survey - ingeominas: mineral resource assessment of Colombia: ore deposit models. Menlo Park, United States of the Interior, Geological Survey.

Cox, D.P. and Singer, D.A. (1992). Mineral deposit models. Denver, U.S. Geological Survey.

Dzigbodi-Adjimah, K. (1991). "On the genesis of the Birimian Gold Deposits of Ghana"; in G.O. Kesse (ed), Proceedings of the International Conference on the Geology of Ghana (1988), Geological Society of Ghana, Accra, pp. F1 to F29.

Dzigbodi-Adjimah, K. (1993). "Geology and geochemical patterns of the Birimian gold deposits, Ghana, West Africa." Journal of Geochemical Exploration 47(1-3): 305-320.

George, H. and Bonham-Carter, G.F., 1989. Spatial modeling of geological data for gold exploration, Star lake area, Saskatchewan. In: F.P. Agterberg and G.F. Bonham-Carter (eds.). Statistical Applications in the Earth Sciences. Geological Survey of Canada, Paper 89-9, pp.157-169.

Griffis, R.J., (1998). Explanatory Notes - Geological Interpretation of Geophysical Data from Southwestern Ghana. Minerals Commission, Accra, 51p.

Howarth, R.J. (ed.), 1983. Statistics and data analysis in Geochemical Prospecting. Handbook of Exploration Geochemistry, volume2, Elsevier, Amsterdam, 230pp.

Leube, A., Hirdes, W., Mauer, R. and Kesse, G.O. (1990). "The early Proterozoic Birimian Supergroup of Ghana and some aspects of its associated gold mineralization." Precambrian Research 48(4): 415.

Loh, G., and Hirdes, W. (1996). "Explanatory Notes for Geological Map of Southwest Ghana-1: 100,000 scale (Axim and Takoradi sheets)", Ghana Geological Survey Bull. 49, 63p, Accra.

Milesi, J.P., (1989). Map of West Africa Gold Deposit, 1:2,000,000 scale map attached to report RM25 Orleans, France.

Ramsey, M.H., Thompson, M., and Hale, M. (1992). "Objective evaluation of precision requirements for geochemical analysis using robust analysis of variance." In: Journal of Geochemical Exploration, 44(1992), pp. 23-36.

Rose, A.W., Hawkes, H.E., and Webb, J.S. (1979). Geochemistry in Mineral Exploration. London etc., Academic Press.

Stanley, C.R. (2006). "Numerical transformation of geochemical data: 1. maximizing geochemical contrast to facilitate information extraction and improve data presentation." Geochemistry – Exploration Environment Analysis 6: 69-78

Sylvester, P.J., and Attoh, K. (1992). Lithostratigraphy and composition of 2.1 Ga greenstone belts of the West African Craton and their bearing on crustal evolution and the Archaean-Proterozoic boundary. Journal of Geology, v. 100, pp. 337-393.

Thompson, M. and Howarth, R.J. (1978). "A new approach to the estimation of analytical precision." Journal of Geochemical Exploration 9(1): 23-30.

Thompson, M. (1983). "Control procedures in geochemical analysis. In: Howarth, R.J. (Editor), Handbook of Geochemical Exploration Volume 2 - Statistics and Data Analysis in Geochemical Prospecting." Handbook of Geochemical Exploration Volume 2: 437.